THERMAL HYDRAULIC PERFORMANCE OF AN OSCILLATING HEAT PIPE FOR AXIAL HEAT TRANSFER AND AS A HEAT SPREADER

THERMAL HYDRAULIC PERFORMANCE OF AN OSCILLATING HEAT PIPE FOR AXIAL HEAT TRANSFER AND AS A HEAT SPREADER

By MOHAMED ABDELNABI, B.Sc.

A Thesis Submitted to the School of Graduate Studies in Partial Fulfilment of the Requirements for the Degree of Master of Applied Science in Mechanical Engineering

McMaster University M.A.Sc (2022) Hamilton, Ontario (Mechanical Engineering)

TITLE:	THERMAL HYDRAULIC PERFORMANCE OF AN OSCILLATING HEAT PIPE FOR AXIAL HEAT TRANSFER AND AS A HEAT SPREADER
AUTHOR:	Mohamed Abdelnabi, B.Sc.
SUPERVISOR:	Dr. Chan Y. Ching, Professor, Dept. of Mechanical Engineering
NUMBER OF PAGES:	x, 113

Abstract

In this thesis, a stacked double-layer flat plate oscillating heat pipe charged with degassed DI water was designed, fabricated and characterized under different operating conditions (orientation, system or cooling water temperature and heat load). The oscillating heat pipe was designed to dissipate 500 W within a footprint of 170 x 100 mm^2. The oscillating heat pipe had a total of 46 channels (23 channels per layer) with a nominal diameter of 2 mm. Tests were performed to characterize the performance of the oscillating heat pipe for (i) axial heat transfer and (ii) as a heat spreader. The stacked oscillating heat pipe showed a distinctive feature in that it overcame the absence of the gravity effect when operated in a horizontal orientation. The thermal performance was found to be greatly dependent on the operational parameters. The oscillating heat pipe was able to dissipate a heat load greater than 500 W without any indication of dry-out. An increase in the cooling water temperature enhanced the performance and was accompanied with an increase in the on/off oscillation ratio. The lowest thermal resistance of 0.06 K/W was achieved at 500 W with a 50°C cooling water temperature, with a corresponding evaporator heat transfer coefficient of 0.78 W/cm^2K. The oscillating heat pipe improved the heat spreading capability when locally heated at the middle and end locations. The thermal performance was enhanced by 27 percent and 21 percent, respectively, when compared to a plain heat spreader.

Keywords: Flat plate oscillating heat pipe; Stacked; Thermo-hydrodynamics; Orientation; Heat spreading.

Acknowledgments

In the name of Allah, the Most Gracious and the Most Merciful, all praises to Allah for blessing me with patience, knowledge, and strength to complete this work.

It is a pleasure to express my deepest thanks to my supervisors Dr. Chan Ching and Dr. Dan Ewing for their guidance, help and support all the time during my M.Sc. degree. Without their guidance and president support, this work would have not been completed.

Special thanks to Dr. James Cotton, Jeff Girard, Zaher, Dr. Vickram Lakhian, Dr. Saber Mohamed, and Dr. Mohamed Yasser, you never hesitate to offer help and guidance whenever I ask.

My thanks to Mechanical Engineering technicians, John Colenbrander, Michael Lee, Mark Mackenzie, Justin Bernar, and Rob Sluban. You are very helpful; without your help It could not have been done.

My thanks to Mechanical Engineering administrators, Nicole, Lily and Leslie. Whenever I ask for help you instantly do you best to help, you always make it easy for us.

My special and deepest thanks to my father Ali and my mother Abla. I can not express my thanks for your overseas support, praying and love. One word I would say “I love you”. I know it has been three years without meeting you, but I believe that one day we will gather again.

I would like to express all my thanks to my brother Ahmed. Since I came to Canada you always help and support me and always do your best to make it easy for me. You always have my back; I owe you a lot. I hope all the best with your new job. And my thanks to Maryam, Ahmed’s wife, you literally make it different and you were so supportive. All my best wishes with your PhD.

I would like to express my warm thanks to my siblings Mariam and Mahmoud. You always try to do your best to support me and show your empathy. Thank you for lending an ear when nobody else would. I am looking forward to seeing you here in Canada and having your own career that you love.

Thank you to my lab mates, Hammouda, Saksham, Safy, Saber and Hassan. We almost spent all our time together in the lab “before Covid-19”. Without you It would have been boring. All my best wishes with your study and your career in the near future.

My special thanks to my friends, Fathallah, Abdallah, Alaa, Helal, Nour, Amira, Amira, Dana, Moemen, Salma, Muna, Mariam, Omar and Ahmed Ragheeb for your friendship, empathy, and great sense of humour. Wish you all the best.

Table of Contents

List of Tables

List of Figures

Nomenclature

A	Area	[m^2]
C	Heat capacity	[J/K]
$Circ$	Circumference	[m]
Cp	Specific heat	[J/kg. K]
d	Diameter	[m]
g	Gravitational acceleration	[m/sec^2]
h	Heat transfer coefficient	[W/m^2K]
h_{fg}	Latent heat	[J/kg]
k	Thermal conductivity	[W/m. K]
L	Length	[m]
M	Number of liquid slugs	
m	Mass	[kg]
N	Number of turns	
n	Number of channels	
P	Pressure	[kPa]
q	Heat flux	[W/m^2]
Q	Heat load	[W]
r	Radius	[m]
$\bar{R}$	Air gas constant	
R	Resistance	[K/W]
S	Suppression factor	
slp	Slope	
V	Voltage	[V]
$\dot{V}$	Volume flow rate	[m^3/sec]
Vol	Volume	[m^3]
X	Martinelli parameter	
Z	Height from sea level	[m]
z	Number of samples	

Greek symbols

ρ	Density	[kg/m^3]
β	Inclination angle to horiz.	[deg]
γ	Specific weight	[N/m^3]
υ	Mean velocity	[m/sec]
ε	Uncertainty	
μ	Viscosity	[kg/m. sec]
σ	Surface tension	[N/m]
φ	Filling ratio	

Dimensionless number

Bo	Bond number	$Bo = \frac{(\rho_l - \rho_v)D^2 g}{\sigma}$
Ja	Jacob number	$Ja = \frac{Cp_l(T_e - T_c)}{h_{fg}}$
*Ja**	Modified Jacob number	$Ja = \frac{\emptyset . Cp_l(T_e - T_c)}{(1-\emptyset)h_{fg}}$
Ka	Karman number	$Ka = \frac{h_{fg}}{Cp_l(T_e - T_c)}$
Ku	Kutateladze number	$Ku = \frac{q}{h_{fg}\rho_v\left(\frac{\sigma g(\rho_l - \rho_v)}{\rho_v^2}\right)^{0.25}}$
Mo	Morton number	$Mo = \frac{g.(\rho_l - \rho_v).{\mu_l}^4}{{\rho_l}^2.\sigma^3}$
Pr	Prandtl number	$Pr = \frac{\mu . Cp}{k}$
Re	Reynolds number	$Re = \frac{\rho . v . d_h}{\mu}$

Subscripts

abs	Absolute	*max*	Maximum
atm	Atmospheric	*meas*	Measured
avg	Average	*mic*	Microscopic
c	Condenser	*min*	Minimum
cr	Critical	*NCG*	Non-condensable gases
e	Evaporator	*o*	Outer
h	Hydraulic	*sat*	Saturation
i	Inner	*t*	Total
l	Liquid	*v*	Vapour
mac	Macroscopic	*w*	Wall

1 Introduction

Thermal management has been and continues to be a major challenge in many different applications and industries, such as in energy renewable and storage systems, refrigeration cycles, power electronics and the automotive industry. For example, there is a growing need for high performance heat dissipation systems for batteries and the advanced power electronic devices as the automotive industry moves towards fully electric vehicles. There is also a growing tendency towards more compact high-power electronic devices that leads to the need for heat transfer devices that have much higher heat flux capacities. Typically, the heat generated in battery and power electronic devices need to be transferred to a different location for dissipation to the ambient due to space constraints. This is done by coupling the heat spreader plates at the source with a heat exchanger for dissipation to the ambient using an active (e.g. forced liquid cooling) or a passive heat transport system. Heat pipes are passive heat transport devices that have been used extensively in such systems. In heat pipes, a working fluid is evaporated at the hot end and the vapor travels to the colder end where it is condensed due to heat transfer. There are several mechanisms used to transport the condensed liquid back to the heated end. In the simplest case, the condensate is returned via gravity (thermosyphons) and in other cases an internal wick along the wall is used to return the liquid through the capillary action (wicked heat pipes). There are also several other variations that include rotating and revolving heat pipes. Due to the two-phase

heat transport mechanism, these devices have a high heat transport capacity with very low thermal resistance compared to other methods.

There is growing interest in the use of oscillating heat pipes in many applications. Oscillating heat pipes have several advantage over traditional heat pipes: (i) there is no need for wick structures to transport the fluid, (ii) the simple structure and low fabrication cost, (iii) they can be fabricated in very small sizes due to its small inner diameter and (iv) they can work in different orientations efficiently compared to traditional heat pipes. An Oscillating heat pipe (OHP) or Pulsating heat pipe (PHP) consists of a long meandering capillary tube typically made of copper that is vacuumed and then filled with a working fluid with a specific filling ratio. A train of vapor bubbles and liquid slugs is formed due to the surface tension as shown in Figure 1-1. At the evaporator section, the liquid slugs are evaporated, increasing the volume of the vapor as well as its pressure. This increase forces the fluid to be pushed to the condenser section where cooling is applied, and the vapor condenses and the pressure decreases. The continuous vaporization and condensation of the fluid creates the oscillatory motion of the fluid. The higher the heat flux, the greater the oscillatory motion which leads to higher heat transfer performance. The heat transfer is through forced convection (oscillatory motion) and phase change (latent heat), so it has a higher heat transfer capacity than traditional heat pipes.

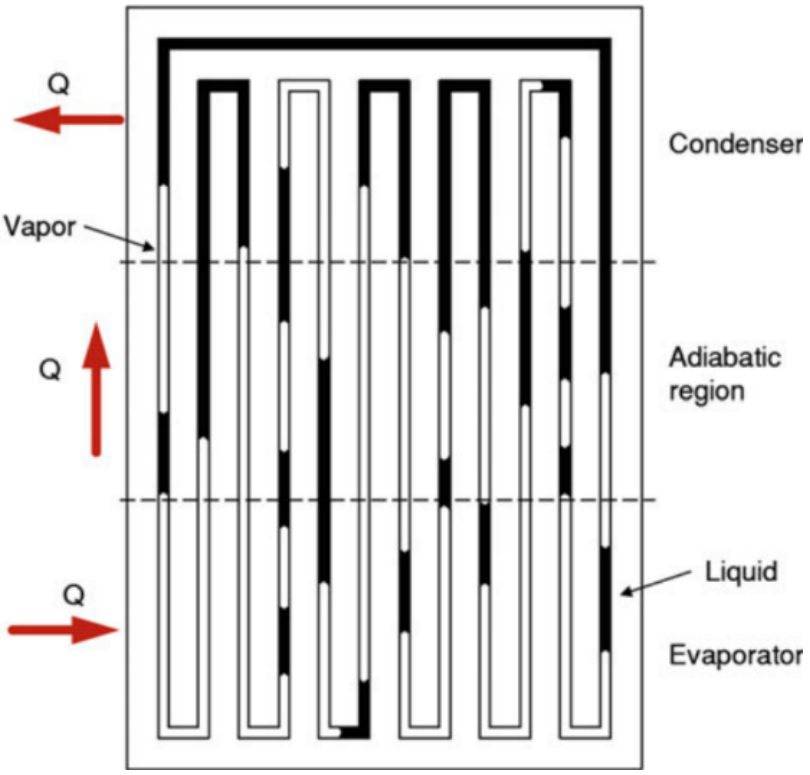

Figure 1-1: Oscillating heat pipe (OHP) structure.

Despite the progress that has been made during the past decades on development of heat transfer devices (heat exchangers, heat sinks and heat pipes), there are still challenges in thermal management that needs more enhancement in their performance, particularly when dealing with hot spots due to local heat generation. One method of alleviating hot spots is to embed heat pipes on the heat spreader plate to transport the heat away from the hot spots and provide a more isothermal heat spreader condition. An example of this is shown in the heat spreader plate manufactured by MERSEN (Figure 1-2) where wicked heat pipes are embedded in the heat spreader plate. Oscillating heat pipes provide an attractive alternative to heat pipes because its geometry is well suited for such applications.

Figure 1-2 Mersen® heat spreader with embedded heat pipes.

The focus of this thesis is on power electronics cooling which generates a high heat flux, which is of interest to our industrial partner MERSEN. In particular, the key objective is to investigate the feasibility of a flat plate oscillating heat pipe to transport heat powers greater than 400 Watts with an evaporator wall temperature not exceeding 100℃. There have been several studies of this configuration and these are reviewed in the next chapter. However, to the author's knowledge, there are no guidelines or estimated heat transfer coefficients to aid in designing oscillating heat pipes for use in heat spreader plates for different application conditions.

The specific objectives of this study are:

(1) To experimentally investigate the thermo-hydrodynamic performance of a flat plate oscillating heat pipe and investigate its performance at different operating conditions. In addition, the advantages of stacked flat plate oscillating heat pipes over single layer ones are considered.

(2) To investigate the capability of the fabricated oscillating heat pipe to function as a heat spreader to eliminate hot spots on power electronics cooling system, specifically replacing the embedded heat pipes on MERSEN® heat spreaders.

This thesis consists of five chapters. Chapter two present a literature review pertinent to this study that includes the design and operation parameters. Emphasis is placed on oscillating heat pipes that deal with high heating power. Chapter three discusses the design methodology and manufacture of the Oscillating Heat Pipe, the experimental facilities, and data analysis. The results and discussion are summarized in chapter four and finally the conclusion and recommendations from the study are presented in chapter five.

2 Literature Review

Oscillating heat pipes consisting of a closed continuous loop of U-shaped evacuated channels that are partially filled with a working fluid were invented by Akachi [1] in 1990s to transport heat passively with a low thermal resistance. The working principle of oscillating heat pipes is based on the oscillations of the working fluid which is present in the channels in the form of a train of water slugs and vapour plugs. The thermodynamics behind the oscillations was initially explained by Karimi [2]. The pressure enthalpy diagram is shown in Figure 2-1, where the working fluid initially is at point A and oscillates between point B and point C. The heating at the evaporator end results in the growth of the vapour plugs due to the liquid evaporation and forces point A to move to point B at a higher pressure, temperature, and quality. Simultaneously, the cooling at the condenser section leads to shrinkage in the vapour plugs because of condensation, moving point A to point C at a lower pressure, temperature, and quality. In this way the system is in a non-equilibrium state which results in the oscillating motion.

The channels in an oscillating heat pipe has a defined hydraulic diameter and it can be constructed out of copper tubing or be machined on a flat plate and are called flat plate oscillating heat pipes. Many experiments have been conducted to understand the working principle of oscillating heat pipes and its performance under different operating conditions with different designs. The parameters that can affect the performance of an oscillating heat pipe can be divided into three categories (Han et al.[3]): (i) geometric parameters, (ii)

physical properties of the working fluid and (iii) operational parameters. The geometric parameters define the physical geometry of oscillating heat pipes and include the inner hydraulic diameter, number of turns and area of the evaporator and condenser sections. The physical properties of the working fluid can significantly affect the performance and include the surface tension, latent heat, specific heat capacity, viscosity, and thermal conductivity. Finally, the operational parameters or operating conditions will define the charging ratio, heat flux, and inclination angle. In most applications that use oscillating heat pipes, the challenge is to design the oscillating heat pipe to transport a given heat flux over a given geometric footprint while maintaining the temperature difference between the evaporator and condenser sections (hot and cold regions) to within the allowable range.

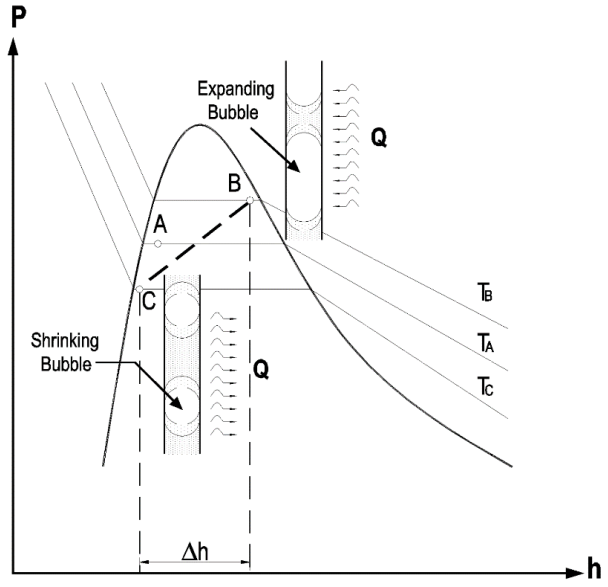

Figure 2-1 Pressure enthalpy diagram of a working fluid during the operation of the oscillating heat pipe [2].

This chapter reviews previous studies on oscillating heat pipes, starting with the different parameters that affect the performance. The effect of each parameter is presented with a summary on its effect on the design of oscillating heat pipes. The limitations on oscillating heat pipes are then discussed. The chapter concludes with previous work done on investigating the performance of oscillating heat pipes as a heat spreader.

2.1 Parameters that affect the performance of Oscillating Heat Pipes.

2.1.1 Channel dimensions.

The dimensions of the channel have a significant effect on the performance of oscillating heat pipes. The appropriate channel hydraulic diameter is determined based on the fluid properties, specifically the surface tension to maintain the presence of the liquid slug and vapor plug trains. The Bond number (Bo) expressed as

$$Bo = \frac{(\rho_l - \rho_v)D^2 g}{\sigma} \qquad 2\text{-}1$$

is used to define the suitable range of the hydraulic diameter. It is a dimensionless number that characterizes the ratio of the gravitational force to the surface tension forces. The appropriate maximum diameter is determined when the capillary force, which is a function of the surface tension σ of the fluid, is almost equal to the gravitational force [4]. Based on the study by Qu et al [5], the Bond number should be in the range between 0.49 and 4 and given as

$$0.7 < Bo^{0.5} < 2 \qquad 2\text{-}2$$

Thus, it follows that the diameter should be in the range given by equation (2-3) to have the appropriate slug and plug trains.

$$0.7\sqrt{\frac{\sigma}{g(\rho_l-\rho_g)}} < D < 2\sqrt{\frac{\sigma}{g(\rho_l-\rho_g)}} \qquad 2\text{-}3$$

An analytical model was developed by Jian et al. [6] to predict the lower limit of the channel diameter D_{min}. The effect of different parameters on the minimum diameter were studied. It is found that the minimum diameter increases with an increase in the number of turns to overcome the increase of the flow resistance. By increasing the inclination angle from 0° to 90° (horizontal to vertical), the minimum diameter decreases as gravity plays an increasing role as the orientation gets closer to the vertical position.

The cross-sectional shape of the channels also affects the thermal performance of an oscillating heat pipe. It has an important role in the slug and plug train distribution and flow pattern transition. Angled corners can have a significant effect on the flow pattern. Mehta et al. [7] experimentally investigated three oscillating heat pipes, two of them having the same hydraulic diameter of 2 mm with different cross-sectional shapes, one with a square cross-section and the other with a circular cross-section, and the third one with a square section with 5 mm hydraulic diameter. The square cross-sectional channel had better thermal performance compared to the circular channel with a decrease in the thermal resistance by about 25 percent. This is because of the wetting film created by the square channel around the vapour plugs which connects both parts of the liquid above and below the vapour plug, resulting in higher rising velocity compared to the circular channel [8]. The larger square channel oscillating heat pipe also performed better than the smaller

circular channel oscillating heat pipe. Zhou and Qu [9] concluded for an experimental study that oscillating heat pipes with triangular channels perform thermally better than ones with rectangular channels. Lee et al. [10] performed a study on micro channel oscillating heat pipes with different channel geometry. It was found that the square channel compared to circular channels extended the power limitation and showed better thermal performance. The liquid film thickness that was visualized by a high-speed camera was found to decrease with an increase of the heat load in contrast to the circular channels which is constant with the heat load. The same was concluded by Hua et al. [11] in their study on the effect of channel geometry on the performance of oscillating heat pipes.

The effect of the evaporator section length was considered in Meena et al. [12], who conducted experiments to study the effect of evaporator length on the critical heat flux for different working fluids. It was found that for the range of their study, the critical heat flux increased as the evaporator length was reduced. Similar conclusions were made by Rittidech et al [13], where the maximum heat flux decreased from 7646 to 4506 W/m^2 with an increase in the evaporator length from 50 to 150 mm for R123 as the working fluid. Charoensawan and Terdtoon [14] studied the effect of the evaporator length with different working fluids, filling ratios and hydraulic diameter. Having a smaller evaporator length enhanced the thermal performance for all the configurations. Previous studies have concluded that it is better to have a condenser length longer than the evaporator length [15],[16].

There are no clear guidelines for determining the optimal condenser length. The numerical investigation done by Wang et al. [17] found a shorter condenser length resulted

in a higher the thermal performance, but the study was done at a fixed condenser temperature of 27℃. Kim et al. [18] reported that other parameters, particularly the temperature, affect the selection of the condenser length. They studied the effect of the condenser length at different conditions and found that a higher condenser section temperature needed a longer condenser length. For example, an optimum condenser length of 10 mm was found suitable when the condenser temperature was lower than 30℃ but a condenser length of 50 mm was required for condenser temperatures higher than 60℃. The results show that the condenser length and its temperature is linked which means that each condenser temperature (cooling water temperature) affects the condenser length selection.

2.1.2 Number of turns

The number of turns is one of the most important parameters that greatly influence the thermal performance of oscillating heat pipes and determine its heat flux limitations. Increasing the number of turns enhances the thermal performance, as the perturbations inside the oscillating heat pipe are increased and this enhances the pressure disturbances, which consequently increases the motion of the working fluid [19]. In addition to the enhancement in the thermal performance, oscillating heat pipes with a high number of turns tend to work better at different inclination angles [20]–[23]. It has been shown that the higher the number of turns the lower the gravitational effect, and thus the effect of orientation on the oscillating heat pipe. Past a certain number of turns, oscillating heat pipes work efficiently in horizontal orientation, though not as the same as in a vertical orientation where gravity assists the fluid circulation. Charoensawan et al. [24] demonstrated that an

oscillating heat pipe with the number of turns greater than 16 operated similarly for all inclination angles. The results showed that a 23-turn oscillating heat pipe filled with water in the horizontal orientation transported about 80 percent of the heat that could be transported in the vertical position, while a 7-turn oscillating heat pipe filled with water transported less than 20 percent of the maximum heat load. On the other hand, several studies support that there is a critical number of turns. Khandekar et al. [25] showed that increasing the of turns past a critical value leads to a degradation in thermal performance caused by the reduction in pressure difference inside the oscillating heat pipe. It is commonly concluded that the number of turns affects how much heat can be dissipated but there is no correlation found to link it with the thermal performance and what is the critical number of turns.

2.1.3 Working fluid

The working fluid properties (surface tension, latent heat, viscosity, and thermal conductivity) affect the performance of the oscillating heat pipe and needs to be considered in its design. Using fluids with a large surface tension would lead to an increase in the critical diameter according to eq. (2-3) and result in a low friction resistance. However, the capillary resistance which effects the contact angle hysteresis is proportional to the surface tension [26]. Hence, there is a compromise to have a fluid with optimal surface tension to maintain the presence of the liquid slugs and vapor plugs train and at the same time to have the lowest flow friction. The latent heat plays a key role in determining the working fluid based on the heat flux. Fluids with low latent heat is better and desirable for low heat flux

applications, as it minimizes the excess temperature needed for start-up of the oscillating heat pipe. For high heat flux applications, fluids with a high latent heat would be needed [27], [28]. Fluids with lower dynamic viscosity is better for oscillating heat pipes. Low dynamics viscosity leads to lower viscous damping which hinders the fluid motion and reduces the shear stress, resulting in a decrease in the pressure. This leads to minimize the heat flux needed to maintain fluid motion [26], [29].

Experiments have been performed to investigate the effect of working fluid properties on the performance of oscillating heat pipes. Wang et al. [30] conducted an experimental study using three different working fluids (water, ethanol and R141B). The oscillating heat pipe with water performed better than the other two fluids, having the largest maximum heat flux and a wider range in operating temperature differences. This is due to its high latent heat and specific heat capacity relative to the other two. However, the oscillating heat pipe filled with water experienced a delay in the start-up as it required more heat to initiate the oscillations due to its higher latent heat. These results were similar to those obtained by Tseng el al. [31]. At low heating powers (less than 60W), the fluids with low specific heat and latent heat performed better as they experienced a lower thermal resistance and an earlier start-up. Water was found to work much better for higher heating powers. Finally, the working fluid selection is mainly based on the application and dry-out limitations which will be discussed later in this chapter and needs to be considered in selecting the working fluid.

2.1.4 Fluid charge ratio

The charge ratio is the volume of the working fluid to the total volume of the oscillating heat pipe channels. As oscillating heat pipes are filled under a vacuum, the charge ratio defines the vapor to liquid ratio which influences the thermal performance. At zero charge ratio, the heat is transferred purely by conduction through the oscillating heat pipe walls which has a relatively high thermal resistance. At low charge ratios, there is insufficient liquid to contribute to the sensible heating mode and the tendency to reach the dry out limit is more likely to occur. On the other hand, very high charge ratios mean the presence of more liquid which can obstruct the oscillating motion as there are not enough vapor slugs which are responsible for the driving force. At 100 percent charge ratio, the oscillating heat pipe becomes a single-phase heat transfer device. Different experiments have been conducted to investigate the optimal charge ratio under different conditions, and it is concluded that the charge ratio depends on different parameters like working fluid, heating power and orientation. Han et al. [3] reviewed experiments done on the charge ratio, and summarized that the optimal range is typically from 35 percent to 65 percent, and in most cases determined that a charge ratio of 50 percent was optimal for higher thermal performance. The optimal range reported in [3] is for the conditions where these experiments were done. The charge ratio, however, is not only a function of one parameter but a combination of the parameters. Mehta et al. [32], conducted an experiment to study the effect of the charge ratio on the performance for a vertical oscillating heat pipe charged with acetone. The performance enhanced with an increase of the charge ratio till a charge ratio of 60 percent before deteriorating with a further increase. The thermal performance

with different working fluids at 70 percent charge ratio was found to give different thermal performance which mean the optimal charge ratio depends on the working fluid and other operating conditions. Khandekar et al. [33] found that the sensitivity of the charge ratio to the performance was not significant within the range of 35 to 70 percent for water as a working fluid

2.1.5 Cooling water temperature

The temperature of the cooling water affects the performance of oscillating heat pipes. By increasing the temperature of the cooling water the overall thermal performance increases and it enhances the start-up conditions by decreasing the power needed for steady start-up as found by Chao Hua et al.[11]. Several studies[20], [34], [35] were done to investigate the effect of the cooling water temperature and the key finding is that by increasing its temperature the thermal performance is enhanced. Kun Xie et al.[36] performed a study on an oscillating heat pipe with different cooling water temperatures in the range of 20-80℃. A higher cooling water temperature resulted in a lower thermal resistance.

2.1.6 Orientation (inclination angle)

Experiments have been performed to study the effect of the orientation on the performance of oscillating heat pipes [20], [37], [35], [38]. The vertical orientation with bottom heating gives the best performance due to the gravitational effect. The gravitational force helps in moving the fluid back to the evaporator section, overcoming the resistance forces represented in the buoyancy force. Charoensawan et al. [24] carried out various experiments to study the effect of orientation on the maximum heat transfer of oscillating

heat pipes. The results show that for different working fluids, the oscillating heat pipe performance degrades as the orientation tends to the horizontal position. In order to predict the thermal performance of oscillating heat pipes at different orientations, Hudakorn et al. [39] formulated a correlation to predict the relationship between the inclination angle and the critical heat flux as

$$\frac{q_{cr,\beta}}{q_{cr,90}} = \left(1.164 \sin\beta + 0.53 \cos\beta - 0.484 \left(\frac{L_e}{D_i}\right)\right)^{0.1} \qquad 2\text{-}4$$

The above correlation is developed for a single-layered oscillating heat pipe. Multi-layered or stacked oscillating heat pipes perform differently at low angle orientations. The effect of orientation is significantly reduced for stacked oscillating heat pipes, where Thompson et al. [40] found similar thermal performance for both vertical and horizontal orientations.

2.1.7 Number of layers (stacked/three-dimensional)

Most previous research has been on the performance of single layer oscillating heat pipes. More recently, there have been studies to investigate the thermal performance of multi layered or stacked oscillating heat pipes which consist of more than one layer of channels connected to create a closed loop. Stacked oscillating heat pipes have an advantage over single-layered oscillating heat pipes as it reduces the problems of operating in a horizontal orientation by reducing the effect of gravity. Stacked oscillating heat pipes have lower thermal resistance than single-layered ones with better start-up conditions. Qu et al. [41] conducted a study to investigate the effect of increasing the number of layers for

both vertical and horizontal orientations. The results showed that by increasing the layers, the thermal resistance decreased, and the maximum heating power range increased. By increasing the number of layers, the thermal resistance in both the horizontal and vertical orientations were very similar. Smoot and Ma [42] investigated the number of layers on the thermal performance of oscillating heat pipes and compared the thermal performance when the number of layers was increased. Single-layer, double-layer and triple-layer oscillating heat pipes were tested in both horizontal and vertical orientations. The results showed an increase in performance with an increase in number of layers and the gravity influence was significantly reduced as the number of layers was increased. In summary, an oscillating heat pipe for horizontal operation requires a specific number of turns. A stacked oscillating heat pipe provides an attractive design alternative for compact applications and can also avoid difficulties in start-up and instabilities associated with operation in the horizontal position. In vertical operation, the performance is improved due to the increased number of turns due to the layers.

2.1.8 Heat transfer coefficients

One of the most complex phenomena in oscillating heat pipes is the heat transfer mechanism in the evaporator and condenser sections. It is a two-phase convective heat transfer where convective evaporation occurs in the evaporator section and convective condensation in the condenser section. There have been several studies to understand the heat transfer processes in the evaporator and condenser sections. In some studies [43], the heat transfer coefficients are calculated using the measured evaporator, condenser and

adiabatic or internal fluid temperatures. In other studies, the heat transfer coefficients are estimated using two-phase flow correlations. Ma et al [44] used the Chen correlation [45] for convective flow to describe the heat transfer in the evaporator section. The Chen correlation combines a nucleate boiling term (h_{mic} - microscopic) with a bulk convective term to account for the oscillating motion (h_{mac} - macroscopic) as

$$h = h_{mic} + h_{mac} \tag{2-5}$$

Chen developed a model for the nucleate boiling heat transfer term as

$$h_{mic} = 0.00122\left[\frac{k_l^{0.79} c_{pl}^{0.45} \rho_l^{0.49}}{\sigma^{0.5} \mu_l^{0.29} h_{lv}^{0.24} \rho_v^{0.24}}\right][T_w - T_{sat}(P_l)]^{0.24}[P_{sat}(T_w) - P_l]^{0.75} S \tag{2-6}$$

The forced convection term caused by the oscillating motions is modeled using the Martinelli parameter as

$$h_{mac} = F(X_{tt}) h_l \tag{2-7}$$

where h_l is the liquid-phase heat transfer coefficient and expressed as

$$h_l = 0.023\left(\frac{k_l}{D}\right) Re_l^{0.8} Pr_l^{0.4} \tag{2-8}$$

Cheng et al [20] suggested using the Shah correlation [46] for film condensation inside a pipe for the condenser heat transfer coefficient. The Shah correlation is given as

$$\frac{h}{h_l} = (1-\varphi)^{0.8} + \frac{3.8.\varphi^{0.76}.(1-\varphi).0.04}{(P/P_{cr})^{0.38}} \tag{2-9}$$

where P and P_{cr} are the absolute pressure and the critical pressure of the working fluid, respectively.

Most previous work that used measured temperatures use the adiabatic temperature instead of the actual fluid temperature to calculate the heat transfer coefficients in the evaporator and condenser sections. It mostly leads to errors in the heat transfer coefficient as shown by Monroe et al [47], where he compared the internal and external temperature measurements for the adiabatic section. They found that the conduction through the walls damps the frequency of the temperature leading to errors in the temperature readings, whereas the internal measurements can capture higher amplitude and frequencies of the temperature.

Installing sensors within the channels for internal measurements to obtain the fluid properties to compute the heat transfer coefficients is challenging. Gonzalez et al. [48] installed pressure transducers and internal thermocouples to obtain the fluid properties. The saturation temperature calculated from the saturation pressure data was compared to the fluid temperature at the evaporator and condenser sections. The fluid at the evaporator section was found to be at the saturation state but at the condenser it was in the subcooled state. This leads to an underestimation of the heat transfer coefficient at the condenser when using the saturation temperature instead of the actual fluid temperature. Previous studies [49]–[53] concluded from different mathematical and numerical models that the sensible heat transfer is the dominant heat transfer mode and not the latent heat. An experimental study by Jo et al. [54], however, showed that the latent heat transfer is the major mode due to the annular flow being dominant. The fluid temperature in the thin film region is higher than the saturation temperature and the opposite in the condenser section and thus leads to overestimation and underestimation of the heat transfer coefficients in the evaporator and

condenser sections, respectively, by assuming the fluid to be at the saturation temperature. The error, however, was found to not exceed 3.8 percent in Jo et al. [54]. Hao et al. [34] reported that the heat transfer coefficient in the evaporator contributed more to the oscillating heat pipe heat transfer than in the condenser but the adiabatic temperature was used instead of the internal fluid temperature in this case. Several other studies [55],[56],[57] have used the evaporator and condenser wall temperatures to compute the convective heat transfer coefficient of oscillating heat pipes without any internal measurements. Sun et al. [43] concluded that internal measurements are more accurate for computing the heat transfer coefficients but could affect the flow pattern and local nucleation sites.

2.2 Non-condensable gases in oscillating heat pipes

In general, the presence of non condensable gases (NCG) is one of the key issues in the operation of heat pipes. It affects the performance negatively as they accumulate at the condenser section and hinders the condensation process. The same was found by [58], [59] for oscillating heat pipes. It is found that in addition to adversely affecting the condensation process, it negatively affects the oscillatory motions leading to higher thermal resistance. The effect of the non-condensable gas can be minimized through good vacuuming and degassing of the fluid during the charging process.

2.3 Limitations

Several studies have been performed to determine the limitations of oscillating heat pipes. Yin et al [60] proposed a limitation for oscillating heat pipes where the mass-spring system disappears when the flow changed to annular flow because of high heat flux. At high heat flux, the increased flow velocities can lead to the vapor penetrating the liquid slugs and forming an annular flow. The operation limitation is defined by the critical heat flux given by

$$q = \frac{3\pi\mu_l h_{lv} L\varphi}{NM} \qquad 2\text{-}10$$

Khandekar et al [61] proposed a correlation to predict the maximum heat flux for oscillating heat pipes with filling ratio of 50 percent. The correlation fit 280 data point with a standard deviation of ±30% and is given by

$$q = \frac{Q}{\pi D_i . n. l_e} = 0.54.\left(e^{\beta}\right)^{0.48}.Ka^{0.47}Pr_l^{0.27}Ja^{1.43}(N)^{-0.27} \qquad 2\text{-}11$$

Several researchers use the Kutateladze number to determine the thermal performance and the critical heat flux. The Kutateladze number is commonly used to identify the performance limitations of heat pipes and is the ratio between the input heat flux to the critical heat flux for pool boiling and is given by

$$Ku = \frac{q}{h_{fg}\rho_v \left(\frac{\sigma g(\rho_l - \rho_v)}{\rho_v^2}\right)^{0.25}} \quad 2\text{-}12$$

Qu et al. [62] formulated a correlation for the critical Kutateladze number based on experimental data on the basis of the nondimensional numbers Bo, Mo, Pr and a modified Jacob number Ja in addition to the two ratios (D_i/L_e) and (L_e/L_c) as

$$ku_{max} = 8.3Bo^{-1.598}Mo^{0.026}Pr^{-3.458}Ja^{*(-0.157)}\left(\frac{D_i}{L_e}\right)^{1.21}\left(\frac{L_e}{L_c}\right)^{-0.232} \quad 2\text{-}13$$

The correlation predicted the maximum or critical Ku number with a standard deviation of about 28 percent for vertical single layered oscillating heat pipes with a 50 percent filling ratio. Rittidech et al. [13] derived a correlation for the critical Ku number for oscillating heat pipes in horizontal orientation with standard deviation of ±30 percent as

$$ku_{max} = 0.0052.\left[\frac{D^{4.3}{L_t}^{0.1}}{{L_e}^{4.4}}.n^{0.5}.\left(\frac{\rho_v}{\rho_l}\right)^{-0.2}.{Pr_v}^{-25}\right]^{0.116} \quad 2\text{-}14$$

The correlation is valid for the following range,

$$1.2 \times 10^{-9} < \frac{D^{4.3}{L_t}^{0.1}}{{L_e}^{4.4}}.n^{0.5}.\left(\frac{\rho_v}{\rho_l}\right)^{-0.2}.{Pr_v}^{-25} < 0.0551$$

Two other correlations were developed by Katpradit el al [63] for both horizontal and vertical orientations expressed as equation [2-15] and [2-16], respectively.

$$ku_{max} = 53680.\left(\frac{D}{L_e}\right)^{1.127}.Ja^{1.417}.Bo^{-1.32} \quad 2\text{-}15$$

$$ku_{max} = 0.0002.\left(\frac{D}{L_e}\right)^{0.92}.Ja^{-0.212}.Bo^{-0.59}.\left[1+\left(\frac{\rho_v}{\rho_l}\right)^{0.25}\right]^{13.06} \quad 2\text{-}16$$

The correlations are valid for working fluids R123, ethanol, water and MP39 and limited to the following range

$$10^{-10} < \left(\frac{D}{L_e}\right)^{1.127}.Ja^{1.417}.Bo^{-1.32} < 10^{-8}$$

High heat flux oscillating heat pipes.

Power electronics typically generates high heat flux that needs high-performance heat transfer devices. Different studies investigated the ability of oscillating heat pipes to handle high heating powers. Smoot et al. [42] tested a stacked oscillating heat pipe of three layers for a power range of 10-8000 W. The results did not show any dry-out. Karthikeyan et al. [64] investigated a single layered oscillating heat pipe for 500 W heating power. The performance increased with an increase of the power and did not show any evidence of dry-out. The experiments of Hao et al. [34] showed similar conclusions.

Table 2-1 presents the findings of previous work done on oscillating heat pipe filled with water as a working fluid that operate for high heat power ranges greater than 100 W.

Table 2-1 Previous studies done on oscillating heat pipe performance with high heat load.

Investigator	*Type*	*Working fluid*	*No. Of layers*	*Heat load (w)*	*Key findings*
Karthikeyan et al. [64]	Copper tubing	Water	Single layer, 8 turns 2 mm	30-500	1. The thermal performance increases with the increase in heat power which affect the dynamics of the internal two-phase flow fluid. 2. Different flow patterns were identified, and the oscillatory motion is the dominant mechanism.
Smoot et al. [42]	Flat plate	water	Stacked layers	10-8000	1- Stacked oscillating heat pipe perform similarly in horizontal and vertical orientations. 2- Stacked oscillating heat pipe with water as a working fluid can handle more than 8 kW heating power. 3- The increase in power does not affect the performance of the triple-layer unlike the single-layer.
Chang et al.[20]	Flat plate	Water, Acetone, Nano fluids	3d staggered, 8 turns, 1.7*1.175& 1.175*1.175	100-350	1. Vertical bottom heating has the best thermal performance compared to horizontal and vertical top heating which has the worst performance, but they all show almost the same performance has high power (350w) 2. The rectangular channels 1.7*1.175 shows better thermal performance compared to square channels 1.175*1.175. 3. Increase the cooling water temp. (20c to 60c) enhance the performance by about 65% 4. Using diamond/acetone nanofluid extended the power limit to 360 w compared to pure acetone of 140 w power limit.
Hao et al. [34]	Flat plat	Water	Single layer, 6 turns, 2*2	30-400	1. Increasing the cooling water temperature decrease the power needed for start-up. 5. The evaporator section contributes more to the heat transfer process than the condenser section as it has higher heat transfer coefficient.
Abraham et al. [35]	Copper tubing	Water	Double layer,16 turns, circular	20-240	1. Increasing the cooling water temperature leads to decrease in the thermal performance.

			2 mm		2. For horizontal cases, the bottom heating mode shows better performance than the double and top heating modes. 3. The 80% filling ratio fits with the horizontal orientations which extend the power limit to 240 w compared to 120 w power limit for other filling ratios. 4. At high heat load (120 w to 240 w), the vertical orientation does not show much change in thermal performance with the increase in the filling ratio from 40% to 80%
Chao Hua et al.[11]	Copper tubing	Water	Single layer, 10 turns, 4*4	80-360	1. Increasing the starting power leads to smoother start-up. 2. The thermal resistance decreases by increasing the power as it leads to more oscillations.
Kun Xie et al. [36]	Chrome coated al tubing	Water	6 turns, 2 mm	20-200	1- The thermal resistance decreases as the power increase. 2- Increasing the cooling water temperature decrease the temperature difference between the evaporator and condenser sections and enhances the thermal performance. 3- The thermal performance of the coated tubing is consistence with the operation for several days while the performance of the uncoated one deteriorates due to the reaction between water and al.

2.4 Heat spreader

In many applications, such as in power electronics, the heat generation is not uniform and results in local hot spots that can significantly affect the performance of such devices. Eliminating these hot spots is a significant challenge since these can lead to failure. Usually solid copper or aluminum plates are used as a heat spreader to reduce the hot spots. For high heat flux applications, other solutions have been developed such as embedding heat pipes within the heat spreader as shown in Figure 2-2.

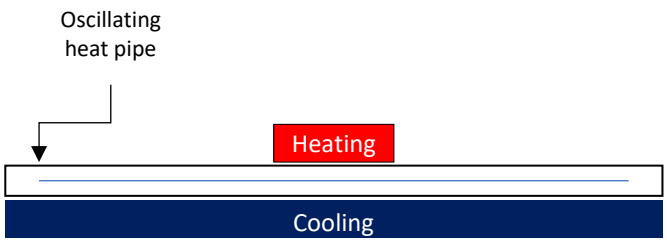

Figure 2-2 Heat spreader configuration

Mansouri et al. [65] conducted a study to compare the thermal performance of a heat spreader with and without embedded heat pipes. There was a significant enhancement using the heat spreader with embedded heat pipes, with the average wall temperature of the heating block reduced by about 25 percent compared to the heat spreader without the heat pipes.

There are several studies on using oscillating heat pipes to eliminate hot spots and to be used as a heat spreader but most of them were tested for heating power less than 250 W. Lu et al. [66] compared the performance of a copper heat spreader with one embedded with an oscillating heat pipe for heating power in the range of 50-500 W. The maximum temperature was reduced when using the heat spreader with the embedded oscillating heat pipe. Lin et al. [23] tested a heat spreader with a 10 turn oscillating heat pipe. The results showed that the heat spreader with the embedded oscillating heat pipe performed thermally better than the basic heat spreader. Hemadri et al. [67] compared heat spreaders made with different materials. Embedding an oscillating heat pipe on an aluminum heat spreader had

no significant enhancement but showed a significant improvement in the thermal performance with a mild steel heat spreader.

Table 2-2 presents the pertinent literature on using oscillating heat pipes as a heat spreader.

Table 2-2 Previous studies done on oscillating heat pipe performance as a heat spreader.

Investigator	*Working fluid*	*No. Of turns*	*Heat load (w)*	*Key findings*
Lin et al. [23]	Acetone	10	40-120	1- The heat spreader with embedded OHP performs thermally better than the basic heat spreader 2- It shows better results than the one with embedded conventional heat pipe below 80 W otherwise the conventional heat pipe performs better
Thompson et al. [68]	Acetone	NA 3D Double-layer	10-240	1- The oscillating heat pipe can operate with middle heating (as a heat spreader) 2- The thermal performance was enhanced by about 10-15% compared to the copper slab.
Khandekar et al.[69]	water	11	120-250	1- The heat spreader with embedded oscillating heat pipe does not make that significant change in the performance.
Lu et al. [66]	Acetone	40	25-500	1- Compared to copper heat spreader, the heat spreader with the embedded oscillating heat pipe shows reduction in the max. system temperature. 2- Increasing the cooling water flow rate delaying the start-up but at the same time enhance the overall thermal performance.
Thompson et al. [70]	water	Quad-layer (additive manufactured)	5-50	1- A significant enhancement of the thermal performance of about 500% compared to empty one. 2- Below 20 W, the horizontal orientation shows no oscillating. 3- At higher power, the vertical and horizontal almost show the same performance
Hemadri et al. [67]	Water Ethanol	11	50-150	1- No significant enhancement when comparing between al plate and al plate with embedded oscillating heat pipe due to the high thermal conductivity of the aluminum 2- For the mild steel, the performance enhanced significantly.

3 Experimental facility

An Oscillating Heat Pipe (OHP) was designed and manufactured to characterize its thermo-hydraulic performance and validate the design methodology that was developed for the oscillating heat pipe. An experimental test facility was designed and built to: (i) characterize the Oscillating Heat Pipe performance and (ii) investigate the effectiveness of using the Oscillating Heat Pipe as a heat spreader to reduce hot spots. The experimental facility included instrumentation to measure temperature, pressure, power, and flow rate to characterize the Oscillating Heat Pipe performance. This chapter presents the Oscillating Heat Pipe design methodology and the manufacture of the Oscillating Heat Pipe. It then provides details of the experimental facility and methodology and the data reduction techniques.

3.1 Design of Oscillating Heat Pipe

The objective here was to design an oscillating heat pipe that fits within a footprint of 170 x 100 mm^2 that could be embedded on a heat spreader of 18 mm thickness and capable of dissipating 500 Watts. The evaporator length for the heat spreader application was 40 mm, and the condenser occupies the entire surface. The design temperature of the evaporator section was not to exceed 100°C. The working fluid in this design was selected as water as it is a good candidate for high heat loads up to 8 kW [71] because of its high

latent heat[26], [29]. The hydraulic diameter determined from the Bond number to fall between 0.7 to 2 as proposed by Qu et al [5] was 2 mm.

The minimum number of channels required was obtained from equation (3-1). The internal heat transfer coefficients for the evaporator and condenser sections were assumed to be the same as those in Karthikeyan et al. [64] for a single layer oscillating heat pipe with the same working fluid, hydraulic diameter and heat load. The internal fluid temperature and wall temperature measurements in addition to the thermal resistance calculated were used to obtain the heat transfer coefficients. A relation between the number of turns and the temperature difference between the hot and cold sides is derived based on heat transfer principles as shown in equation (3-1). For the current design constraints, setting the condenser length to be quadruple the length of the 40mm evaporator length, the relation between the temperature difference and number of turns for a heat load of 500 W is shown in Figure 1. From this figure, it is seen that to maintain a temperature difference smaller than 80°C, the number of turns must be greater than 20.

$$\boldsymbol{\Delta T} = Q\left[\frac{1}{h_e(\pi D \boldsymbol{n} l_e)} + \frac{1}{h_c(\pi D \boldsymbol{n} l_c)}\right] \qquad 3\text{-}1$$

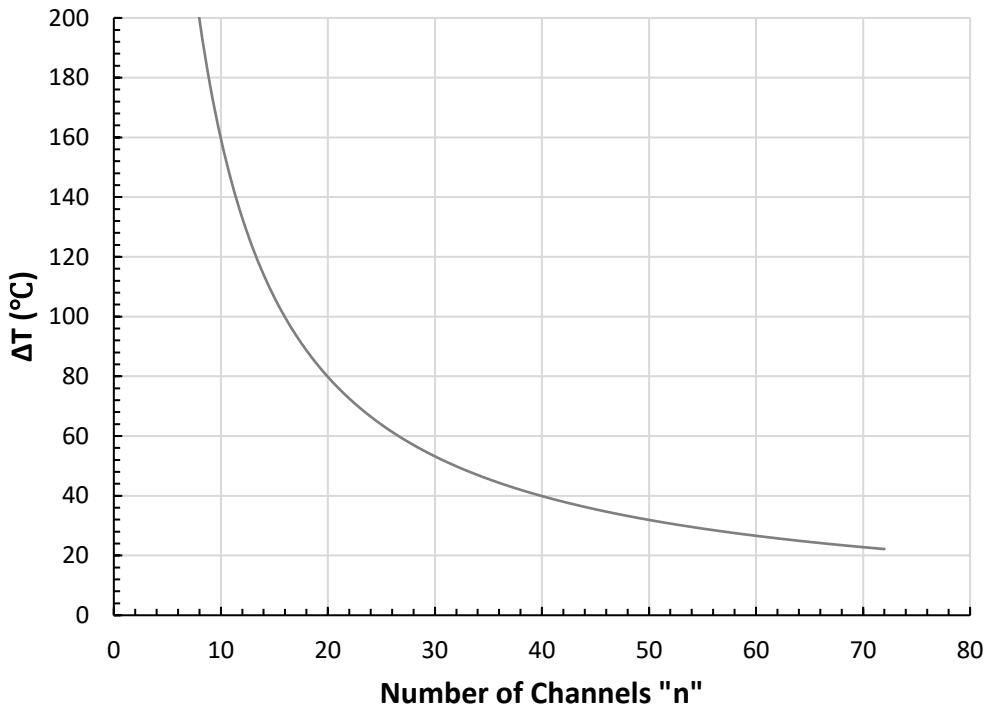

Figure 3-1 Temperature difference with the required number of channels at 500 W.

For the application under consideration, the oscillating heat pipe would need to operate in the horizontal orientation. A stacked oscillating heat pipe was found to reduce the effect of inclination on its performance as outlined in the literature review. Thus, in this instance a stacked oscillating heat pipe was chosen. This configuration also allows for a greater number of channels for the same area when compared to a single layer oscillating heat pipe. Machining 2 mm channels spaced by 2 mm results in 11-turn (23 channels) for each layer in the allowable surface area. The thickness limitation of 18 mm allows for two layers of channels. There are several designs in the literature to connect the two layers. The most common are the two designs introduced by Thompson et al [72],[40]. The first has

the channels of the two layers in parallel, while in the second it has the channels staggered. To have a high-density of channels, the parallel design is chosen for this study. The machining option has one more advantage as the cross-section of the channels are square and it was found that a square cross-section shows better performance than a circular cross section [7], [10].

There are several studies to determine the best charge ratio, which varies with the working fluid and operating conditions as outlined in the literature review. Khandekar et al. [33] determined that the sensitivity of the charge ratio to the performance is not significant within the range of 35% to 70% for water as a working fluid. In our design a 70 percent charge ratio was selected. The final design parameters for our oscillating heat pipe are summarized in Table 3-1.

Table 3-1 Design parameters for the oscillating heat pipe.

Term	***Value***
Evaporator length	40 mm
Inner diameter	2 mm
Filling ratio	70%
Working fluid	Degassed DI Water
Number of turns	23 turns (46 channels)
Number of layers	Two layers
Channel cross section	Square

3.2 Fabrication of Oscillating Heat Pipe

Two option were considered for the fabrication of the Oscillating Heat Pipe: (i) copper tubing for the channels and (ii) directly machining the channels on an aluminum or copper plate. The first option was not feasible since maintaining the recommended bending radius (6mm in this instance for an outer tube diameter of 3mm) would result in a very limited number of turns over the Oscillating Heat Pipe footprint of 175mm x 100mm. This would require a multi-stacked Oscillating Heat Pipe to achieve the required number of turns, which would not be possible to fit within the 18 mm thickness of the heat spreader.

$$R = 2 * D_o \qquad 3\text{-}2$$

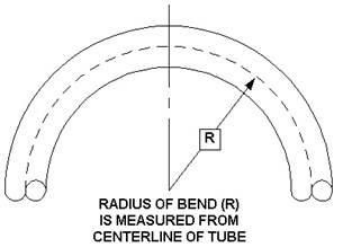

Figure 3-2 Bending radius of a copper tube.

As such, the Oscillating Heat Pipe was fabricated by machining 2 mm channels at a spacing of 2 mm and a length of 153 mm to obtain 11 turns (23 channels) over the 175mm x 100mm area as shown in Figure 3-3. To meet the required number of turns, a stacked configuration of two layers was chosen by machining the channels on both surfaces of the plate that resulted in 23 turns. The channels are aligned parallel and interconnected by drilling a 2 mm hole on each channel to connect it to the corresponding channel on the other side as

illustrated in Figure 3-4A. This connection is made to create a complete closed loop and to allow the working fluid to traverse between the two sides. On each end, six holes with 10-32 UNF thread are drilled. The first hole in each end is for the filling and vacuuming and the rest of the holes are for internal measurements. Each hole is connected to the channels through a smaller hole of 2 mm.

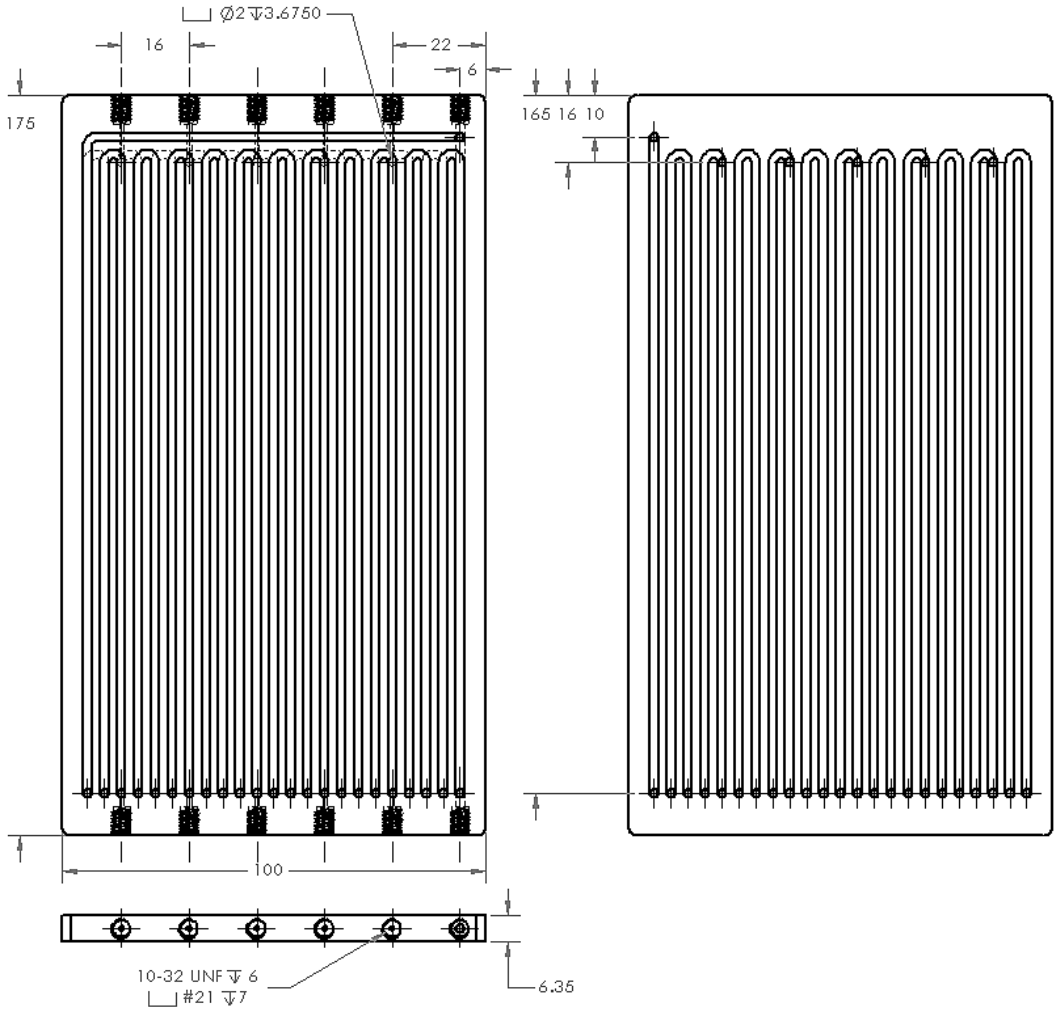

Figure 3-3 Engineering drawing of Oscillating Heat Pipe

The second stage of the manufacturing process is to braze cover plates on the machined plate to fully seal the oscillating heat pipe. Here, 2 mm plates were brazed on each side as shown in Figure 3-4B, to achieve a total thickness of 10.35 mm and keep it below the allowable thickness for the heat spreader.

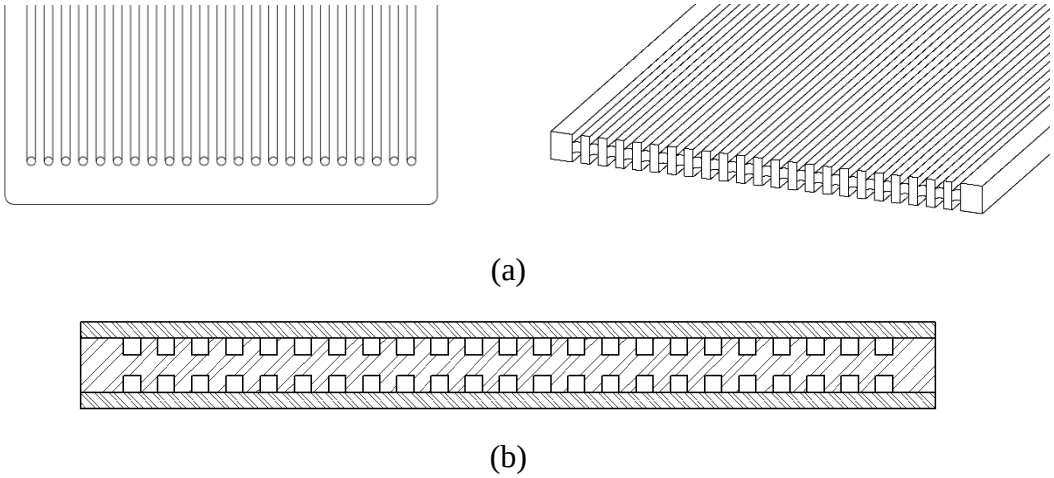

(a)

(b)

Figure 3-4 (a) 2 mm connecting holes between the two layers, (b) cross-sectional view of Oscillating Heat Pipe with the brazed plates.

Prototype oscillating heat pipes were manufactured in-house using both an aluminum and copper plate. The machining of the channels on the aluminum plate using a CNC mill (Figure 3-5) was successful; however, the brazing of the aluminum sheets proved challenging. Aluminum brazing needs to be done in a vacuum or inert gas oven, which was not available in-house. Several attempts were made to braze using alternate techniques which proved unsuccessful. Copper was considered as the cover plates could be soldered onto the machined plate instead of brazing. The machining of the channels on the copper plate was more problematic and the surface finish was not as good as on the aluminum plate (Figure 3-6). The machined channels were sand blasted to achieve the desired surface

finish. Copper tubes were soldered to the openings for the internal measurements and the other end to Swagelok fittings as shown in Figure 3-6. The soldering was found to be not sufficiently good to maintain a vacuum, and threaded holes were made directly on the machined plate for direct connection.

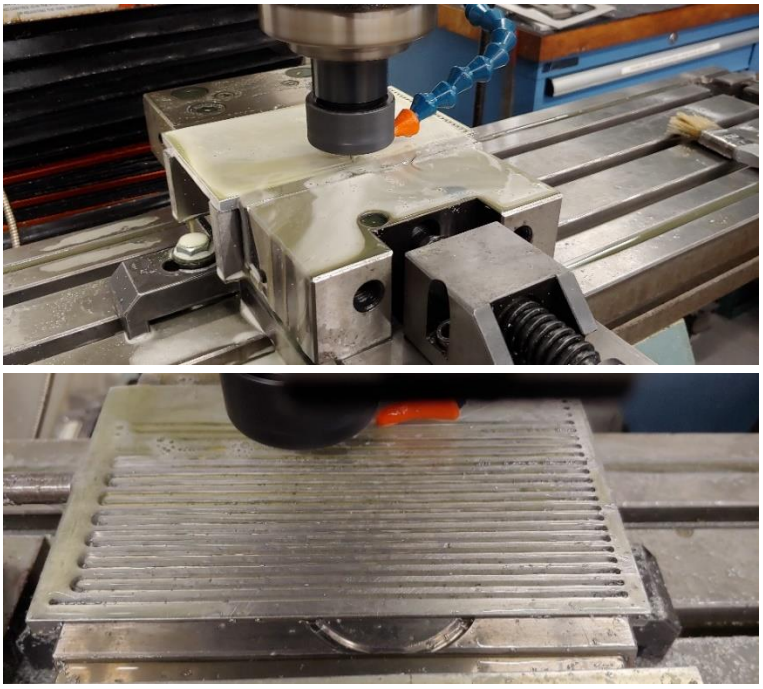

Figure 3-5 Aluminum plate CNC machining process.

Figure 3-6 The soldered copper Oscillating Heat Pipe with the Swagelok fittings.

Finally, a third prototype was manufactured by MERSEN France. MERSEN France has excellent aluminum brazing facilities, in addition to experience in machining such devices. A full detailed shop drawing was sent to MERSEN France with the necessary instructions and the protypes fabricated by MERSEN France was found to withstand a vacuum well and was used for this testing.

3.3 Experimental Facility

The oscillating heat pipe was tested in the test facility shown schematically in Figure 3-8. Two heating and cooling configurations were used to: (i) study the thermo-hydrodynamics performance of the Oscillating Heat Pipe for axial heat transfer and (ii) study the performance of the Oscillating Heat Pipe as a heat spreader. The heating unit in both was a heater block with two 300 W-240 V heating cartridges. It was machined in-house from aluminum with dimensions of 100 mm x 40 mm x 8 mm as shown in Figure 3-7. Two holes with 6.35 mm diameter were drilled for the heater cartridges. The holes were machined first with a one size smaller drill bit and then a 6.35 mm straight flute reamer to

achieve an accurate size with a good surface finish. TECHSPRAY® thermal compound was applied on each heat cartridge to minimize the contact resistance before placing them in the holes on the heater plate. The cooling units are a series of off-the shelf cold plates of 100mm x 40mm x 12mm as shown in Figure 3-7. They are made of aluminum and have two U-tube channels. A single plate was used for the thermo-hydraulic system while four were used in series for the heat spreader facility (Figure 3-7).

The two test facilities have the same components and equipment, but they have different cooling and heating configurations. The first test facility has heating on one end using two heating blocks, one on each side, and has cooling on the other end also using two cold plates, one on each side as shown in Figure 3-8A. The second configuration has cooling all over the back side using four cold plates and one heater block on the front side as shown on Figure 3-8B. All the heater blocks and cold plates are attached firmly to the Oscillating Heat Pipe using in-house metal clamps. TECHSPRAY® thermal compound is applied between the contact surfaces to minimize the contact resistance.

The heater cartridges are connected to a VARIAC® variable transformer to control the input heating power, and a power transducer is used to measure the power input. The power transducer was calibrated using a high accuracy multimeter (Equation 3-3). The calibration data and the resulting calibration curve

$$Power(Watts) = 198.441 \times V(volt) - 0.627 \qquad 3\text{-}3$$

is shown in Figure 3-9A. The cooling water was provided by a water chiller for cooling water temperatures below 30℃ and a thermal bath for water temperatures 30℃ to 50℃. A turbine flow meter is connected to the outlet port of both the water chiller and thermal bath to measure the flow rate of the cooling water. The turbine flow meter sensor was calibrated using a high accuracy Proline® Promass 80E Coriolis flowmeter. The calibration data with the resulting calibration curve given by

$$\dot{V}(LPM) = 6.285 \times V(volt) + 0.098 \qquad 3\text{-}4$$

is shown in Figure 3-9B. The cold plates are connected to have one water inlet and one water outlet, and each port is instrumented with a 0.5 mm thermocouple to measure the inlet and outlet water temperatures.

The surface temperature at different locations of the oscillating heat pipe and the water inlet and outlet temperatures were measured with 0.5 mm grounded Omega® T-type thermocouples. For the surface temperature measurements, 1 mm wide and 0.5 mm deep grooves were machined on both surfaces of the oscillating heat pipe as shown in Figure 3-10. The lengthwise grooves correspond to the internal channel locations. The thermocouples were placed along these grooves, so they did not interfere with the contact between the heater block and cold plates with the oscillating heat pipe body. The first configuration shown in Figure 3-8A has a total of six thermocouples for the evaporator section (three for each heater block) and a total of six thermocouples for the condenser section (three for each cold plate). Two thermocouples were also placed on the adiabatic section, one on each side. The second configuration has a total of twelve thermocouples for

the cooling side. These are placed along four rows, with three thermocouples in each row. Five thermocouples were placed on the heating side underneath the heater block. The thermocouples were calibrated against an RTD temperature sensor using a thermal water bath for temperature range from 5℃ to 90℃ and for higher temperature ranges up to 150℃ in an oil bath. The temperature calibration equations for each thermocouple are directly entered to the recording software.

The internal pressure is measured using a Validyne® diaphragm pressure transducer connected to the middle hole on the heating end. It was connected through the 10-32 thread through a 10-32 to 1/8" male to female adapter. A gas thread seal tape was applied on all threads with vacuum grease to prevent any leakage. The pressure transducer is calibrated for vacuum pressure readings using and AMETEK® is33 pressure calibrator The pressure calibration equation

$$P(kPa) = 12.307 \times V(volt) + 0.6183 \qquad 3\text{-}5$$

and the calibration graph is shown in Figure 3-9C.

The measured saturation pressure data is used to calculate the saturation temperature. The pressure transducer measures the gauge pressure and the absolute pressure is needed for the saturation temperature calculations. The data recorded for the hourly atmospheric pressure and temperature at Hamilton airport, Canada [73] are used to calculate the absolute pressure and the elevation difference Z between our lab location and Hamilton airport is taken into consideration through equation (3-6).

$$P_{meas,abs} = slp \times (V_{meas} - V_0) + (P_{atm} - \gamma_{air} \times Z) \quad 3\text{-}6$$

where γ_{air} is the air specific gravity and is calculated using EES® with Hamilton airport, Canada data, slp is the calibration slope and V_0 is voltage at zero-gauge pressure before the charging process of each test.

The thermocouple data is collected through Measuring Computing® temperature data acquisition board and recorded using their own software at a sampling rate of 3 Hz. A second data acquisition board (NI USB- 4431) is used to record and collect the voltage data of the flow meter, pressure transducer and power transducer at sampling rate of 1000 Hz. A LabView® code was used to record and monitor the data and the data was down sampled using LabView® to match the temperature sampling rate.

A gas thread seal tape was applied on all fittings and valves thread and a vacuum grease is applied on the tape to avoid any leaks. A fiber glass insulation is used to insulate the test rig to ensure a good energy balance and minimize heat loss.

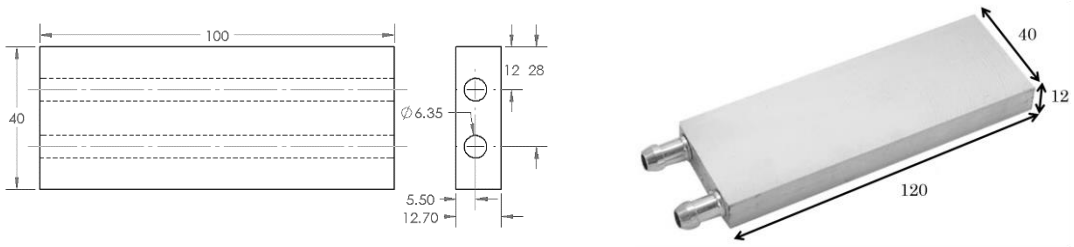

(a) (b)

Figure 3-7 Dimensions of (a) Heater block and (b) cold plate dimensions.

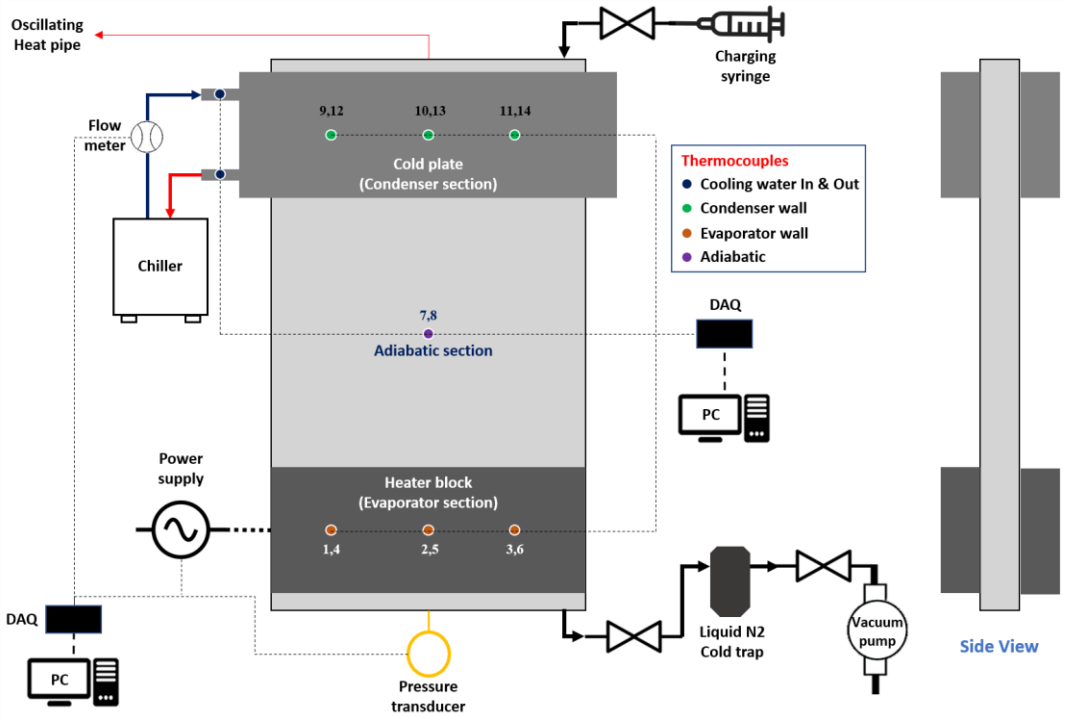

(a)

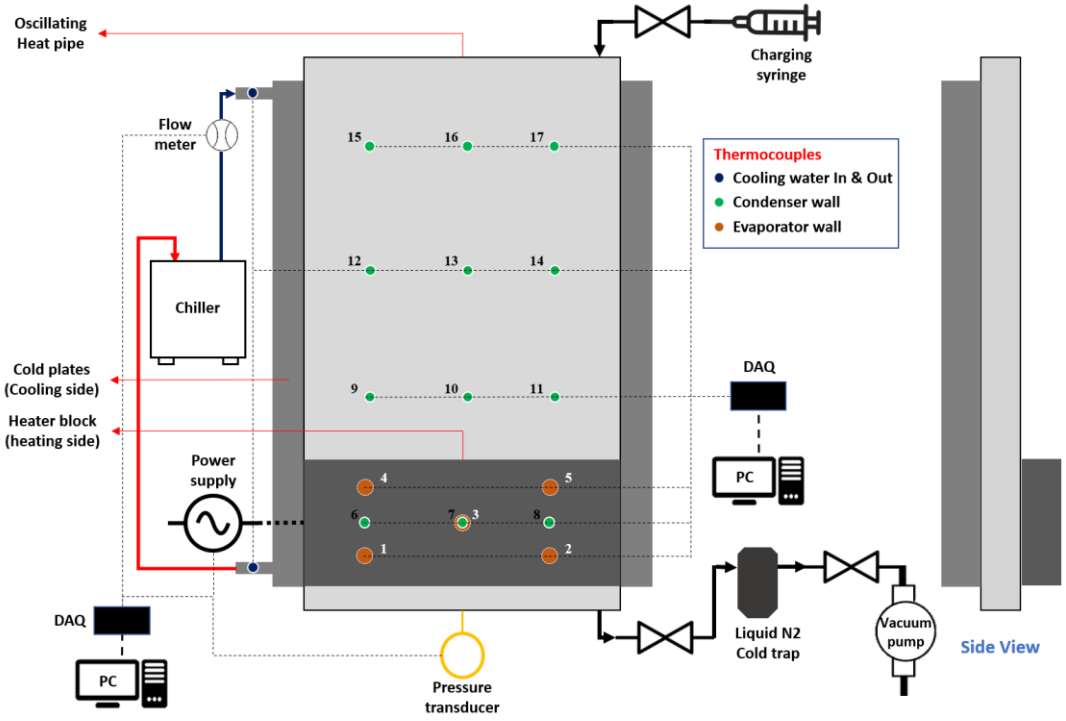

(b)

Figure 3-8 Schematic drawing of the test setup for **(a)** thermo-hydrodynamic performance and **(b)** performance as a heat spreader.

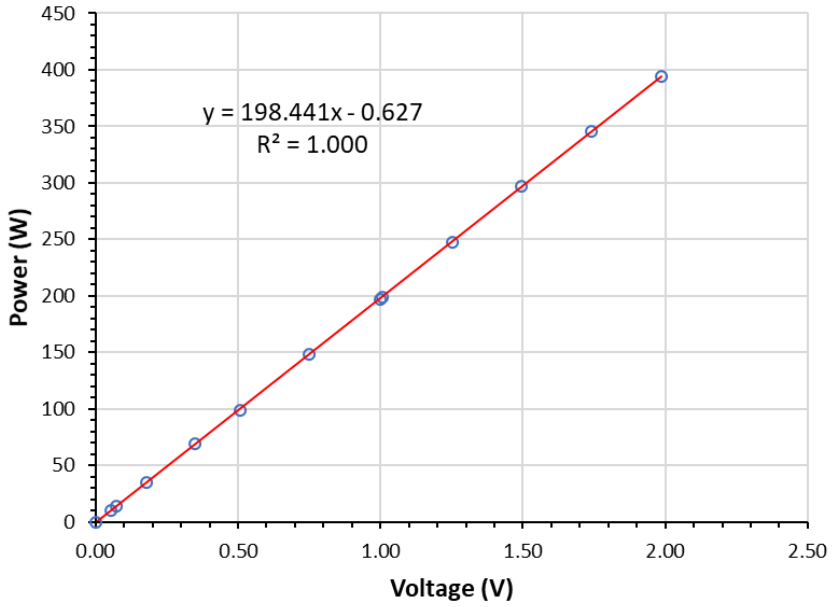
y = 198.441x - 0.627
R² = 1.000
Power (W)
Voltage (V)
0
50
100
150
200
250
300
350
400
450
0.00
0.50
1.00
1.50
2.00
2.50

(a)

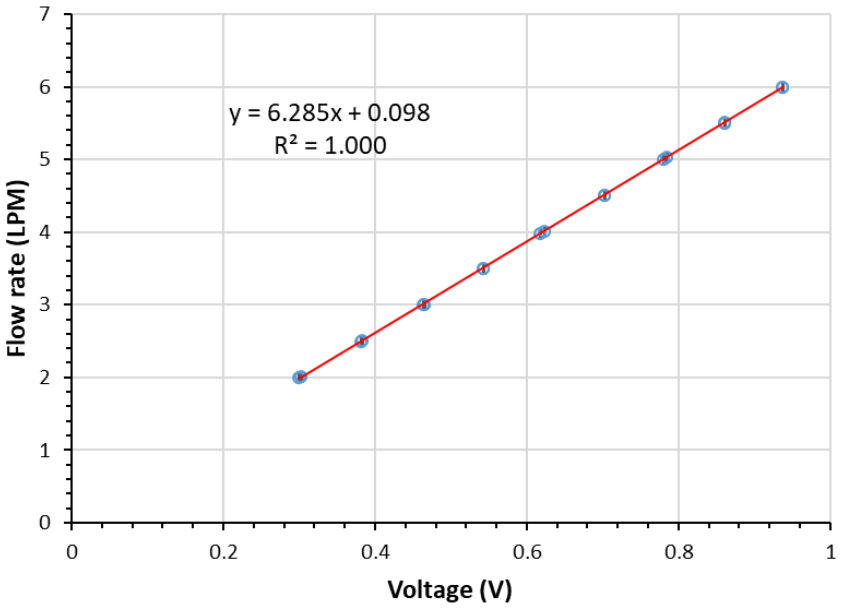
y = 6.285x + 0.098
R² = 1.000
Flow rate (LPM)
Voltage (V)
0
1
2
3
4
5
6
7
0
0.2
0.4
0.6
0.8
1

(b)

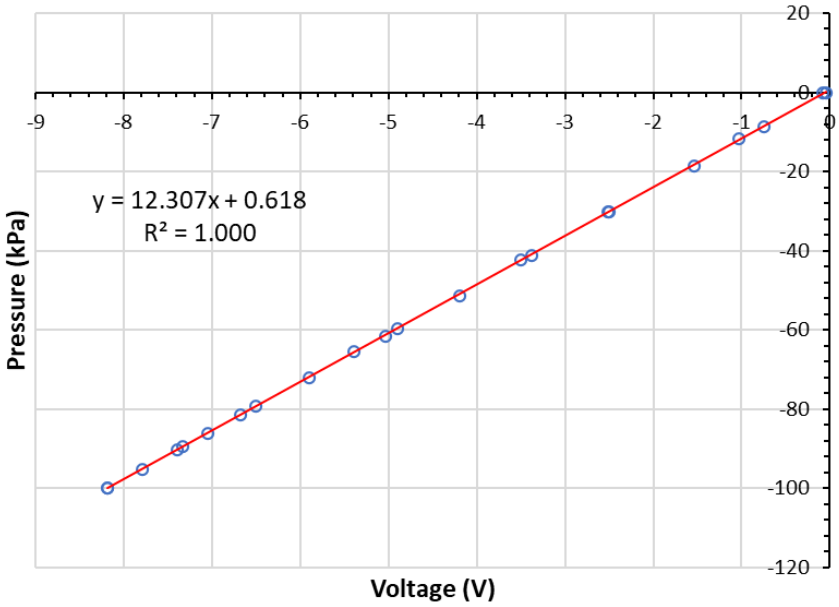

(c)

Figure 3-9 Sensors calibration data, (a) Power transducer, (b) Flow meter sensor, and (c) Pressure transducer.

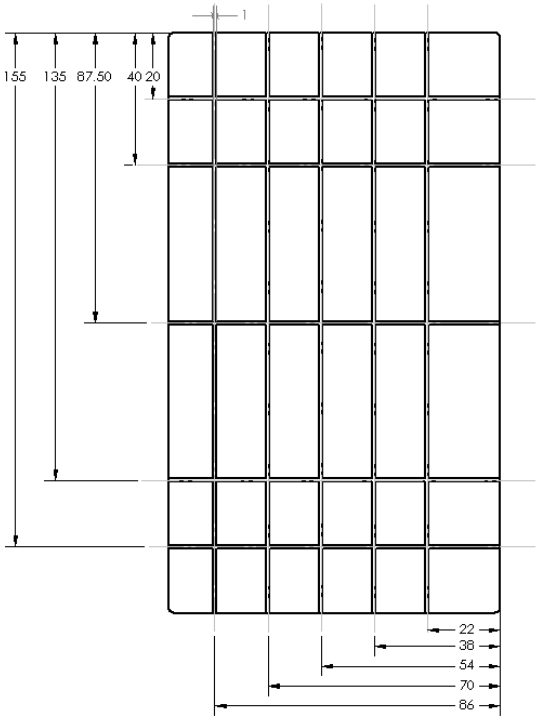

Figure 3-10 Groove geometry on surface of oscillating heat pipe for placement of thermocouples.

3.4 Charging of Oscillating Heat Pipe.

The oscillating heat pipe was vacuumed and charged with water using the two charging ports on opposite ends. A PFEIFFER® Pascal 2015 I vacuum pump is used to vacuum the air out of the oscillating heat pipe. It is a two-stage rotary vane pump with minimum pressure of $5x10^{-5}$ kPa. The pump is connected to the bottom end through fittings with a ball valve and a liquid nitrogen cold trap is connected midway to prevent any water vapor entering the pump as shown in Figure 3-8. The charging is done using a 30 ml syringe with a Luer lock fitting connected through an adapter with a ball valve to the top first hole. Distilled water is used, and it is degassed first by boiling for about three hours. The vacuuming and charging process followed the procedure given below:

1- Remove all water from the channels (in case it has been used before) by passing pressurized air through the channels for at least 30 minutes.
2- Heat the entire oscillating heat pipe to 30°C.
3- Use the vacuum pump to vacuum the oscillating heat pipe.
4- Remove any gases trapped inside the charging valve by connecting the fitting shown in Figure 3-11 while vacuuming and then open and close the valve a few times. Thereafter, leave it open for about five minutes and then finally close the valve and detach the fitting.
5- Use the syringe with a thin needle filled with degassed water to fill the charging valve to minimize the gases in the system.
6- Attach the syringe and open the charging valve to inject 3 ml of water to purge all the gases in the passage between the syringe and the internal channels.
7- Turn off the vacuum pump for 30 mins then turn it on again and continue vacuuming to suck all the fluid within the oscillating heat pipe for one hour.
8- Close the vacuuming valve and open the charging valve to inject the desired amount of working fluid corresponding to the desired charging ratio.

Once the charging process as described above is completed, the oscillating heat pipe is ready for testing.

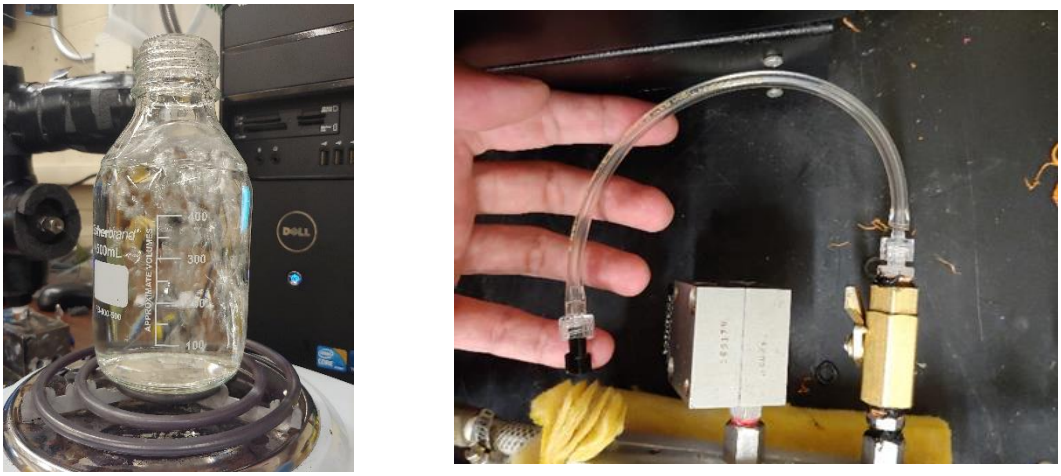

Figure 3-11 Degassing process by boiling on the left and the fitting to remove trapped air in the charging valve on the right.

3.5 Modelling Effect of Non-Condensable Gases

The presence of non-condensable gases will affect the calculation of the saturation temperature from the measured pressure. Thus, the saturation pressure is computed by subtracting the partial pressure of any non-condensable gas from the measured pressure. The mass of any non-condensable gas in the oscillating heat pipe was estimated for the measurement at the start of the test before heat was applied. The non-condensable gas is assumed to be fully mixed with the working fluid vapor so that the volume of the non-condensable gas is assumed to be the volume of the device not filled with liquid working fluid or $(100 - \phi)$ where ϕ is the filling ratio by neglecting the mass of the working fluid vapour

Firstly, the device is brought to thermal equilibrium by using the cold plates and the heater block. Using the average temperature at this initial condition where $T_{meas} = T_{NCG}$ is assumed and assuming ideal gas behavior, the mass of the NCG is estimated by assuming a partial pressure P_1 initial value of 0.1 kPa.

$$m_{NCG} = \frac{(P_1 \times T_{meas})}{(Vol_{NCG} \times R)} \quad 3\text{-}7$$

The saturation pressure P_{sat} is calculated by subtracting the P_1 from P_{meas} the measured pressure, equation (3-7),

$$P_{sat} = P_{meas} - P_1 \quad 3\text{-}8$$

The T_{sat1} is obtained using EES® software,

$$T_{sat1} = f\ P_{sat} \quad 3\text{-}9$$

and the non condensable gases pressure P_{NCG} is obtained as

$$P_{NCG} = \frac{m_{NCG} \times R \times T_{NCG}}{Vol_{NCG}} \quad 3\text{-}10$$

This is iterated by substituting the new value of P_{NCG} for the initial P_1 in equation (3-6) till an error less than 10^{-3} is obtained, where

$$T_{NCG} = T_{sat1} \quad 3\text{-}11$$

and $\not{R}$ is air gas constant,

$$\not{R} = 0.287\ \left(\frac{KJ}{Kg.K}\right) \quad 3\text{-}12$$

and Vol_{NCG} as mention before is the volume occupied by the NCG inside the channels which is assumed to be a percentage of the total channels volume Vol_{total}.

$$Vol_{NCG} = (1 - \phi) \times Vol_{total} \quad 3\text{-}13$$

The final equation used for the pressure incorporating all the corrections is equation (3-14)

$$P_{sat} = P_{meas,abs} - P_{NCG} = [Slp \times (V_{meas} - V_0) + (P_{atm} - \gamma_{air} \times Z)] - P_{NCG} \quad 3\text{-}14$$

3.6 Data Analysis

Averaged quantities are computed over a time interval of 1000 sec and 600 sec for the first test rig and second test rig, respectively. An energy balance between the power input and the heat removed by the cooling water was performed to qualify the test set-up and ensure there are no large losses to the ambient. First the inlet and outlet temperatures and the flow rate of the cooling water are averaged over the specified time interval (equation 3-15 to 3-17)

$$\bar{T}_{in} = \frac{\sum T_{in}}{z} \quad 3\text{-}15$$

$$\bar{T}_{out} = \frac{\sum T_{out}}{z} \quad 3\text{-}16$$

$$\dot{\bar{V}}_{avg} = \frac{\sum \dot{V}}{z} \quad 3\text{-}17$$

The output power is calculated using equation 3-18 where ρ_{water} is the density of water at ambient conditions and C_{water} is the water heat capacity at ambient conditions

$$\overline{Power}_{out} = \dot{\bar{V}}_{avg} \times \rho_{water} \times C_{water} \times (\bar{T}_{out} - \bar{T}_{in}) \quad 3\text{-}18$$

while the input power is obtained from the power transducer as

$$\overline{Power}_{in} = \frac{\sum Power_{in}}{z} \quad 3\text{-}19$$

A representative energy balance for the case with cooling water at 30°C is shown in Figure 3-12. Typically, the energy balance was within ±10 percent for all cases.

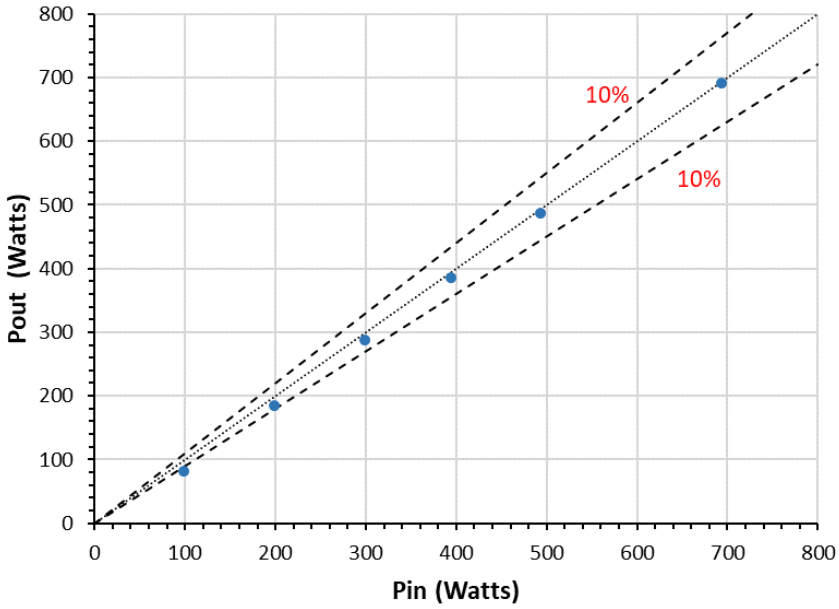

Figure 3-12 Energy balance example for 30C vertical case.

The thermal resistance for the different sections, heat transfer coefficients and total thermal resistance were computed as follows. The first test rig has three sections: evaporator, adiabatic and condenser as shown in Figure 3-8A. The averaged wall temperature of each section is calculated from the thermocouples designated for each section. The saturation temperature is computed from the measured saturation pressure using the following correlation [74],

$$T_{sat} = 39.31 + \left(\frac{3991.11}{18.5916 - \ln \frac{15 \times P_{sat}}{2}} \right) \qquad 3\text{-}20$$

and then the average saturation temperature over the time interval is calculated as

$$\bar{T}_{sat} = \frac{\sum_1^z (T_{sat})}{z} \quad 3\text{-}21$$

The temperature difference of each section relative to the saturation temperature is used to calculate the thermal resistance

$$\Delta T_e = \bar{T}_{evap} - \bar{T}_{sat} \quad 3\text{-}22$$

$$\Delta T_c = \bar{T}_{sat} - \bar{T}_c \quad 3\text{-}23$$

$$\Delta T_t = \bar{T}_e - \bar{T}_c \quad 3\text{-}24$$

The average thermal resistance of the evaporator and condenser in addition to the total average thermal resistance is calculated as

$$\bar{R}_e = \frac{\overline{\Delta T}_e}{\overline{Power}_{in}} \quad 3\text{-}25$$

$$\bar{R}_c = \frac{\overline{\Delta T}_c}{\overline{Power}_{in}} \quad 3\text{-}26$$

$$\bar{R}_t = \frac{\overline{\Delta T}_t}{\overline{Power}_{in}} \quad 3\text{-}27$$

The heat transfer coefficients for each section are based on the lateral area of the channels in each section. In this test rig the condenser area is the same as the evaporator area

$$A_{evap} = Circ \times L_e \times n_e \quad 3\text{-}28$$

$$A_{cond} = Circ \times L_c \times n_c \quad 3\text{-}29$$

where $Circ$ is the circumference of the channel

$$Circ = 4 \times D \tag{3-30}$$

where D_h is the hydraulic diameter, L_e and L_c are the evaporator and condenser lengths respectively, and the n_e and n_c are the number of channels exposed to the heating and cooling, respectively. The heat transfer coefficients for each section are calculated as

$$\bar{h}_e = \frac{1}{A_e \times \bar{R}_e} \tag{3-31}$$

$$\bar{h}_c = \frac{1}{A_c \times \bar{R}_c} \tag{3-32}$$

The same procedure is used for the second test rig except that the second one has different cooling and heating locations and areas and does not have an adiabatic section which leads to changes in the area calculated for each section in addition to having more thermocouples for each section as shown in figure 3-8B.

3.7 Uncertainty analysis

The temperature is the main measured quantity on which the performance is based. The thermocouples are calibrated against an RTD sensor accurate to ±0.01℃. The saturation temperature is calculated using the measured saturation pressure. The Validyne® pressure transducer is calibrated against Ametek® pressure calibrator with an uncertainty of ±0.25% of the pressure reading for vacuum. The input power is measured using a power

transducer that has been calibrated against a multimeter with current accuracy of ±0.7% of the current reading and voltage accuracy of ±0.4% of the voltage reading.

Most of the properties that determine the performance in this study are not directly measured but calculated from another measured properties. The error of each measured property is considered using the root-sum-square method according to Moffat [75] to get the propagated uncertainty

$$\varepsilon_P = \pm \sqrt{\sum_{i=1}^{N} \left(\frac{\partial R}{\partial x_i} \, \varepsilon_{x_i} \right)^2} \qquad 3\text{-}33$$

According to this method the propagated uncertainty of the different calculated properties is summarized in Table 3-2.

Table 3-2 The propagate uncertainty.

PROPERTY	LOW POWER		HIGH POWER	
	Value	***Uncertainty***	***Value***	***Uncertainty***
Saturation temp	49℃	±0.59℃	82.4℃	±0.16℃
Thermal resistance	0.197℃/W	±0.002℃/W	0.0522℃/W	±0.0004℃/W
Heat transfer coeff.	2682 W/m^2℃	±152.15 W/m^2℃	6659 W/m^2℃	±191.82 W/m^2℃

The calculations of uncertainty of the heat transfer coefficient is presented as an example to show how the propagated uncertainty is calculated. These calculations are at high heating power

$$h = \frac{Q}{A \times (T_e - T_{sat})} \qquad 3\text{-}34$$

where the values and the uncertainty of each parameter are as following,

$$\begin{aligned} Q &= 694.8\ W & \varepsilon_Q &= \pm 5.6\ W \\ T_e &= 89.5℃ & \varepsilon_{T_e} &= \pm 0.1℃ \\ T_{sat} &= 82.4℃ & \varepsilon_{T_{sat}} &= \pm 0.16℃ \end{aligned} \qquad 3\text{-}35$$

Using equation 3-33,

$$\varepsilon_h = \pm \sqrt{\left(\frac{-\varepsilon_{T_e} \times Q}{A(T_e - T_{sat})^2}\right)^2 + \left(\frac{\varepsilon_{T_{sat}} \times Q}{A(T_e - T_{sat})^2}\right)^2 + \left(\frac{\varepsilon_Q}{A(T_e - T_{sat})}\right)^2} \qquad 3\text{-}36$$

$$\varepsilon_h = \pm 191.82\ W/m^2K$$

therefore, the heat transfer coefficient at these conditions is,

$$h = 6659 \pm 191.82\ W/m^2K \qquad 3\text{-}37$$

4 Results and Discussion

This chapter presents and discusses the results for the thermo-hydraulic performance of the oscillating heat pipe for axial heat transfer and its performance as a heat spreader. In the first section, the effect of orientation (vertical and horizontal) and the cooling water temperature for the horizontal orientation on the thermo-hydrodynamic performance are presented for axial heat transfer. In the second section, the performance of the oscillating heat pipe for a heat spreader application for different orientations, heating locations and cooling water temperatures are presented.

Section 1: Axial heat transfer – Thermal Hydraulic Performance.

The thermal hydraulic performance of the oscillating heat pipe was characterized with the stacked oscillating heat pipe in both the horizontal and vertical orientations. The horizontal orientation was tested at three cooling water temperatures of 10°C, 30°C and 50°C and the vertical orientation at cooling water temperature of 30°C. For each case, the input power was incremented in steps of 100 W, from 100W to 700 W. Table 4-1 summarize the test matrix.

Table 4-1 Axial heat transfer - thermal hydraulic performance test matrix.

	Horizontal	Vertical
10ºC	✓	
30ºC	✓	✓
50ºC	✓	

4.1 Effect of Orientation on Thermal Hydraulic Performance.

A comparison of the transients of the temperatures on the oscillating heat pipe in the vertical and horizontal orientations for a cooling water temperature of 30℃ are shown in Figure 4-1. In the vertical orientation, the temperature traces (Figure 4-1A), including the saturation temperature, show evidence of fluctuations at 100 W suggesting that the heat pipe is active with oscillations at this heat input. The fluctuations, however, vary in magnitude with time suggesting that the operation is intermittent. The results at 200 W show evidence of some variation in the fluctuations over the experimental time though not as large as at 100 W. The temperature fluctuations for 300 W and higher are more consistent with a small increase in the amplitude which suggests a full activation of the oscillating heat pipe. As the heating power increases the temperatures of each section increase and the results do not show evidence of dry-out at 700 W which would be reflected in a dramatic increase in the evaporator temperature.

The results for the oscillating heat pipe in the horizontal orientation (Figure 4-1B) show much larger variations at 100 W. The results suggest that there is intermittent start of oscillations as seen in the large fluctuations, but in the absence of the gravitational force the oscillations are not sustained. At 200 W the fluctuations are more regular but not fully consistent as for the higher power in the vertical case. The fluctuations are consistent at heat inputs greater than 300 W as in the vertical case, but with an increase in amplitude as the power increases suggesting that the oscillation is active. The temperature of each section increases with the heat load, as observed with vertical case, but the results do not show any signs of dry-out at high heating power.

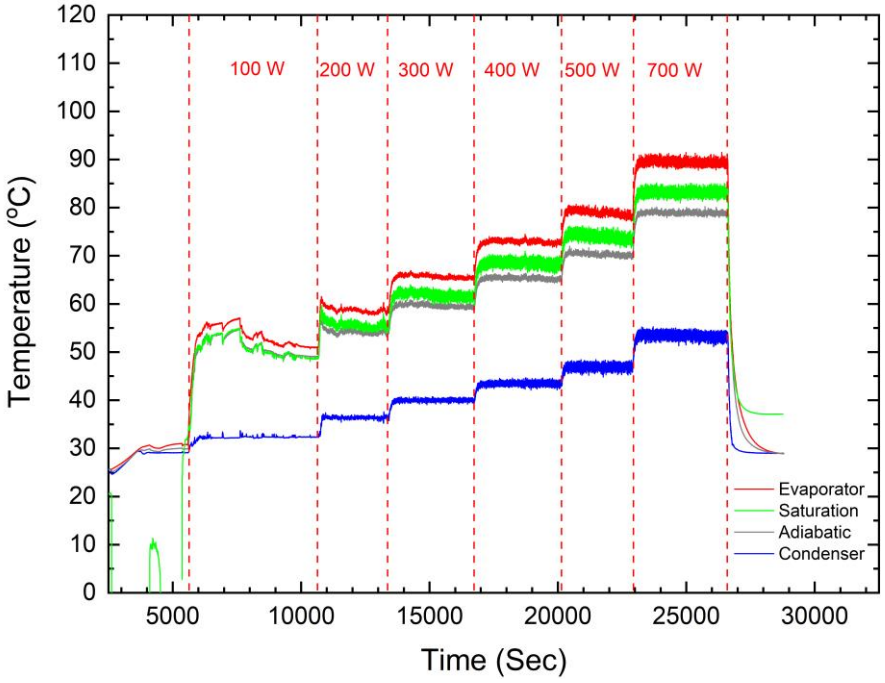

(a)

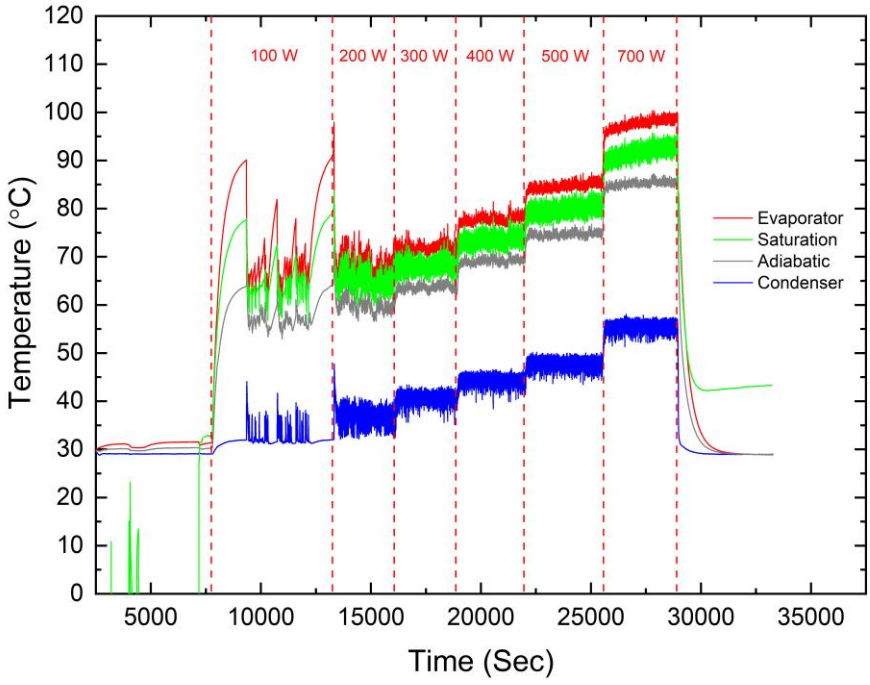

(b)

Figure 4-1 Temperature traces in the different sections for (a) vertical and (b) horizontal orientations at a cooling water temperature of 30°C.

The change in the average temperature of the different sections with heat transfer rates for the two orientations are compared in Figure 4-2. The average is taken for each power setting over 1000 seconds once steady state is reached. The results show that the average wall temperatures in the condenser section are approximately similar for the two orientations. The average wall temperature in the evaporator section for the horizontal orientation is higher, indicating a higher thermal resistance. The saturation temperature was higher for the horizontal section indicating that some of the effect is due to the condenser performance. The average evaporator wall temperature initially decreases with power at the lower power for the horizontal orientation. This corresponds to the period of large fluctuations in the evaporator wall temperature transients in Figure 4-1 where the behavior appeared intermittent.

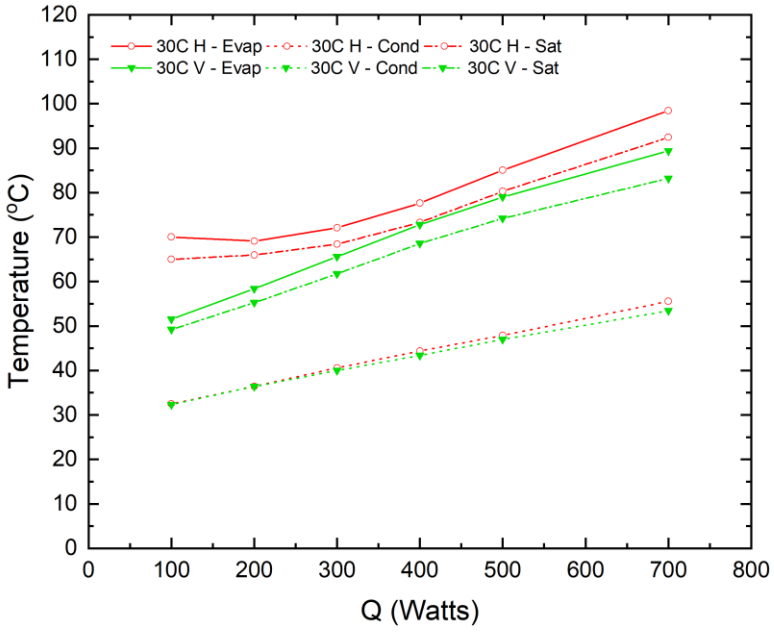

Figure 4-2 Change in the time average temperature of the evaporator and condenser wall, and saturation temperature with the heating power for vertical and horizontal orientation.

The change in the total thermal resistance with heat transfer rate is shown in Figure 4-3. The results show that the total thermal resistance of the oscillating heat pipe decrease with the heat transfer rate for both orientations. At 100 W and 200 W, the oscillating heat pipe in the horizontal orientation has lower thermal performance than in the vertical orientation. This corresponds to the high temperature fluctuations and spikes at low power. As the heating power is increased, the difference in the thermal resistance between the two orientations decrease and the thermal resistance in the horizontal orientation is approximately 14 percent larger than in the vertical orientation. The total thermal resistance can be divided into the thermal resistances for the evaporator and condenser sections, where the resistance is based on the average saturation temperature, i.e.,

$$R_e = \frac{(T_e - T_{sat})}{Q} \tag{4-1}$$

$$R_c = \frac{(T_{sat} - T_c)}{Q} \tag{4-2}$$

The resulting resistances for the evaporator and condenser are included on Figure 4-3. The condenser section resistance is the dominant thermal resistance in both orientations. The device in the horizontal orientation has a higher condenser resistance compared to the vertical orientation that is responsible for much of the difference in the total resistance in the two orientations. The heat transfer coefficient of the evaporator and condenser sections calculated based on the surface area of the channels corresponding to each section as given in equations (3-31) and (3-32) are plotted in Figure 4-4. The results show a significant difference in the heat transfer coefficient between the two sections; the evaporator section

shows a higher heat transfer coefficient of 5 and 6 times that of the condenser section in the vertical and horizontal orientations, respectively. The device in the horizontal orientation has a lower condenser heat transfer coefficient as compared to the vertical orientation with a maximum difference in the heat transfer coefficient of about 24 perecnt at 4.75 W/cm^2. The evaporator heat transfer coefficient is similar for the two orientations, except at 100 W with a 115 perecnt increase in the evaporator heat transfer coefficient for the vertical case where large fluctuations in temperature were observed for the horizontal case. The heat transfer coefficients are significantly larger than the results calculated from the data in Karthikeyan et al. [64] for a single-layer oscillating heat pipe.

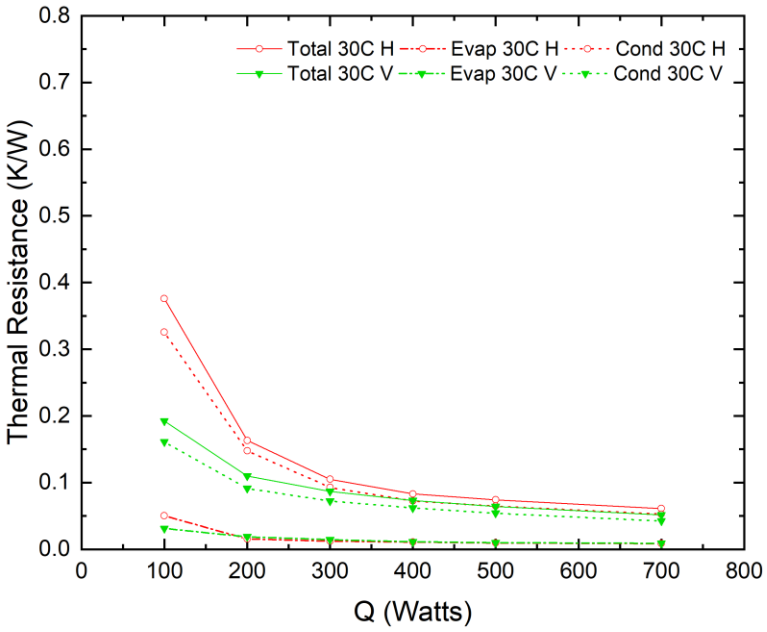

Figure 4-3 Change in the thermal resistance with heating power for vertical and horizontal orientation.

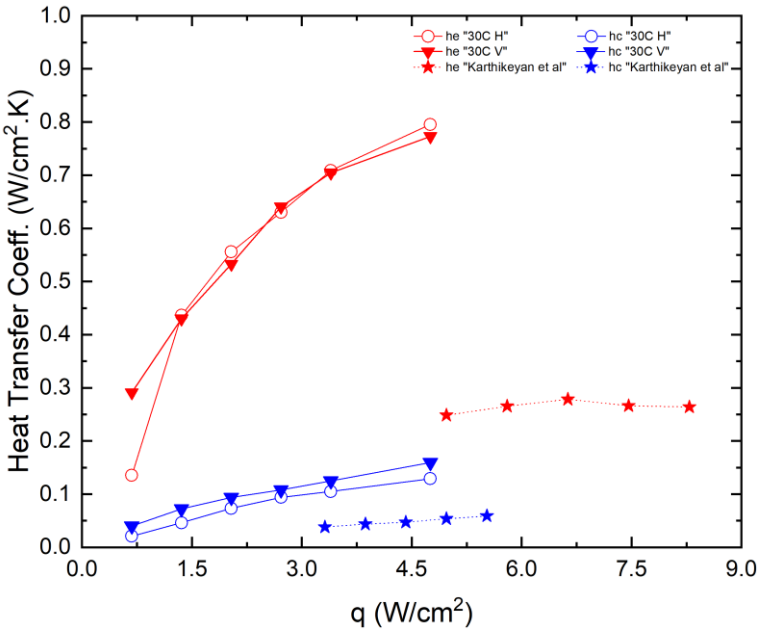

Figure 4-4 Change in the heat transfer coefficient of evaporator and condenser section with heat flux for vertical and horizontal orientation.

The transients of the temperatures measured in the different sections show that there are changes in the instantaneous performance of the devices. Typical transients of the temperatures for heating powers 200 W, 300 W, and 500 W are shown in Figures 4-5 to 4-7 respectively. Two modes were observed from the transients. The first mode is an intermittent oscillation mode, which is characterized by a slow increase in the saturation temperature followed by a sudden drop in the saturation temperature with subsequent oscillations in this temperature. The increase in the saturation temperature is accompanied by an increase in the evaporator temperature and a decrease in the temperature in the condenser section resulting in an increase in the thermal resistance or decrease in the total thermal performance. The decrease in the saturation temperature and subsequent

oscillations suggest the oscillations in the heat pipe are active and are accompanied by a decrease in the evaporator temperature and increase in the condenser temperature suggesting an increase in thermal performance during this phase. The intermittent oscillation mode is observed at 200 W for the horizontal case as shown in Figure 4-5B. The second mode is a continuous oscillation mode where the temperature oscillations are present at all times. This mode is observed in the vertical orientation for heating powers of 200 to 500 W as shown in Figures 4-5A, 4-6A, and 4-7A, but with a higher frequency as the heat input increases. The results for the horizontal orientation at a heating power of 300 W in Figure 4-6B show evidence of both modes. The intermittent oscillation mode is shorter, and the oscillation mode is more dominant as shown. Both orientations show a fully oscillation mode with almost the same frequencies at 500 W as seen in Figure 4-7. The early onset of the continuous oscillation mode for the vertical orientation suggests that gravity assists in maintaining a continuous oscillation.

The effect of the heat transfer rate on the transient operation can be characterized by the difference in the minimum and maximum temperature for the evaporator section shown in Figure 4-8. The oscillation modes are highlighted by different symbols. The magnitude of the evaporator temperature variations increased with heating power for the vertical orientation but decreased with heating power for the horizontal orientation as the intermittent mode is less prominent. The temperature fluctuation for the two orientations shows a similar maximum temperature fluctuation at 700 W.

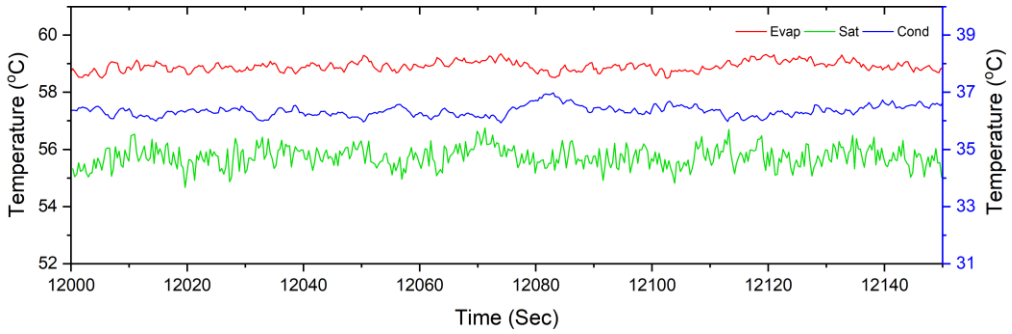

(a)

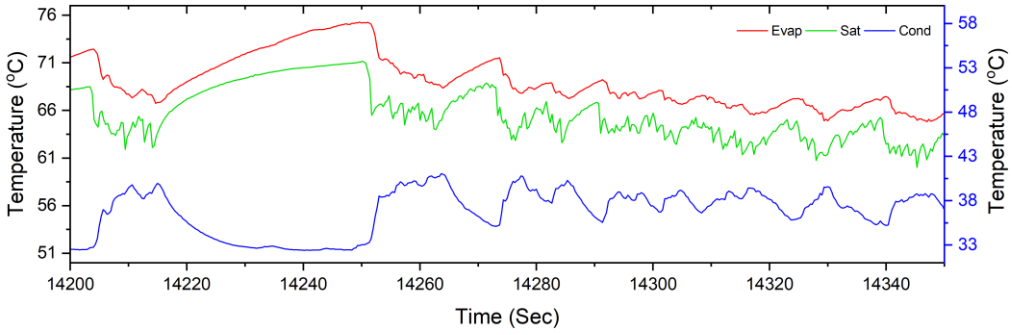

(b)

Figure 4-5 Transients of the temperatures of the evaporator wall, saturation (left axis**)** and condenser wall **(**right axis) at 200 W a) Vertical and b) Horizontal.

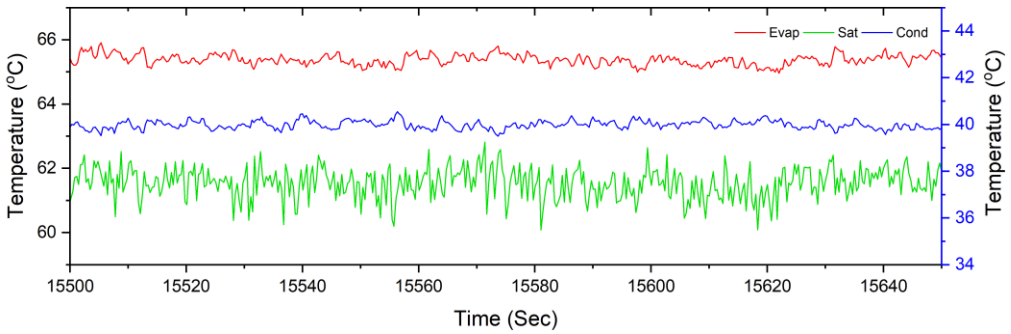

(a)

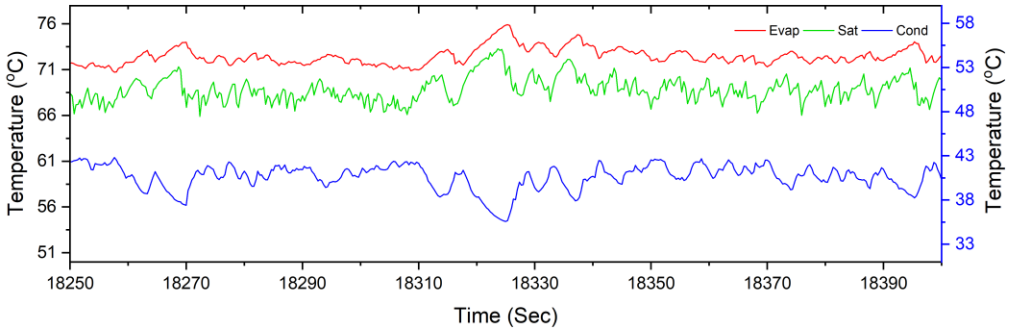

(b)

Figure 4-6 Transients of the temperatures of the evaporator wall, saturation (left axis) and condenser wall (right axis) at 300 W a) Vertical and b) Horizontal.

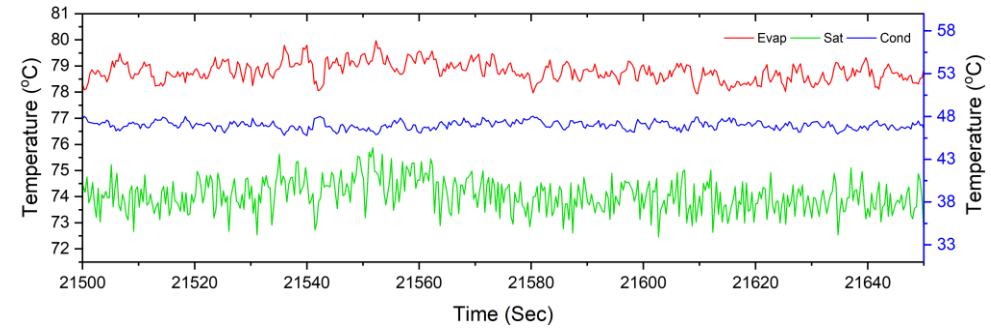

(a)

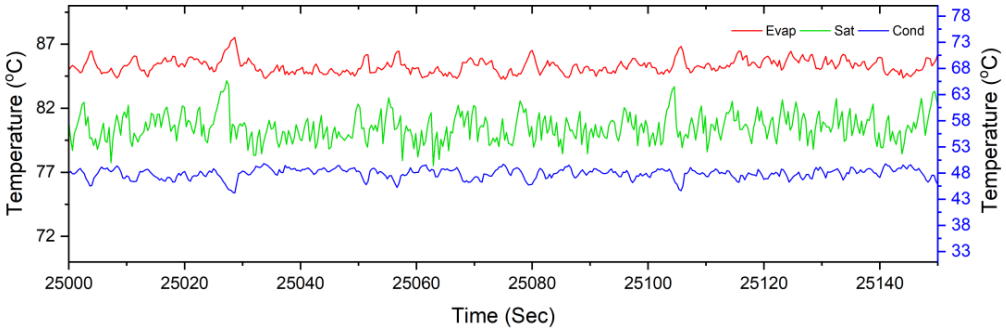

(b)

Figure 4-7 Transients of the temperatures of the evaporator wall, saturation (left axis) and condenser wall (right axis) at 500 W a) Vertical and b) Horizontal.

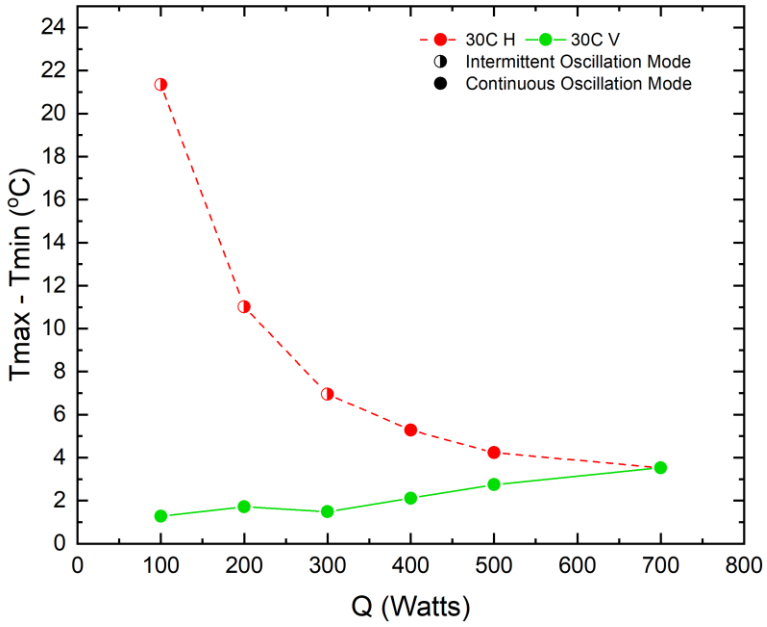

Figure 4-8 Evaporator temperature fluctuations at different heating power for vertical and horizontal orientation.

The boiling or dry-out limit of the oscillating heat pipe is typically characterized by the Kutateladze number (Ku) number defined as the ratio between the input heat flux to the critical heat flux for pool boiling

$$Ku = \frac{q'}{h_{fg}\rho_v \left(\frac{\sigma g(\rho_l - \rho_v)}{\rho_v^2}\right)^{0.25}} \qquad 4\text{-}3$$

The change in Kutateladze number with the saturation temperature is show in Figure 4-9. The results are compared with the correlations for the maximum Ku for a vertical single-layered oscillating heat pipe by Qu et al.[62]

$$Ku_{max} = 8.3Bo^{-1.598}Mo^{0.026}Pr^{-3.458}Ja^{*(-0.157)}\left(\frac{D_i}{L_e}\right)^{1.21}\left(\frac{L_e}{L_c}\right)^{-0.232} \quad 4\text{-}4$$

and the correlation for a horizontal single-layered oscillating heat pipe by Rittidech et al.[13]

$$Ku_{max} = 0.0052.\left[\frac{D^{4.3}{L_t}^{0.1}}{{L_e}^{4.4}}.n^{0.5}.\left(\frac{\rho_v}{\rho_l}\right)^{-0.2}.{Pr_v}^{-25}\right]^{0.116} \quad 4\text{-}5$$

The results show that the vertical case does not exceed the max Ku number proposed by Qu et al.[62]. This agrees with the temperatures transient data that suggest that the vertical case does not experience dry-out. For the horizontal case, the correlation by Rittidech et al.[13] can not predict the dry-out limitation with the present data having a significantly higher Ku number than that predicted by the correlation, even though there is no evidence of dry-out. The correlation was developed for a single-layered oscillating heat pipe and is clearly not valid for a stacked oscillating heat pipe in the horizontal orientation. It is apparent that stacked oscillating heat pipes can handle much higher heat loads than single-layered ones before reaching the dry-out limitation.

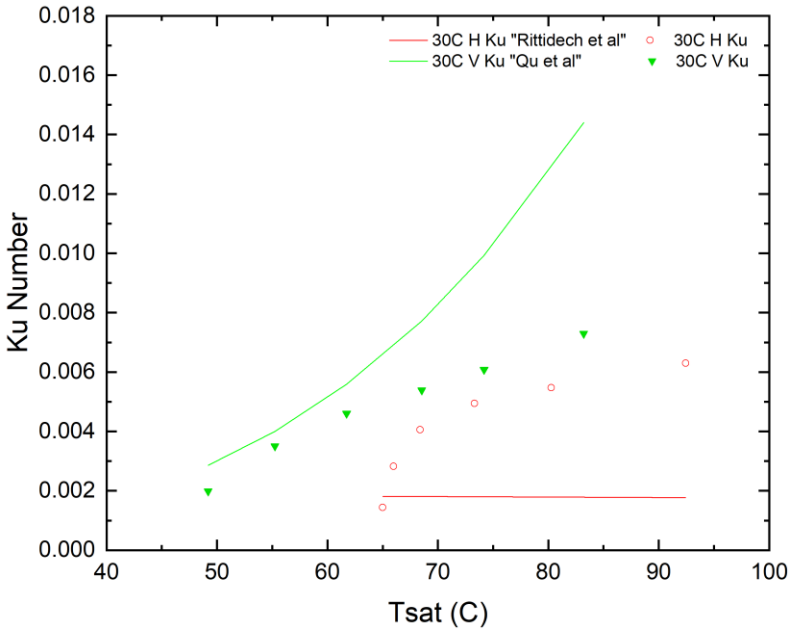

Figure 4-9 Different correlation for maximum Ku compared to Ku number.

4.2 The effect of cooling water temperature.

The effect of the cooling water temperature (10°C to 50°C) on the temperature transients of the horizontal oscillating heat pipe under different heating powers is shown in Figure 4-10. The results in most cases show an increase in the evaporator and adiabatic temperature when the heat transfer was increased except at low heat transfer rates and condenser wall temperatures. For example, when the cooling water temperature was 10°C, the temperature traces show no evidence of temperature fluctuations for the heating power of 100 W. Temperature fluctuations appear for the power of 200 W when the cooling water was 10°C and the condenser wall temperature was approximately 20°C. The evaporator wall temperature in this case was lower than at the power of 100 W. The adiabatic and saturation temperature in this case were at 50 to 60°C that was similar to the temperatures for the experiments when the cooling water temperature was 30°C, despite the much lower condenser wall temperature. The evaporator wall temperature and saturation temperature show large spikes for all heating powers up to 700 W where the data appears to show more consistent oscillations. The results for the cooling water temperature of 50°C show temperature fluctuations at 100 W that appear to be evidence of oscillations, but the oscillations are not fully sustained. The temperature fluctuations decrease as the heating power increases and are consistent beyond 200 W. In all three cases, the temperature oscillations are consistent at the highest power of 700 W with no dramatic increase, which indicates that it is operating below the dry-out limit.

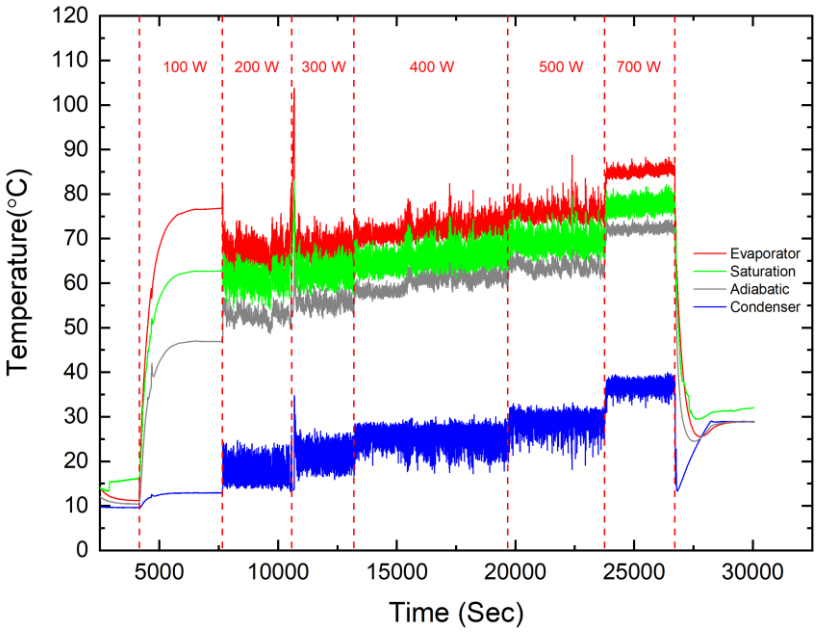
100 W
200 W
300 W
400 W
500 W
700 W
Temperature(°C)
Time (Sec)
Evaporator
Saturation
Adiabatic
Condenser

(a)

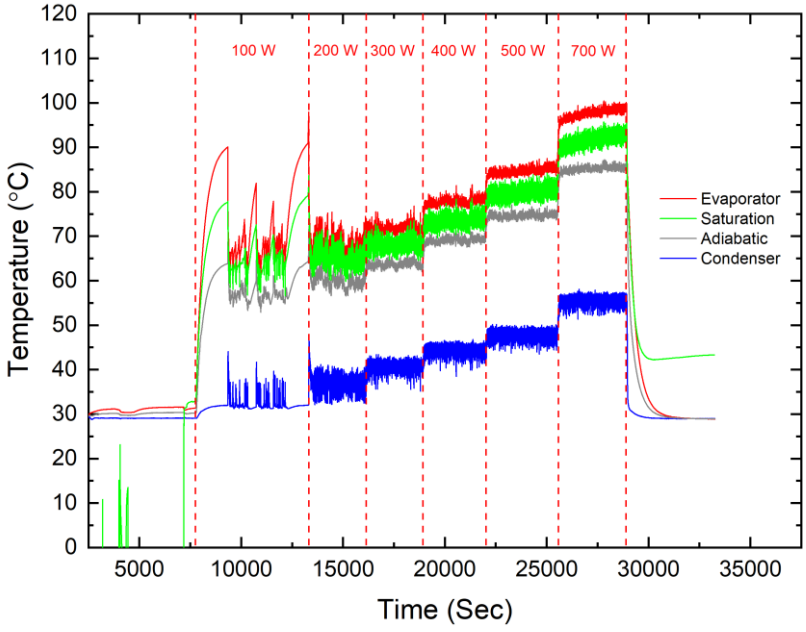
100 W
200 W
300 W
400 W
500 W
700 W
Temperature (°C)
Time (Sec)
Evaporator
Saturation
Adiabatic
Condenser

(b)

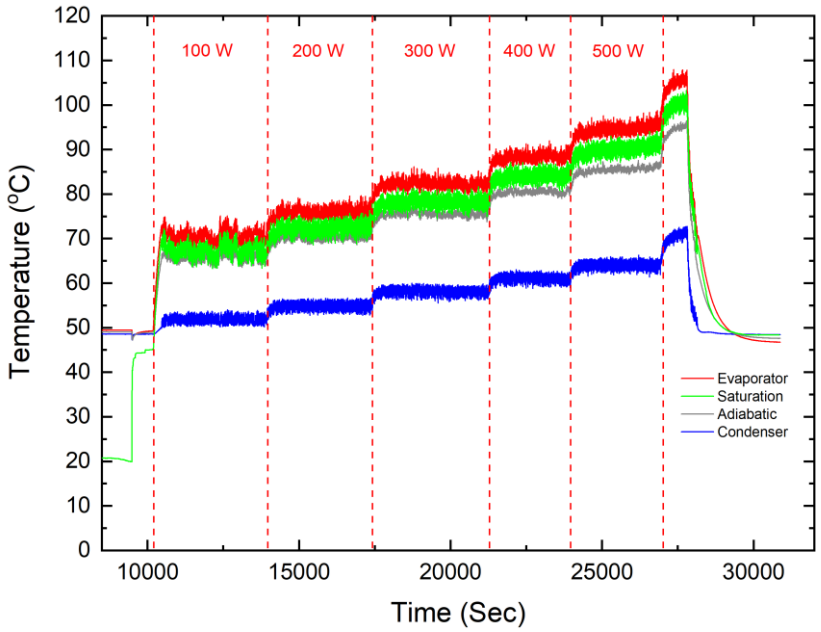

(c)

Figure 4-10 Comparison of the transients of the temperatures measured on the horizontal oscillating heat pipe for cooling water temperatures of a) 10℃, b) 30℃ and c) 50℃.

The change in the average temperature of the evaporator wall, the condenser wall, and the saturation temperature of the oscillating heat pipe with heating power for different cooling water temperatures are shown in Figure 4-11. The change in the condenser wall temperature is much more significant compared to the evaporator wall temperature when the cooling water temperature is changed. At 50℃, the temperatures increase with an increase in the heating power. The results for 10℃ and 30℃ cases show high evaporator temperatures at 100 W. This evaporator temperatures in these cases decrease until 300 W and start increasing after that with the heating power. This low-power high evaporator temperatures correspond to the instabilities and fluctuations seen in figure 4-10 for 10℃ and 30℃. At higher heating powers, which is of interest for power electronics cooling,

despite the big change in the condenser temperature, the evaporator temperature does not exceed 100°C.

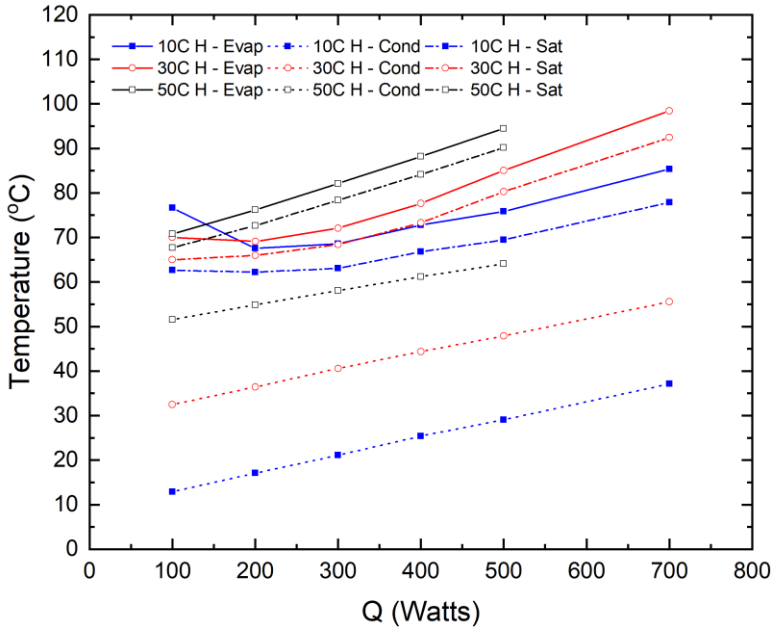

Figure 4-11 Temperature of the evaporator and condenser section, and the saturation temperature vs the heating power for 10°C, 30°C and 50°C cooling water temperature.

The change in component and total thermal resistance of the horizontal oscillating heat pipe for the different cooling water conditions is shown in Figure 4-12. The corresponding heat transfer coefficients for the evaporator and condenser sections are shown in Figure 4-13. The total thermal resistance of the oscillating heat pipe decreases with the heating power in all cases. The oscillating heat pipe resistance for a given heat transfer rate decreases as the cooling water temperature and condenser wall temperature increases as found in the literature [20], [34]–[36]. The large values of the total thermal resistance for the 10°C and 30°C cooling water at 100 W correspond to the conditions with

extended periods without oscillations as shown previously in Figure 4-10. The condenser section makes the larger contribution to the total thermal resistance in all cases. The heat transfer coefficient of the evaporator section in Figure 4-13 was similar for the case where the water temperature was 30℃ and 50℃. The evaporator heat transfer coefficient was lower for the cooling water temperature of 10℃ that leads to a higher evaporator resistance. The heat transfer coefficient for the condenser was smallest for the 10℃ that lead to the highest total thermal resistance and increased significantly when the cooling water temperature was increased leading to a decrease in the condenser and total resistance. Comparing the three cases to the single-layered OHP tested by Karthikeya et al. [64], the stacked oscillating heat pipe shows much better performance from all aspects.

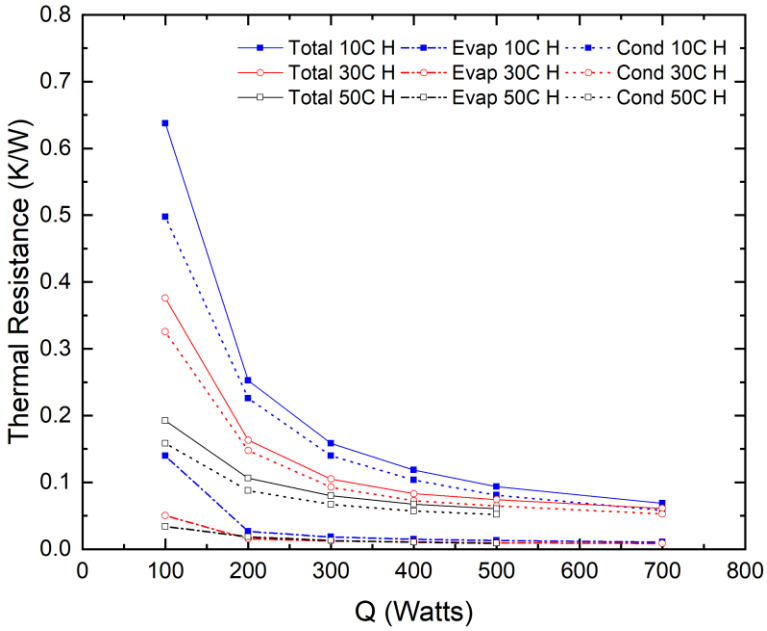

Figure 4-12 Total resistance vs heating power for 10℃, 30℃ and 50℃ cooling water temperature.

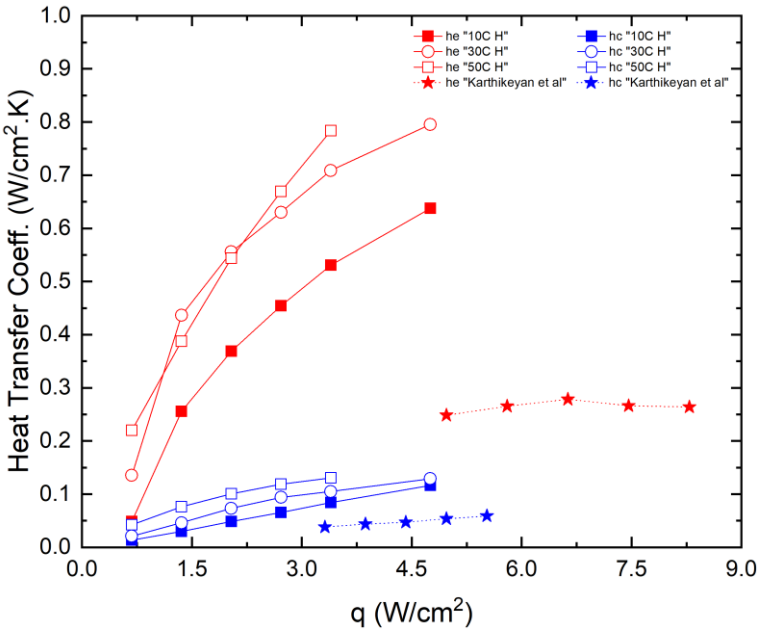

Figure 4-13 Heat transfer coefficient for evaporator and condenser section at 10°C, 30°C and 50°C cooling water temperatures.

The change in the heat transfer coefficient in the condenser appears to be associated with a change in the oscillations in the heat pipe. A more detailed comparison of the transients of the temperatures of the evaporator wall, saturation and condenser wall for 200 W, 300 W and 500 W for the three cooling water temperatures are shown in Figures 4-14, 4-15 and 4-16. The results suggest there are again periods of intermittent oscillations and periods of steady oscillations. The results for the 10°C show the intermittent oscillation mode is dominant at lower heating power more so than observed previously for the 30°C case. The transients for 50°C, on the other hand, show evidence of a continuous oscillation mode for the three presented heating powers with similar amplitude. The cases show evidence of a continuous oscillation mode at 500 W but with a difference in the amplitude

where the 30℃ shows the minimum and 10℃ shows the maximum, in addition to short periods of intermittent oscillation mode. This likely explains the higher thermal resistance for the 10℃ case. The change in the magnitude of the fluctuations in the evaporator temperature for the three cooling water temperatures are shown in Figure 4-17 that also shows the different oscillation modes. At a cooling water temperature of 10℃, there are no fluctuations at 100W. The fluctuations increase with an increase in the power to 400 W and

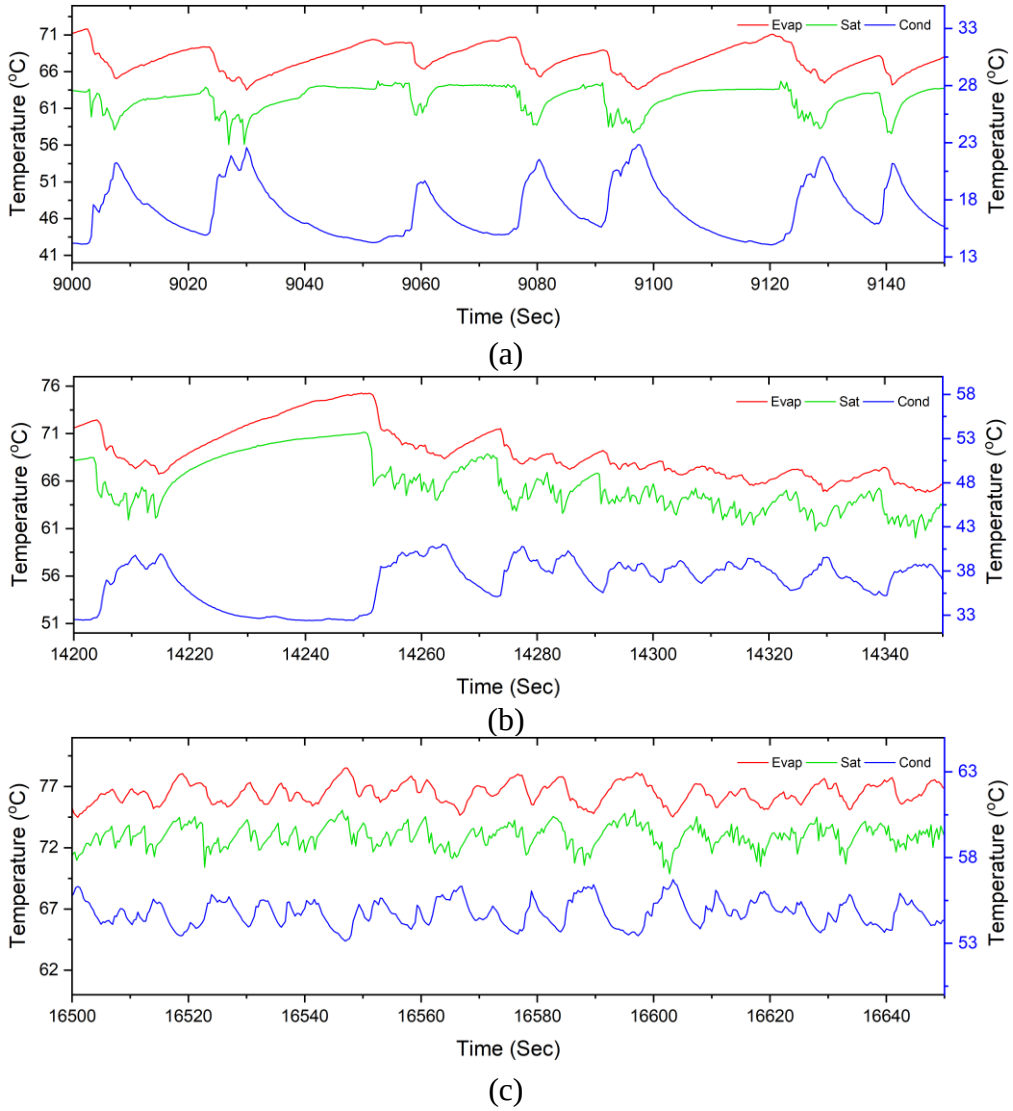

Figure 4-14 Transients of the temperatures of the evaporator wall, saturation and condenser wall at 200 W a) 10℃, b) 30℃ and c) 50℃.

then decreases with a further increase in the power, indicating a stable operation of the oscillating heat pipe. When the cooling water was 30℃, the fluctuations decrease with increasing power as discussed in the previous section. The fluctuations for the evaporator where the cooling water temperature was 50℃ is constant with the heating power which represents the continuous oscillation mode.

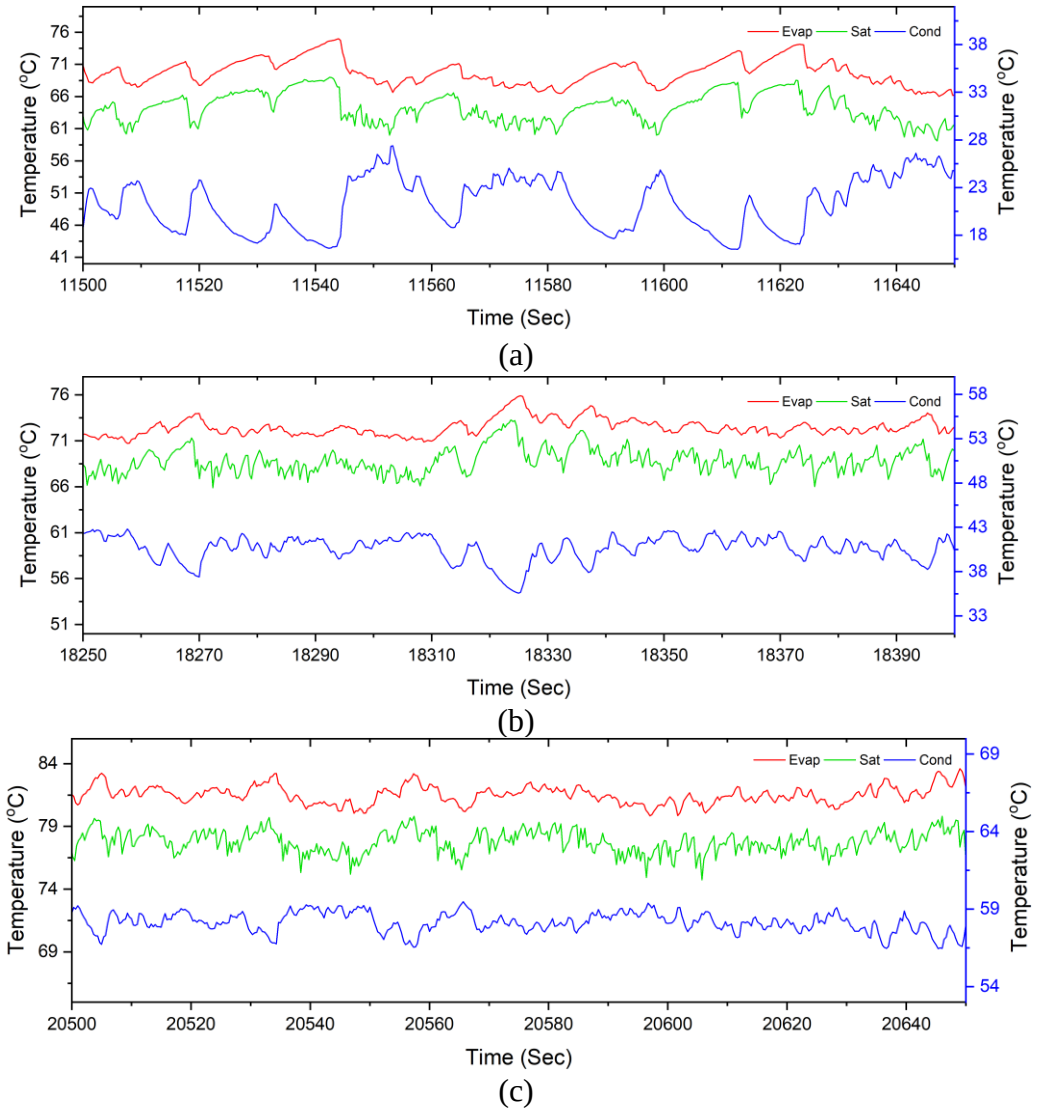

Figure 4-15 Transients of the temperatures of the evaporator wall, saturation and condenser wall at 300 W a) 10C, b) 30C and c) 50C.

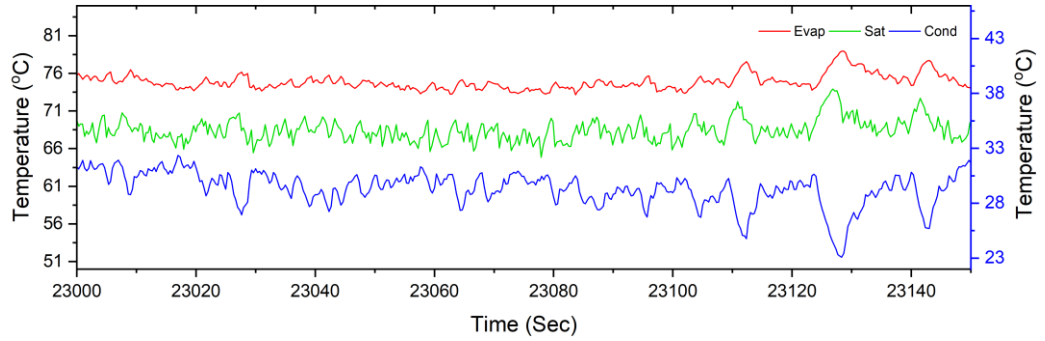

(a)

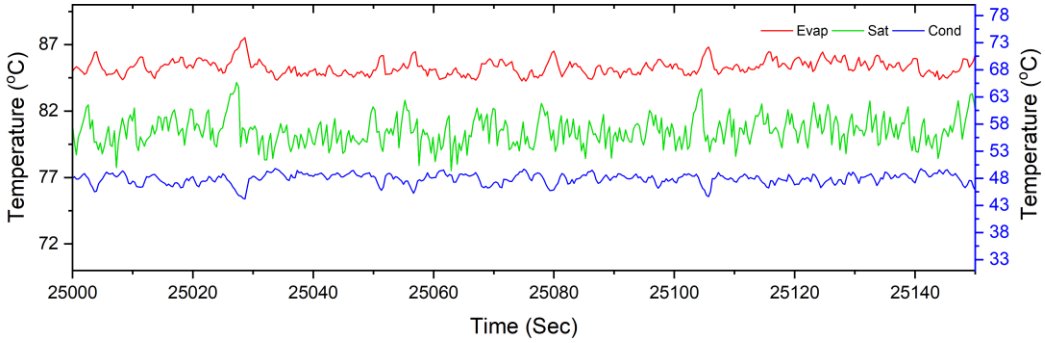

(b)

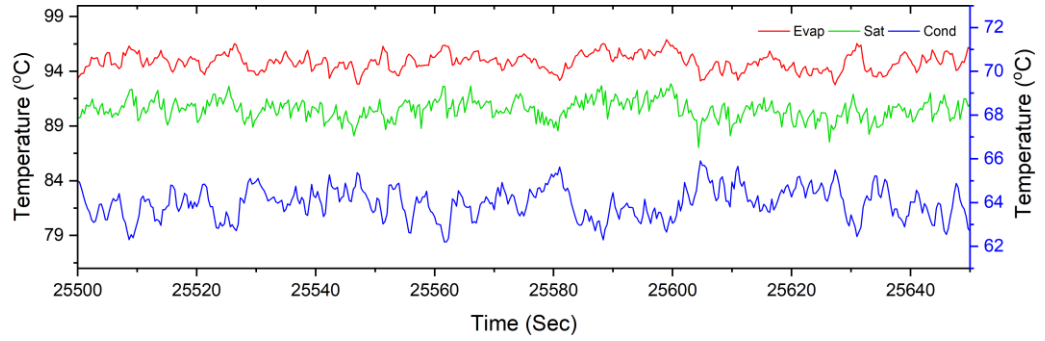

(c)

Figure 4-16 Transients of the temperatures of the evaporator wall, saturation, and condenser wall at 500 W a) 10℃, b) 30℃ and c) 50℃.

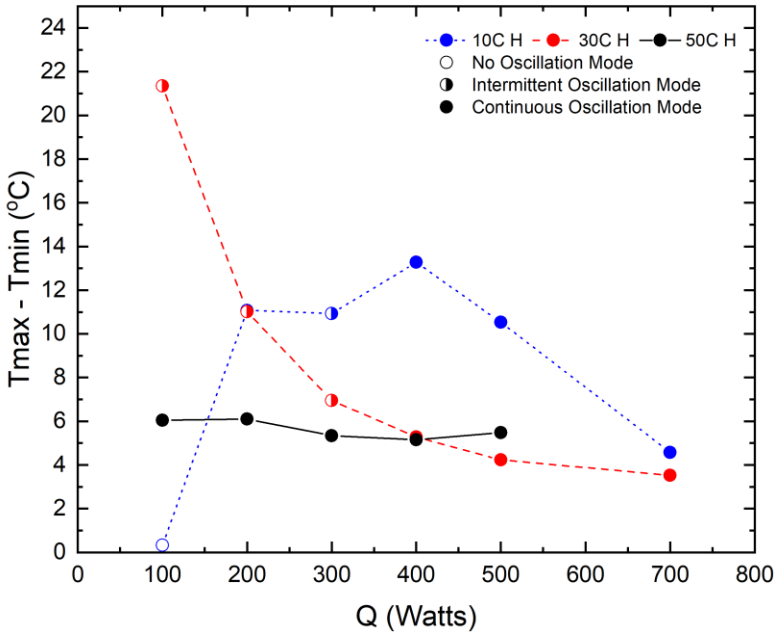

Figure 4-17 Evaporator temperature fluctuations at different heating power for 10℃, 30℃ and 50℃ cooling water temperature.

The Kutateladze number (Ku) for the three cases which is calculated by equation (4-3) is compared with the maximum Ku correlation by Rittidech et al.[13] (equation (4-6)) in Figure 4-18.

$$ku_{max} = 0.0052.\left[\frac{D^{4.3}{L_t}^{0.1}}{{L_e}^{4.4}}.n^{0.5}.\left(\frac{\rho_v}{\rho_l}\right)^{-0.2}.{Pr_v}^{-25}\right]^{0.116} \qquad 4\text{-}6$$

The Ku number for the three cases is higher than that from the correlation, especially at the higher saturation temperatures. The correlation for the single-layered oscillating heat pipe is not valid for a stacked oscillating heat pipe and it is apparent that stacked oscillating heat pipe can handle much higher heat load than a single-layered one before reaching the dry-out limitation. A new correlation is needed to be developed to capture the advantages of the stacked OHP. All the three cases do not exceed the correlation proposed by Qu et al. and the stacked oscillating heat pipe overcomes the lack of gravity assistance.

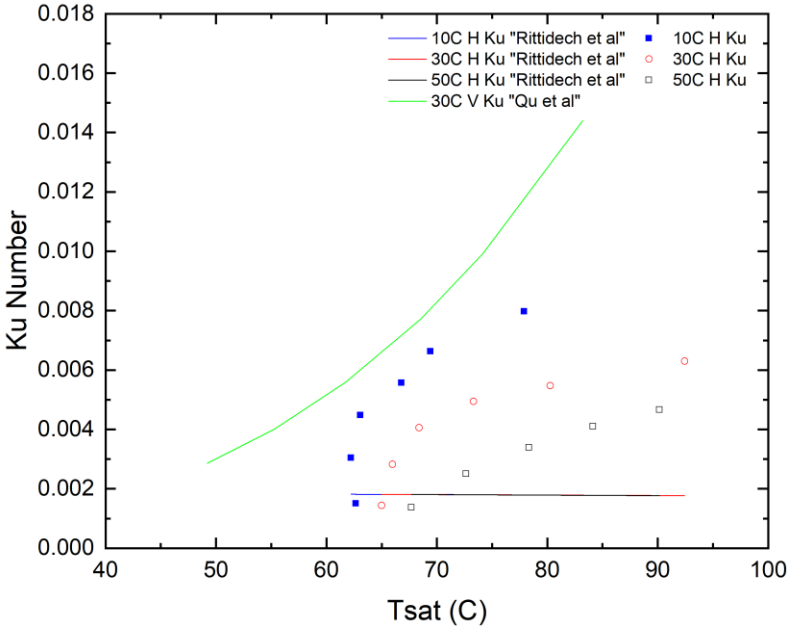

Figure 4-18 Ku Correlations compared to Ku number.

Section 2: Heat Spreader Thermal Performance.

In this section, the performance of the oscillating heat pipe as a heat spreader is presented. The results are presented in two subsections. The first considers the effect of the orientation for different heating locations, while the second one considers the effect of the cooling water temperature for different heating locations. For both parts, tests were performed for three different heating locations, middle heating and two end heating with different cooling water flow direction. Co-flow where the cooling water travels from the heater position and counter-flow where the cooling water travels to the heater position. The test matrix is presented in table 4-2.

Table 4-2 Heat spreader thermal performance test matrix.

	Horizontal			Vertical		
	Middle	Co-flow	Counter-flow	Middle	Co-flow	Counter-flow
30ºC	✓	✓	✓	✓	✓	✓
50ºC	✓	✓	✓			
450 W	✓	✓	✓			

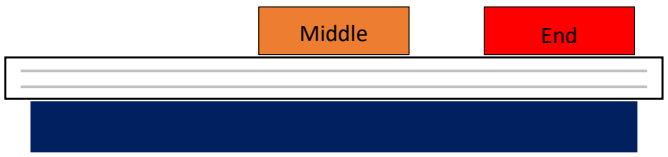

Figure 4-19 Heating locations for the heat spreader test rig.

4.3 Effect of orientation on the performance with different heating locations.

Transients of the temperature on the heater block wall, the cold plates, and the saturation temperature for the horizontal and vertical orientations with a 30℃ cooling water temperature are presented in Figures 4-20 and 4-21 respectively. Other cases are presented in the appendix. The results for the end heating show that there is no oscillation at 100 W for both orientations as shown in Figure 4-20. The vertical orientations results show low amplitude oscillations starting from 200 W heating power until 400 W where a high amplitude oscillation started accompanied with a significant decrease in the saturation temperature. This lead to a decrease in the heater block wall temperature. For the horizontal orientation, the results show no temperature oscillations until 300 W where the oscillations begin but are followed by a non-oscillating period that was accompanied with increase in the saturation temperature and the wall temperature below the heater block. A non-oscillation mode is present again when the power is increased to 400 W. The temperatures resume oscillations at 500 W with a noticeable drop in saturation temperature and the heater block wall temperature. When the heater was in the middle location, the transients as shown in Figure 4-21 do not show oscillations until 400 W and 500 W for the vertical orientation where there are low amplitude oscillations. The results for the horizontal orientation show a small period of oscillation at the transition between 400 W and 500 W heating powers. The saturation temperature for the vertical orientation is almost the same as the condenser temperature for powers up to 300 W except for small increases at 400 W and 500 W where the oscillations occurred. The saturation temperature increases relative to the condenser

wall temperature with heating power for the horizontal orientation. The results show that the heater block has a lower wall temperature in the middle heating case compared with the end heating for the two orientations for the same condenser temperature.

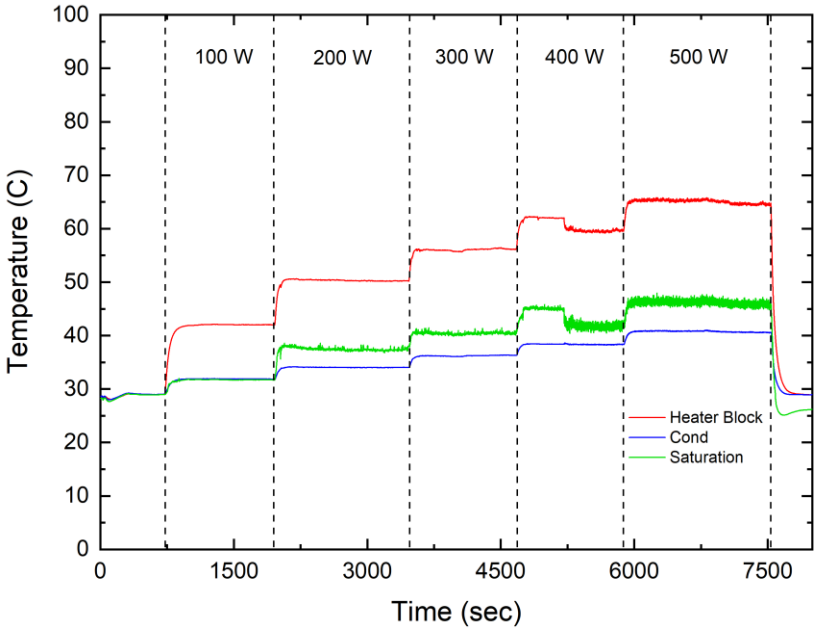

(a)

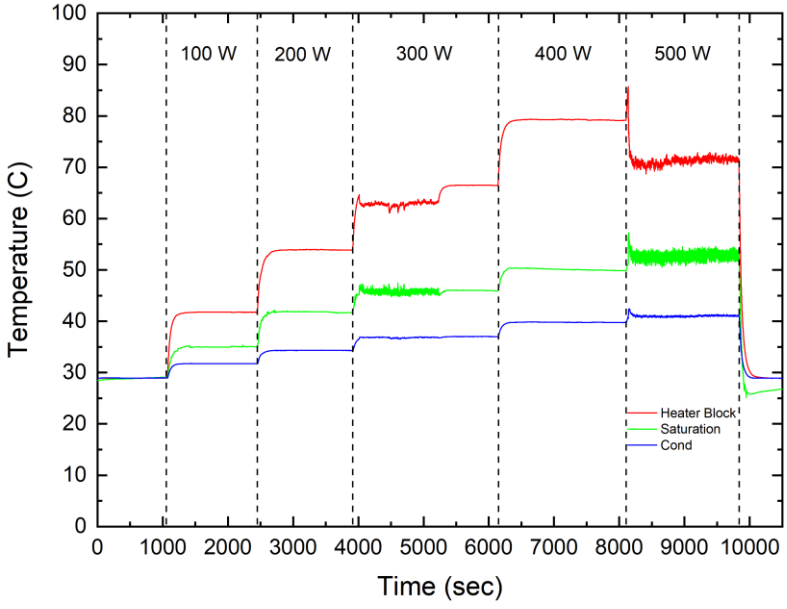

(b)

Figure 4-20 Temperature transients for end heating at 30°C cooling water temperature for two orientations a) vertical and b) horizontal.

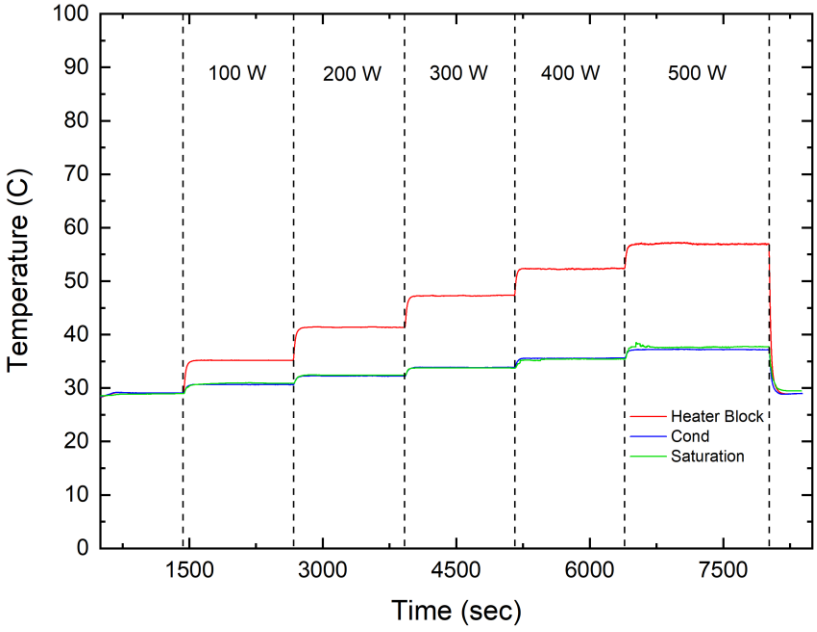

(a)

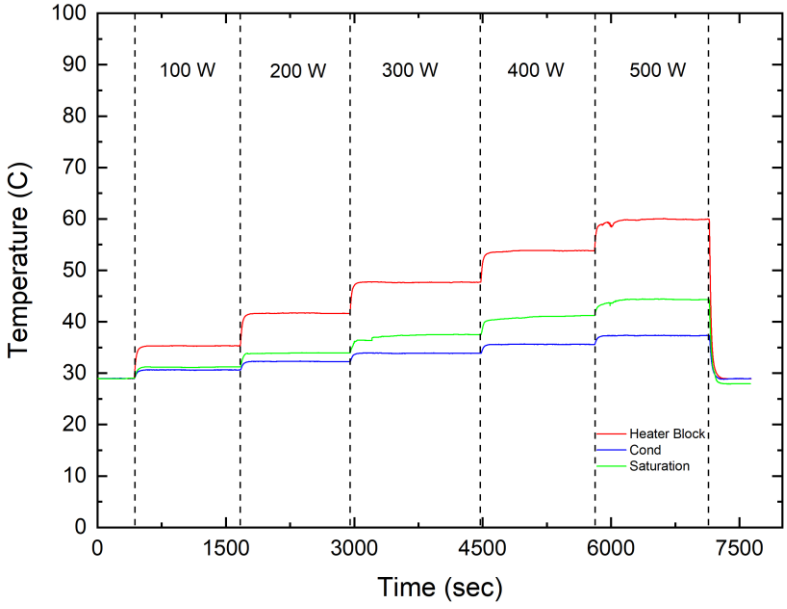

(b)

Figure 4-21 Temperature transients for middle heating at 30°C cooling water temperature for two orientations a) vertical and b) horizontal.

The horizontal cases do not show evidence of continuous oscillations and the vertical middle heating case shows low amplitude oscillations, so the effect of the start up was also studied by stepping the heating power directly to 400 W or 500 W with cooling water temperature of 30℃ for both orientations. The temperature transients for the end heating for the horizontal orientation and the middle heating for both orientations are shown in Figure 4-22. The results show continuous oscillations at the two heating powers for the end heating unlike what was seen in Figure 4-20b. Thus, a large power step up appears to initiate oscillations for the end heating case. The results for the middle heating show low amplitude oscillation with a low saturation temperature near to the condenser temperature for the vertical case and the horizontal case results still show no oscillations similar to the result in in Figure 4-21.

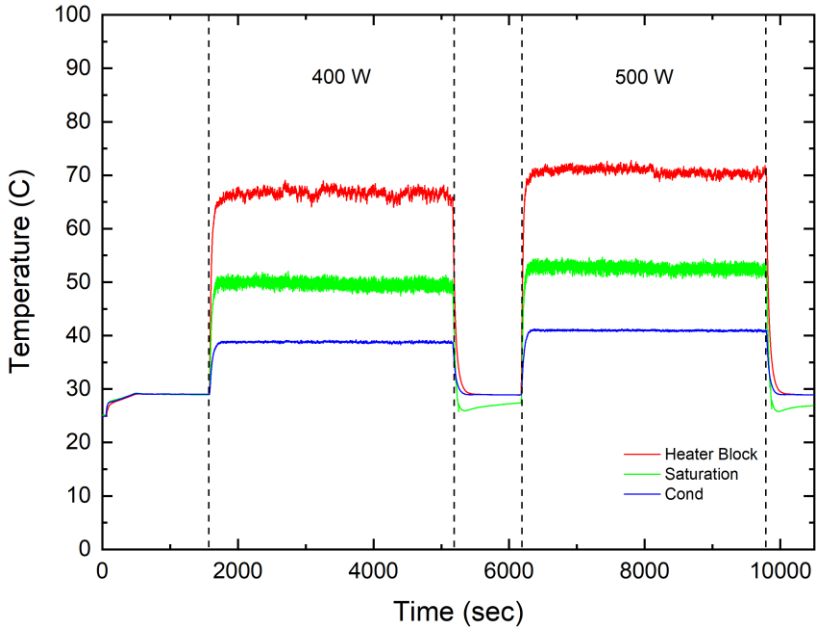

(a)

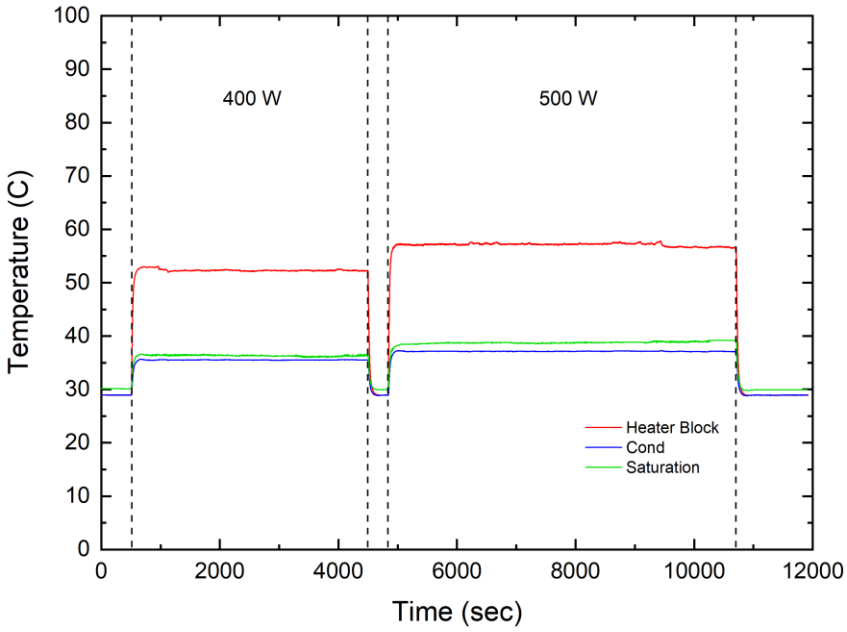

(b)

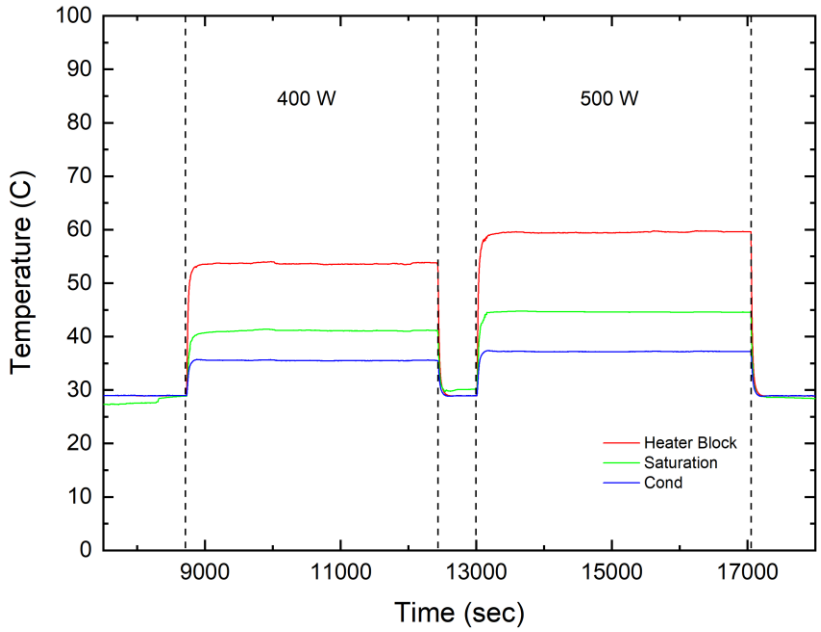

(c)

Figure 4-22 Temperature profiles for 400 W and 500 W tests with 30°C cooling water temperature for a) end – horizontal, b) middle - vertical and c) middle – horizontal

The temperature differences between the average wall temperature below the heater block and the cooling blocks are presented in Figure 4-23 for the two orientations. The temperature differences increase with an increase in the heating power for all cases. The middle heating cases show the lowest temperature differences which mean better thermal performance. At low heating powers of 100 W to 300 W, both orientations show the same temperature difference with a small deviation at 300 W. Starting from 400 W, the vertical case shows lower temperature differences compared to the horizontal case which corresponds to the low amplitude oscillations shown in the transients in Figure 4-21a. The end heating for the both cooling water directions (co-flow and counter-flow) show almost the same results at the same orientation except at 400 W. The results with the co-flow cooling water direction for the horizontal orientation has a large increase in the temperature difference that corresponded to the non-oscillation mode shown in Figure 4-20b. At 500 W both cases show the same temperature difference. The results for the end heating in the vertical orientation have lower temperature differences compared to the horizontal orientation except at 100 W, where all cases have the same temperature difference.

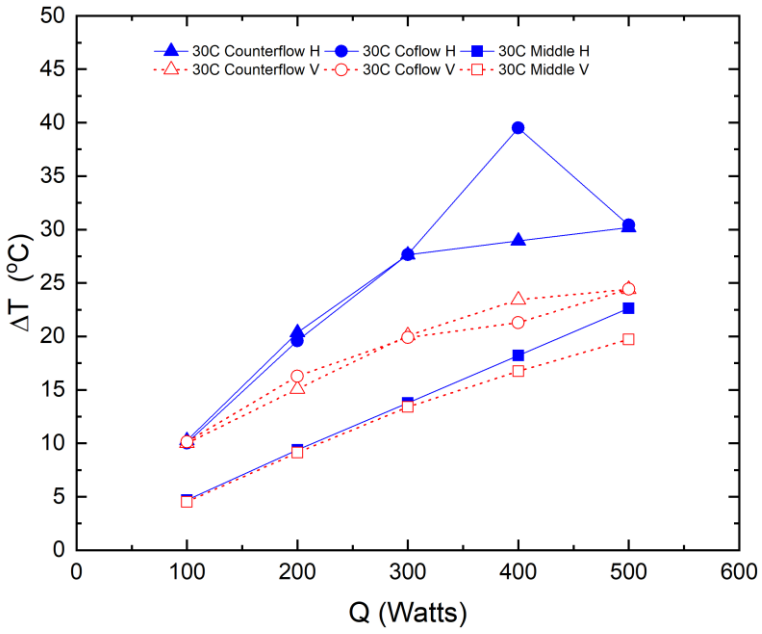

Figure 4-23 The temperature difference between the heater block wall and condenser temperatures with the heating power for vertical and horizontal cases.

The total thermal resistances of both heating locations for the vertical and horizontal orientation are presented in Figure 4-24. The open symbols reflect the non-oscillation mode and the solid ones represent the oscillation mode. The non-oscillation mode has a thermal resistance of 0.1 K/W for the end heating with both cooling water directions and 0.045 k/W for the middle heating position at all heating powers. The thermal resistances for the middle location are essentially the same as the thermal resistance of the non-charged or empty oscillating heat pipe indicating that the heat is transferred mainly through pure conduction despite the presence of the working fluid. The middle heating location has the lowest thermal resistance in these cases and lower than the end heating for the cases considered even when the oscillation mode occurs. When the oscillating heat pipe shows oscillation, the thermal resistance decreases with the heating power. The results for middle heating did

not show any oscillations for the horizontal orientation but did for the vertical orientation starting at 400 W, and this resulted in a decrease in the thermal resistance at 400 W and 500 W. For the end heating, the vertical orientation has a lower resistance except at 100 W that did not show oscillations. The results for this heating locations show similar thermal resistances for the two cooling water directions except for the horizontal case at 400 W where oscillations occurred for the counter-flow cooling water direction but not for the co-flow direction. The results at 300 W that had the oscillation mode at the beginning followed by the non-oscillation mode (in Figure 4-20b) shows the improvement in the thermal performance with oscillations.

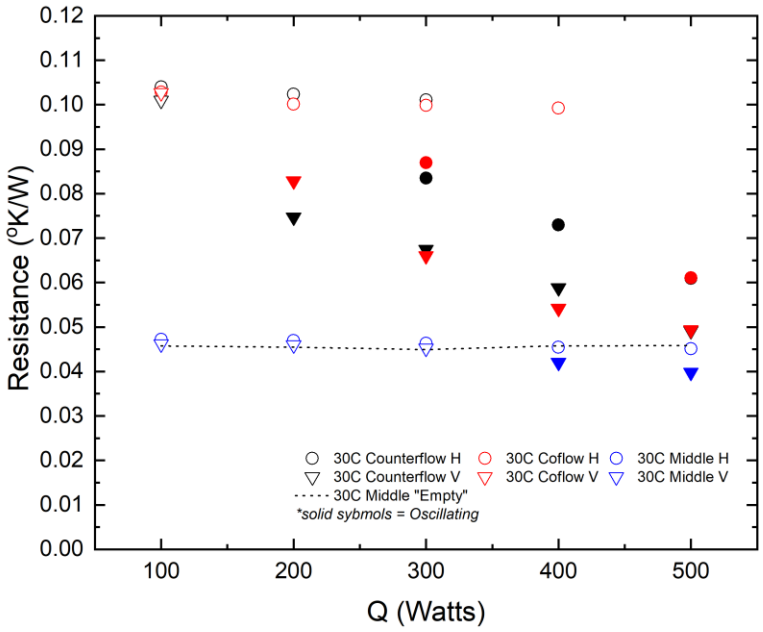

Figure 4-24 The change in total thermal resistance with the heating power for the cooling water temperature of 30°C for middle and end heating in the (○) horizontal and (▽) vertical orientations. Sold symbols indicate oscillating mode.

The temperature distribution of each orientation for end heating for the evaporator section and condenser section are shown in Figure 4-25 and Figure 4-26, respectively. The results show a more uniform temperature distribution on the evaporator side for the vertical orientation compared to the horizontal one as shown in Figure 4-25. The maximum temperature in the vertical case was 67.8℃ compared to the horizontal orientation which shows 75.4℃. For the condenser side the two cases show almost the same temperature distribution as shown in figure 4-26, but a higher max temperature at the corner for the horizontal orientation.

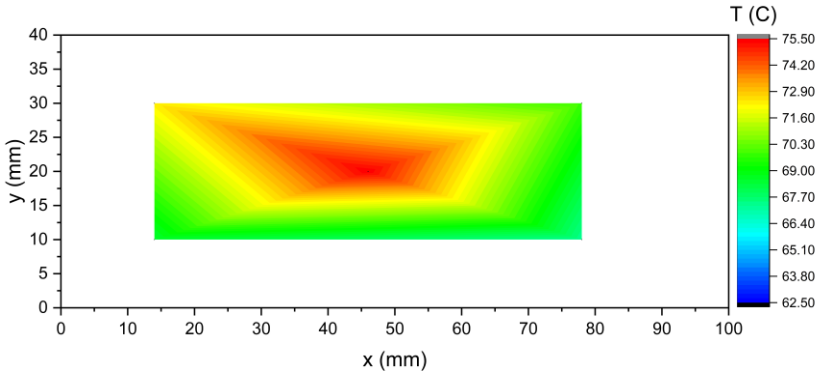

(a)

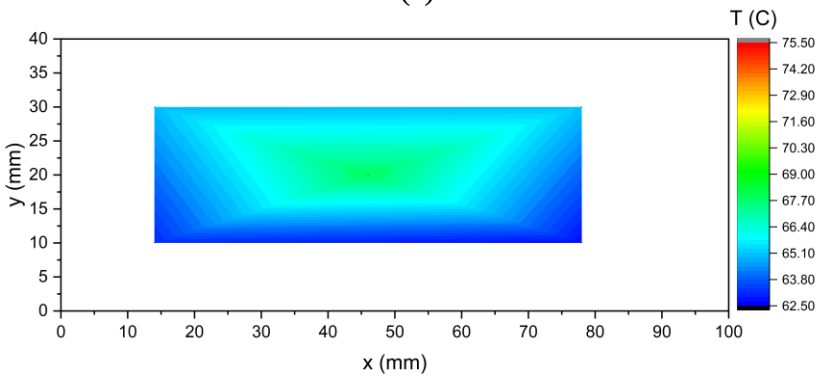

(b)

Figure 4-25 Temperature Distribution of the evaporator side for (a) horizontal and (b) vertical orientations with end heating.

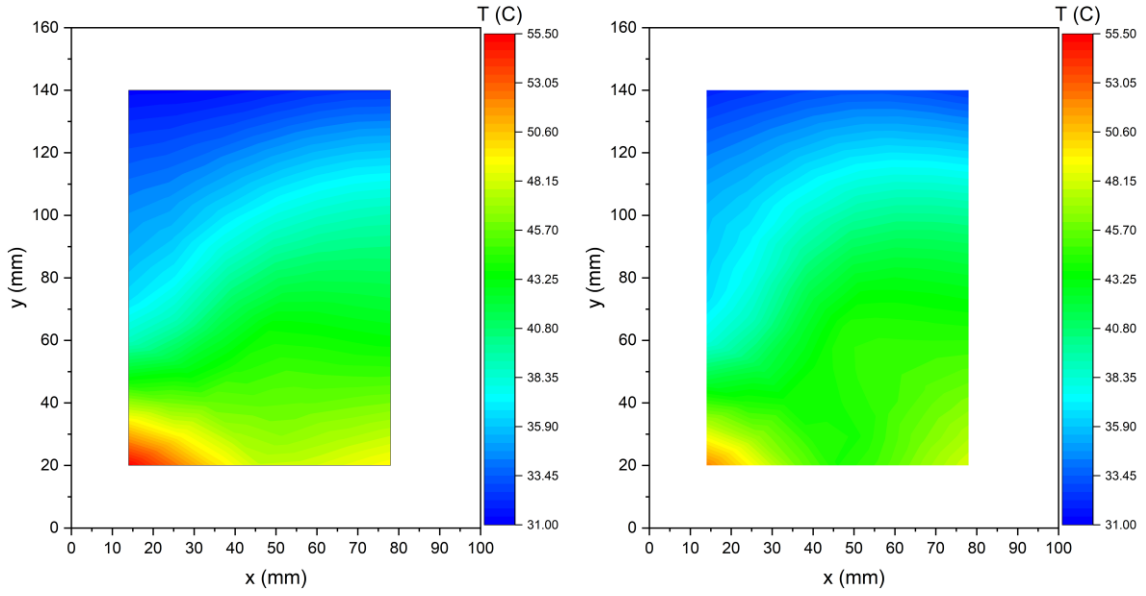

(a) (b)

Figure 4-26 Temperature Distribution of the condenser side for (a) horizontal and (b) vertical orientations with end heating.

4.4 Effect of cooling water temperature on the performance.

The effect of the cooling water temperature on the performance for different heating locations was studied and will be discussed in this section. The performance for middle and end heating in the horizonal orientation for cooling water temperatures of 30 and 50°C were considered. Typical transients of the temperatures are shown in Figures 4-27 and 4-28. Other cases are presented in the appendix. For end heating with a 50°C cooling water temperature, oscillations are evident for the heating powers except at 100 W unlike results at 30°C that show oscillations only at high heating powers as shown in Figure 4-28. The oscillations for the 50°C case are not fully developed at 200 W but start to be steadier at 300 W and reach consistent oscillations at 400 W and 500 W. The 50°C case with middle heating only shows oscillation starting from 400 W while the 30°C case does not show any

oscillations. The middle heating cases results show lower heater block wall temperatures compared to corresponding results with end heating.

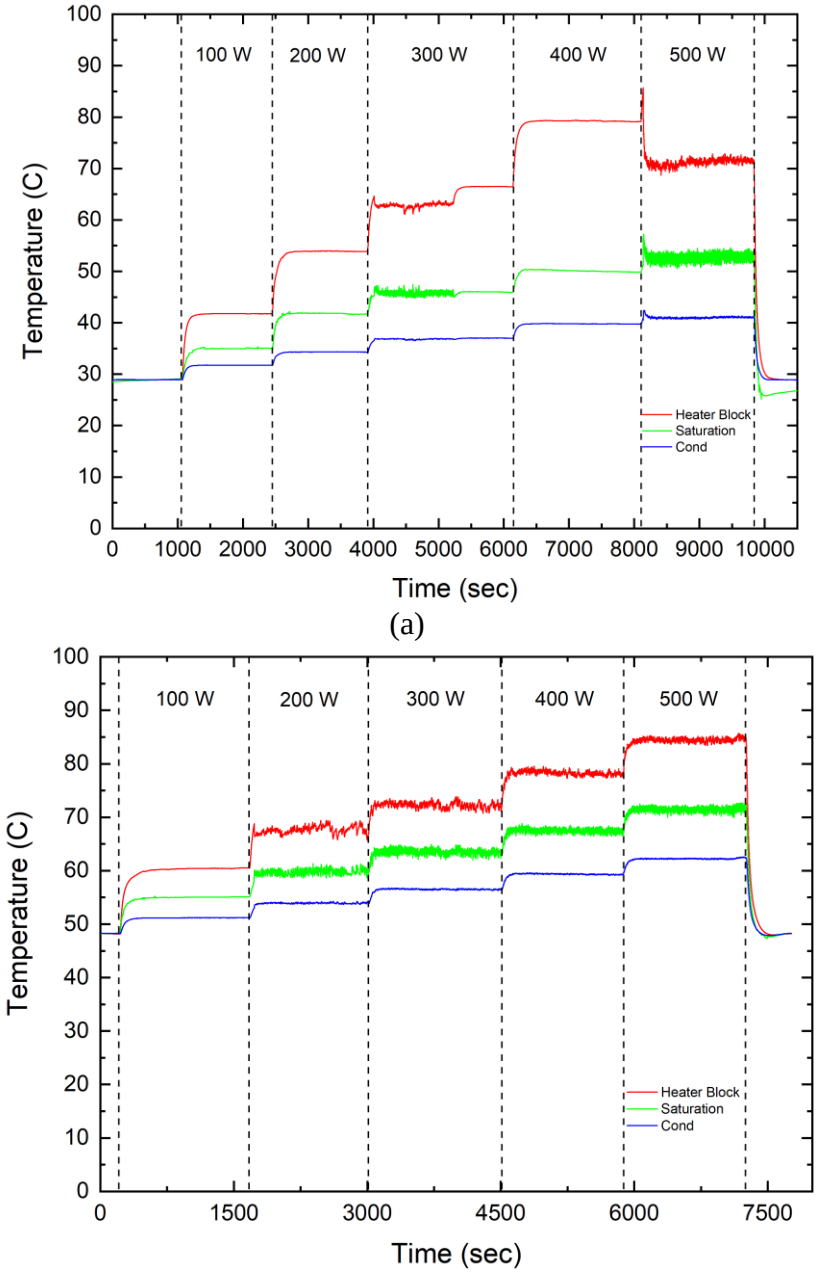

Figure 4-27 Temperature transients for end heating at horizontal orientation for cooling water temperature of a) 30℃ and b) 50℃.

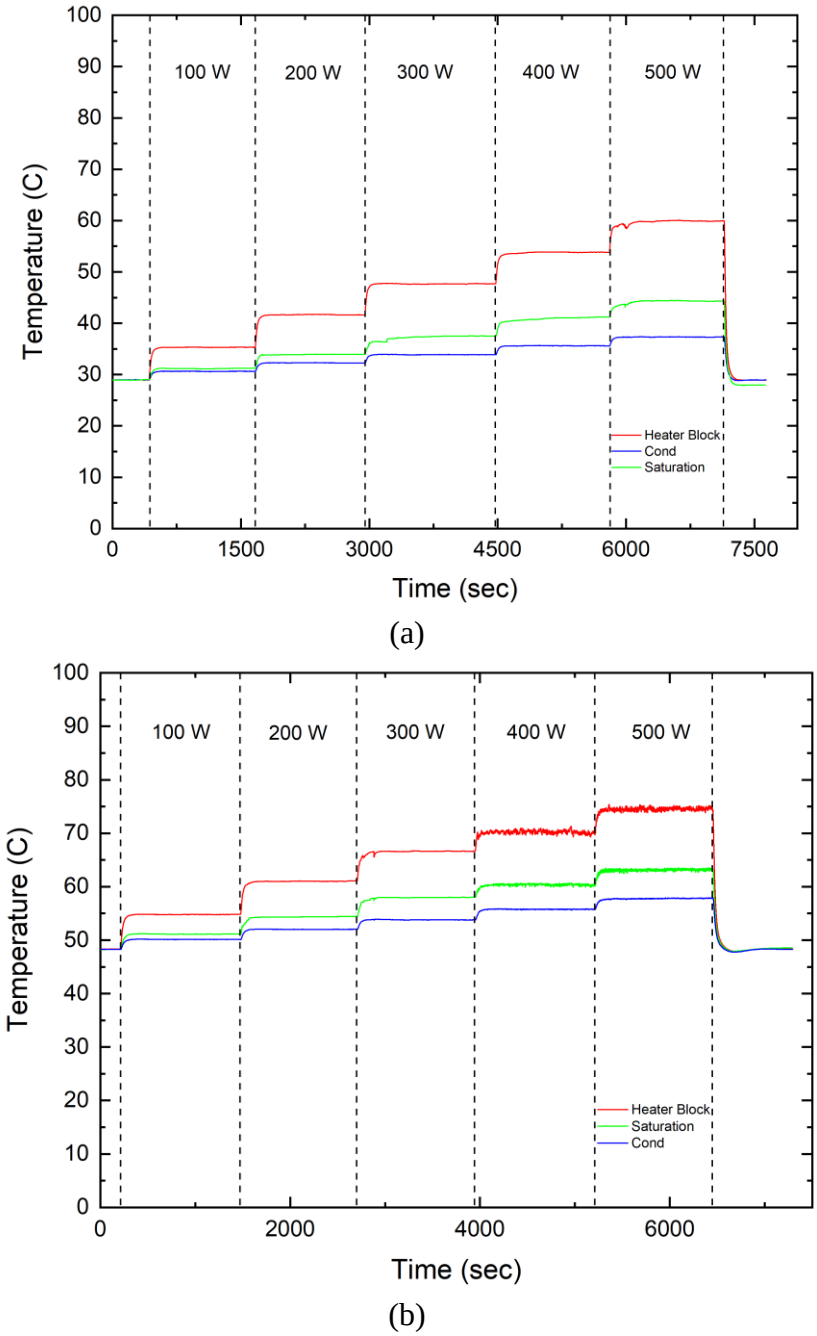

Figure 4-28 Temperature transients for middle heating at horizontal orientation for cooling water temperature of a) 30℃ and b) 50℃.

The temperature differences between the average wall temperatures below the heater block and the condenser are presented in Figure 4-27. The temperature differences increase with the increase in the heating power for all the cases. The middle heating cases show the lowest temperature differences. At low heating powers of 100 W to 300 W, the 30℃ and 50℃ cases show the same temperature difference with a small deviation at 300 W. Starting from 400 W, the 50℃ case shows lower temperature difference compared to the 30℃ case which correspond to the oscillations seen in the transient with the 50℃. The two end heating cases show almost the same results at the same cooling water temperature. All the end heating cases show the same temperature difference at 100 W. Starting from 200 W, the 50℃ cases shows lower temperature difference than the 30℃ cases and they reach almost the same temperature difference as the middle case at 30℃ cooling water temperature at high heating powers of 400 W and 500 W. The 30℃ case with end heating as discussed previously, shows high temperature difference with a big spike shown with the co-flow cooling water direction which correspond to the non-oscillating mode shown in Figure 4-25a.

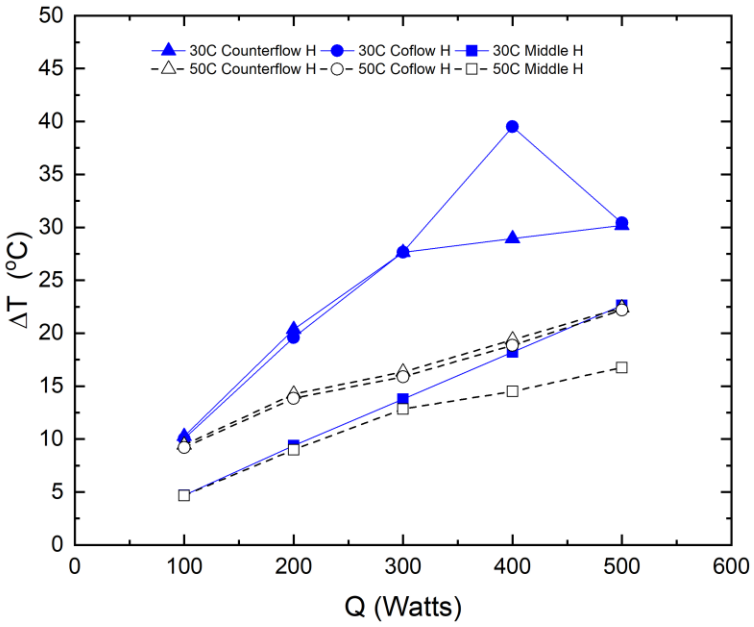

Figure 4-29 The temperature difference between the heater block wall and condenser temperatures with the heating power for 30℃ and 50℃ cooling water temperature cases.

Figure 4-28 presents the total thermal resistance for the 30℃ and 50℃ cooling water. The open symbols represent the non-oscillation mode and the solid ones represent the oscillation mode. The non-oscillation mode has a thermal resistance of approximately 0.1 K/W for the end heating with both cooling water directions and 0.045 k/W for the middle heating position. The results for the end heating at 100 W did appear to vary modestly with cooling water temperature. When oscillations were present, the thermal performance improves with the heating power. The 30℃ case does not show any oscillations and has nearly the same thermal resistance as the empty case. Oscillations accompanied with low thermal resistance are observed at 50℃ at high heating powers. The oscillations improve the performance with about 19% and 25% at 400W and 500 W

respectively. For the end heating, the 50°C results show lower thermal resistance than the 30°C results even once the oscillations occurred in that case until it reached almost the same thermal performance as the middle heating empty 30°C case at 400 W and 500 W.

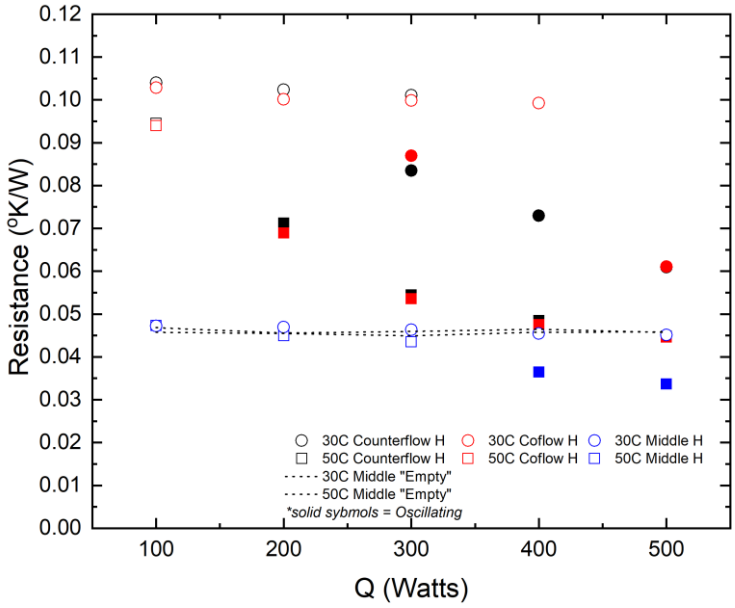

Figure 4-30 The total thermal resistance with the heating power including an oscillation mode map for 30°C and 50°C cooling water temperature cases.

The temperature distribution contours of the filled and unfilled oscillating heat pipe at 50°C with middle heating for the evaporator and condenser sections are shown in Figure 4-31 and Figure 4-32, respectively. The results show a more uniform temperature distribution on the evaporator side for the filled one compared to the unfilled case, which shows a hot spot in the middle with a temperature of approximately 85.5°C. A similar observation can be made on the condenser side as shown in Figure 4-32, where the unfilled one experiences a high temperature region corresponding to the location of the heating block while the filled one dissipates the heat more uniformly.

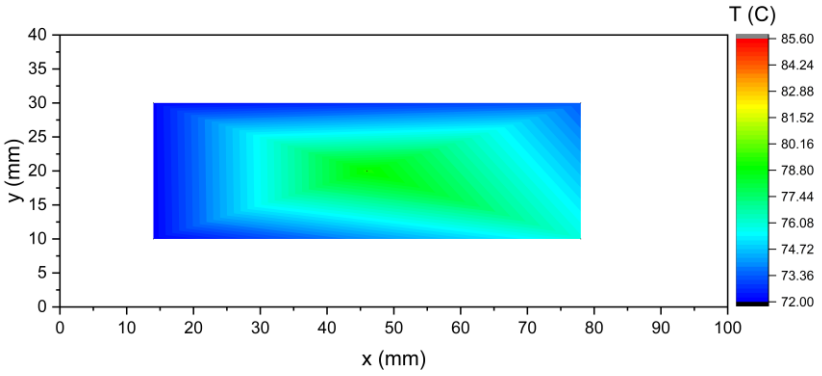

(a)

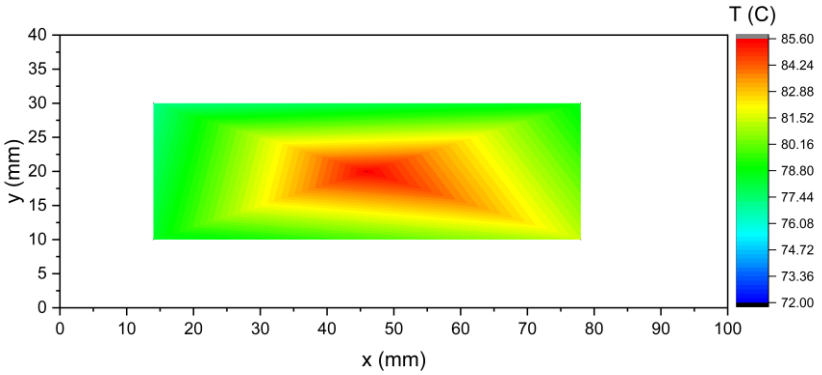

(b)

Figure 4-31 Temperature Distribution of the evaporator side at 50°C for (a) filled and (b) empty oscillating heat pipe with middle heating.

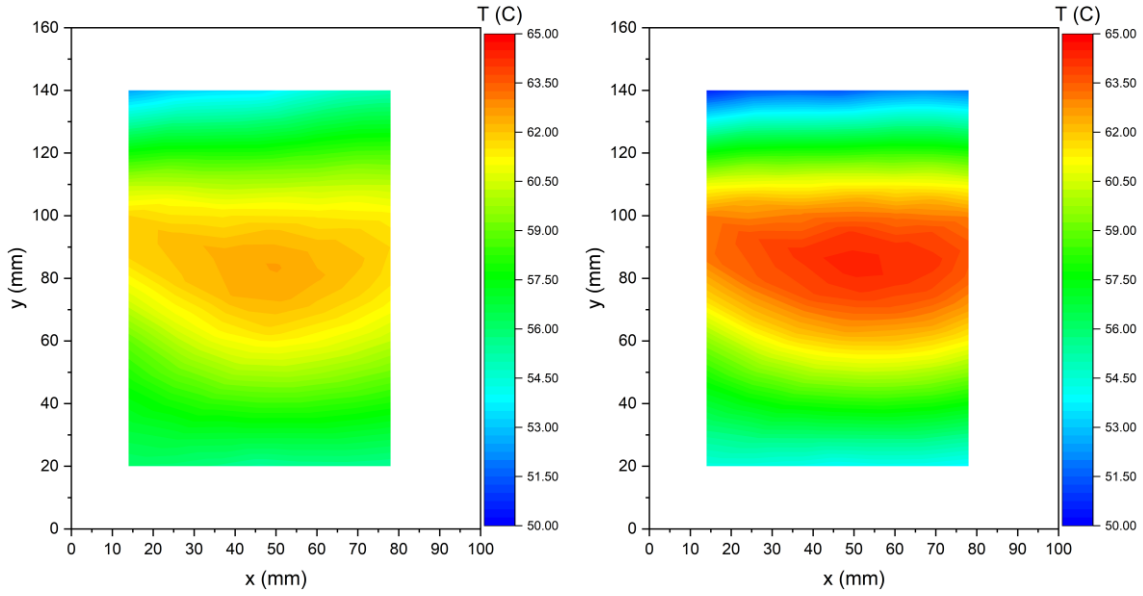

(a) (b)

Figure 4-32 Temperature Distribution of the condenser side at 50°C for (a) filled and (b) empty oscillating heat pipe with middle heating.

The effect of the cooling water temperature for the horizontal orientation was also considered at a heating power of 450 W as the cooling water temperature was increased from 30℃ to 50℃. The transients of the temperatures are presented in the appendix. The change in the average temperature difference between wall below the heater block and below the condenser with the condenser wall temperature are shown in Figure 4-33. The results for end heating show a decrease in the temperature difference across the device with an increase in the condenser wall temperature, while the middle heating case is initially nearly constant before decreasing. The middle heating case has lower temperature difference than the end heating cases in addition to having lower condenser wall temperatures at the same cooling water temperatures.

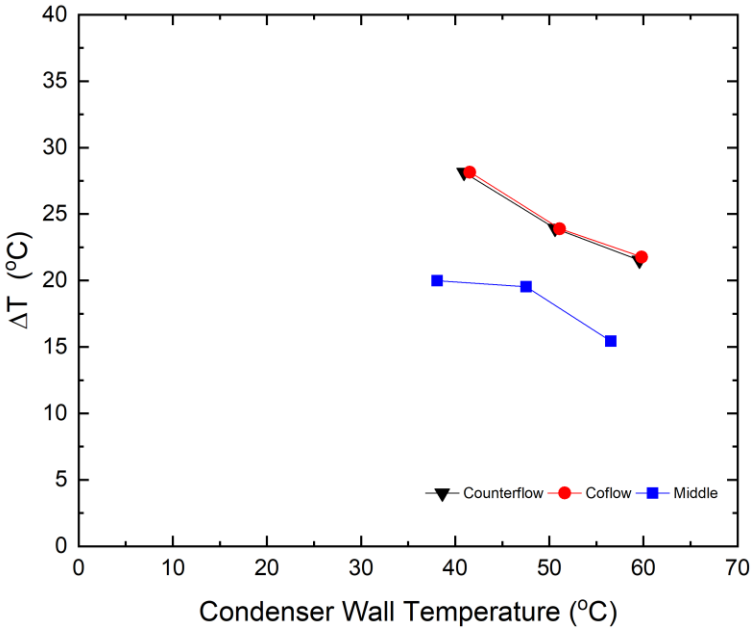

Figure 4-33 The temperature difference with the condenser wall temperature at 450 W for different heating locations.

The change in thermal resistance of the three cases and the oscillation mode observed from the temperature transients are shown in Figure 4-34. The thermal performance improves with an increase in the condenser wall temperature for the two heating locations. The end heating cases of both cooling water directions show oscillations along the test and a similar thermal performance. The middle heating case shows oscillations only at the high condenser wall temperature of about 57°C and this agrees with the previous results. The middle heating case has the lowest thermal resistance for all conditions, even when there are no oscillations. The thermal performance improved by about 20% when the oscillation mode is turned on.

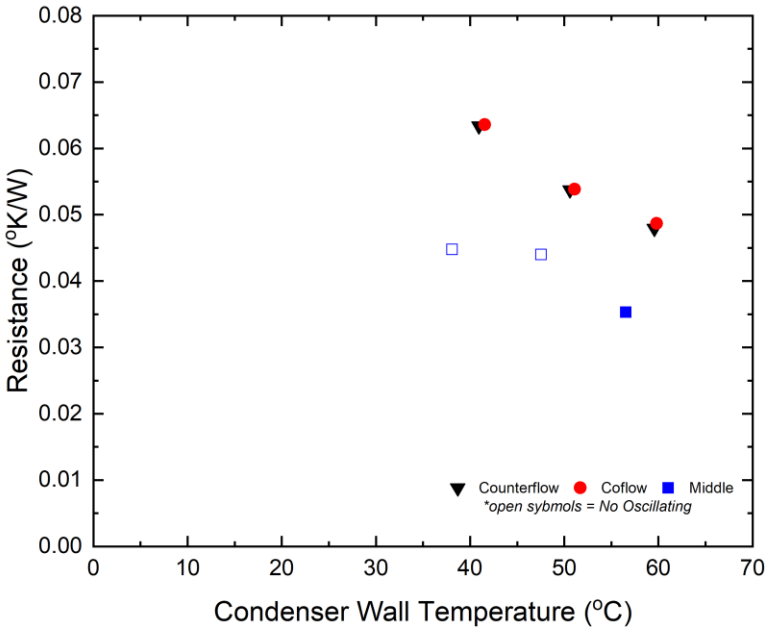

Figure 4-34 The total thermal resistance with the condenser wall temperature at 450 W for different heating locations including an oscillation mode map.

5 Conclusions and recommendations

The performance of a stacked double-layer flat plate oscillating heat pipe was designed, fabricated and tested to investigate its thermo hydraulic performance for axial heat transport and to investigate its capabilities to work as a heat spreader under local heating conditions. For the thermo hydraulic performance, two different sets of experiments were performed to (i) study the effect of the orientation of the oscillating heat pipe and (ii) to study the effect of the change of the cooling water or system temperature. For the heat spreading capability, two different heating locations were investigated: (i) middle heating and (ii) end heating with the cooling water in a co-flow and counter-flow direction. These experiments were performed for different orientations and cooling water temperatures.

Part 1: Axial heating performance.

The overall thermo-hydrodynamic performance analysis shows that the designed stacked oscillating heat pipe was capable of transporting 500W with the average evaporator wall temperature below 100℃ for all axial heat transport cases, even in the horizontal orientation. The oscillation frequency increased with the heating power and with a more damped amplitude, which enhanced the convective heat transfer and led to a lower thermal resistance at high power.

The evaporator heat transfer coefficient is significantly higher than that in the condenser. The condenser represents the major portion of the total thermal resistance, and more research is needed to be understand the condenser heat transfer and methods to improve it. The heat transfer coefficient values are considerably larger at the same heat flux compared with the data measured by Karthikeyan et al for a signal-layered oscillating heat pipe, indicating the superior performance of a stacked oscillating heat pipe. The effect of orientation on the overall thermal performance was small, with the vertical orientation showing an improvement in thermal performance of about 14% over the horizontal orientation at 500W and 30℃ cooling water temperature. This is consistent with the findings in the literature that stacked oscillating heat pipes largely eliminate the effect of gravity. The effect of the condenser temperature was investigated by performing tests at three cooling water temperatures of 10℃, 30℃ and 50℃. The lowest thermal resistance was at a cooling water temperature of 50℃ with a total thermal resistance of 0.06 K/W at 500 W. Despite an increase in the cooling water temperature by 20℃, the average evaporator temperature increased only from about 70℃ to 90℃ at 500 W. Increasing the cooling water temperature resulted in an increase in the condenser heat transfer coefficient as well as of the evaporator section. The change was significant as the temperature was changed from 10℃ to 30℃, but more modest with a further increase from 30℃ and 50℃ cases.

Three different oscillation modes were noted: (i) non-oscillating mode, (ii) continuous oscillating mode, and (iii) intermittent oscillating mode. The non-oscillating mode was observed only at 100 W for the 10℃ cooling water temperature case which leads

to a delay in the start-up of the oscillating heat pipe till 200 W. The continuous oscillating mode was present for the entire power range for the vertical orientation and the horizontal orientation with the 50℃ cooling water temperature case. The continuous oscillation mode results in an enhancement in both the condenser and evaporator heat transfer coefficients. The intermittent oscillating pattern was the dominant at low power for the 10℃ and 30℃ cooling water temperature cases and transitioned to the continuous oscillating pattern as the power was increased. This affects the total thermal performance as the oscillating heat pipe experiences a higher thermal resistance in the intermittent oscillating situation and sets a threshold for the start up power for each case. Previous correlations used to predict the maximum Ku number for single-layered oscillating heat pipes were found to underpredict the current data except for the correlation by Qu el al. for single-layered vertical oscillating heat pipes.

Part 2: Heat spreader.

The heat spreading capacity of the oscillating heat pipe was tested using local heating at the middle and at the end with the cooling water in both a co-flow and counter-flow direction with respect to the heating location in the latter case. There is no significant difference in the heat transfer performance between the co-flow and counter-flow cases. The co-flow and counter-flow cases had a low thermal resistance at high power where the oscillating heat pipe showed oscillations. The lowest thermal resistance achieved was 0.045 K/W at 500 W for the 50℃ cooling water case. At lower powers below 300 W, the oscillating heat pipe did not show oscillations and had a similar thermal performance of an unfilled oscillating heat pipe. For the middle heating case, there is no improvement in the heat transfer or heat spreading capacity over an unfilled oscillating heat pipe, except for high power at 50℃ in the horizontal orientation and 30℃ in the vertical orientation. The thermal performance was improved by 27% and 13%, respectively, for these two cases when compared to the unfilled case. An oscillation on/off map was developed based on the temperature and pressure transients and on the thermal resistance to define conditions under which the oscillations are effective and result in an improved performance. The oscillating heat pipe functions well as a heat spreader for local end heating for all powers and for middle heating at higher powers.

Part 2: Recommendations and Future Work.

Based on the present work of this thesis and previous work reported in the literature, recommendations for future work include:

- Investigation of the effect of the condenser and evaporator lengths on the thermal performance, especially on the heat transfer coefficients.
- Investigate the effect of filling ratio for the stacked oscillating heat pipe.
- Investigate the effect of the number of channels on the thermal performance. For example, the current configuration can be changed to have a space of 1 mm between channels, instead of the current 2 mm which will result in a higher number of channels over the same footprint.
- Investigate the long-term performance of the oscillating heat pipe, particularly when using water as the working fluid to avoid degradation in performance.
- Improve the instrumentation to measure internal pressure and temperature to obtain more accurate results.
- Investigate the heat spreader capacity using smaller heating zones to better represent local hot spots in the applications.

References

[1] H. Akachi, "Structure of a heat pipe," US4921041A, 1990.

[2] G. Karimi and J. R. Culham, "REVIEW AND ASSESSMENT OF PULSATING HEAT PIPE MECHANISM FOR HIGH HEAT FLUX ELECTRONIC COOLING," in *The Ninth Intersociety Conference on Thermal and Thermomechanical Phenomena In Electronic Systems*, 2004, no. vol.2, pp. 52–59.

[3] X. Han, X. Wang, H. Zheng, X. Xu, and G. Chen, "Review of the development of pulsating heat pipe for heat dissipation," *Renew. Sustain. Energy Rev.*, vol. 59, pp. 692–709, 2016.

[4] B. S. Taft, A. D. Williams, and B. L. Drolen, "Review of pulsating heat pipe working fluid selection," *J. Thermophys. Heat Transf.*, vol. 26, no. 4, pp. 651–656, 2012.

[5] R. Dobson and T. Harms, "Lumped parameter analysis of closed and open oscillatory heat pipes," in *Proceedings of the 11th International heat pipe Conference*, 1999, pp. 137–142.

[6] J. Qu, Q. Wang, and Q. Sun, "Lower limit of internal diameter for oscillating heat pipes: A theoretical model," *Int. J. Therm. Sci.*, vol. 110, pp. 174–185, 2016.

[7] K. Mehta, N. Mehta, and V. Patel, "Influence of the channel profile on the thermal resistance of closed-loop flat-plate oscillating heat pipe," *J. Brazilian Soc. Mech. Sci. Eng.*, vol. 42, no. 3, pp. 1–12, 2020.

[8] J. Bico and D. Quéré, "Rise of liquids and bubbles in angular capillary tubes," *J. Colloid Interface Sci.*, vol. 247, no. 1, pp. 162–166, 2002.

[9] Y. Zhou and W. Qu, "Experimental study on capillary structure and size effects of pulsating heat pipes," *J. Eng. Thermophys.*, vol. 28, no. 4, pp. 646–648, 2007.

[10] J. Lee and S. J. Kim, "Effect of channel geometry on the operating limit of micro pulsating heat pipes," *Int. J. Heat Mass Transf.*, vol. 107, pp. 204–212, 2017.

[11] C. Hua, X. Wang, X. Gao, H. Zheng, X. Han, and G. Chen, "Experimental research on the start-up characteristics and heat transfer performance of pulsating heat pipes with rectangular channels," *Appl. Therm. Eng.*, vol. 126, pp. 1058–1062, 2017.

[12] P. Meena, S. Rittidech, and P. Tammasaeng, "Effect of Evaporator Section Lengths and Working Fluids on Operational Limit of Closed Loop Oscillating Heat Pipes with Check Valves (CLOHP/CV)," *Am. J. Appl. Sci.*, vol. 6, no. 1, pp. 136–139, 2009.

[13] S. Rittidech, P. Terdtoon, M. Murakami, P. Kamonpet, and W. Jompakdee,

"Correlation to predict heat transfer characteristics of a closed-end oscillating heat pipe at normal operating condition," *Appl. Therm. Eng.*, vol. 23, pp. 497–510, 2003.

[14] P. Charoensawan and P. Terdtoon, "Thermal performance correlation of horizontal closed-loop oscillating heat pipes," *Proc. Electron. Packag. Technol. Conf. EPTC*, vol. 28, pp. 906–909, 2007.

[15] C. FASULA, "OSCILLATING HEAT PIPES (OHP),MASTERS OF SCIENCE IN MECHANICAL ENGINEERING AND APPLIED MECHANICS,UNIVERSITY OF RHODE ISLAND," 2009.

[16] N. S. Y. and Pachghare P. R., "Parameters Affecting the Functioning of Close Loop Pulsating Heat Pipe : A Review," *Res. J. Eng. Sci.*, vol. 2, no. 1, pp. 35–39, 2013.

[17] J. Wang, H. Ma, and Q. Zhu, "Effects of the evaporator and condenser length on the performance of pulsating heat pipes," *Appl. Therm. Eng.*, vol. 91, pp. 1018–1025, 2015.

[18] J. Kim and S. J. Kim, "Experimental investigation on the effect of the condenser length on the thermal performance of a micro pulsating heat pipe," *Appl. Therm. Eng.*, vol. 130, pp. 439–448, 2018.

[19] L. Quan and L. Jia, "EXPERIMENTAL STUDY ON HEAT TRANSFER CHARACTERISTIC OF PLATE PULSATING HEAT PIPE," in *ASME 2009 2nd Micro/Nanoscale Heat & Mass Transfer International Conference*, 2009, pp. 1–6.

[20] P. Cheng, S. Thompson, J. Boswell, and H. B. Ma, "An Investigation of Flat-Plate Oscillating Heat Pipes," *J. Electron. Packag.*, vol. 132, no. 4, p. 041009, 2010.

[21] J. Lee, Y. Joo, and S. J. Kim, "Effects of the number of turns and the inclination angle on the operating limit of micro pulsating heat pipes," *Int. J. Heat Mass Transf.*, vol. 124, pp. 1172–1180, 2018.

[22] Q. Cai, C. L. Chen, and J. F. Asfia, "Operating characteristic investigations in pulsating heat pipe," *J. Heat Transfer*, vol. 128, no. 12, pp. 1329–1334, 2006.

[23] Z. R. Lin, Z. Y. Lee, L. W. Zhang, S. F. Wang, and G. Refai-Ahmed, "Heat transfer characteristics of aluminum plate pulsating heat pipes," in *ASME 2011 Pacific Rim Technical Conference & Exposition on Packaging and Integration of Electronic and Photonic Systems*, 2011, pp. 1–7.

[24] P. Charoensawan, S. Khandekar, M. Groll, and P. Terdtoon, "Closed loop pulsating heat pipes - Part A: Parametric experimental investigations," *Appl. Therm. Eng.*, vol. 23, no. 16, pp. 2009–2020, 2003.

[25] S. Khandekar and M. Groll, "An insight into thermo-hydrodynamic coupling in closed loop pulsating heat pipes," *Int. J. Therm. Sci.*, vol. 43, no. 1, pp. 13–20, 2004.

[26] B. S. Taft, A. D. Williams, and B. L. Drolen, "Working fluid selection for pulsating

heat pipes," *42nd AIAA Thermophys. Conf.*, no. June, pp. 1–14, 2011.

[27] Y. Zhang and A. Faghri, "Advances and unsolved issues in pulsating heat pipes," *Heat Transf. Eng.*, vol. 29, no. 1, pp. 20–44, 2008.

[28] R. S. Borkar and P. R. Pachghare, "EFFECT OF WORKING FLUID, FILLING RATIO AND NUMBER OF TURNS ON PULSATING HEAT PIPE THERMAL PERFORMANCE," *Front. Heat Pipes*, vol. 4, pp. 1–6, 2015.

[29] M. Groll and S. Khandekar, "STATE OF THE ART ON PULSATING HEAT PIPES," in *The 2nd International Conference on Microchannels and Minichannels*, 2004, pp. 1–12.

[30] S. Wang and S. Nishio, "Heat Transport Characterastics in Closed Loop Oscillating Heat Pipes," in *ASME Summer Heat Transfer Conference*, 2005, pp. 1–6.

[31] C. Y. Tseng, K. S. Yang, K. H. Chien, M. S. Jeng, and C. C. Wang, "Investigation of the performance of pulsating heat pipe subject to uniform/alternating tube diameters," *Exp. Therm. Fluid Sci.*, vol. 54, pp. 85–92, 2014.

[32] K. Mehta, N. Mehta, and V. Patel, "Experimental investigation of the thermal performance of closed loop flat plate oscillating heat pipe," *Exp. Heat Transf.*, vol. 00, no. 00, pp. 1–19, 2020.

[33] S. Khandekar, M. Groll, P. Charoensawan, S. Rittidech, and P. Terdtoon, "Closed and Open Loop Pulsating Heat Pipes," in *Proc. 13th International Heat Pipe Conference*, 2004, vol. 26, p. 38.

[34] T. Hao, X. Ma, Z. Lan, and N. Li, "Effects of Superhydrophobic and Superhydrophilic Surfaces on Heat Transfer and Oscillating Motion of an Oscillating Heat Pipe," *J. Heat Transfer*, vol. 136, no. 12, pp. 1–13, 2014.

[35] S. Abraham, A. Takawale, P. Stephan, and A. Pattamatta, "Thermal characteristics of a three-dimensional coil type pulsating heat pipe at different heating modes," *J. Therm. Sci. Eng. Appl.*, vol. 13, no. August, pp. 1–34, 2020.

[36] K. Xie and Y. Ji, "Experimental investigation on an aluminum oscillating heat pipe charged with water," *Appl. Therm. Eng.*, vol. 162, no. February, p. 114182, 2019.

[37] K. H. Chien, Y. R. Chen, Y. T. Lin, C. C. Wang, and K. S. Yang, "The Experimental Studies of Flat-Plate Closed-Loop Pulsating Heat," *11th IHPS*, pp. 212–216, 2011.

[38] K. K. Mehta, N. Mehta, and V. Patel, "Effect of Operational Parameters on the Thermal Performance of Flat Plate Oscillating Heat Pipe," *J. Heat Transfer*, vol. 141, no. 12, pp. 1–8, 2019.

[39] T. Hudakorn, P. Terdtoon, and P. Sakulchang, "Effect of Inclination Angle on Performance Limit of a Closed-End Oscillating Heat Pipe," *Am. J. Eng. Appl. Sci.*, vol. 1, no. 3, pp. 174–180, 2008.

[40] S. M. Thompson *et al.*, "Robust Thermal Performance of a Flat-Plate Oscillating Heat Pipe During High-Gravity Loading," *J. Heat Transfer*, vol. 133, no. 10, p. 104504, 2011.

[41] J. Qu, J. Zhao, and Z. Rao, "Experimental investigation on thermal performance of multi-layers three-dimensional oscillating heat pipes," *Int. J. Heat Mass Transf.*, vol. 115, pp. 810–819, 2017.

[42] C. D. Smoot and H. B. Ma, "Experimental Investigation of a Three-Layer Oscillating Heat Pipe," *J. Heat Transfer*, vol. 136, no. 051501, pp. 1–6, 2014.

[43] Q. Sun, J. Qu, X. Li, and J. Yuan, "Experimental investigation of thermo-hydrodynamic behavior in a closed loop oscillating heat pipe," *Exp. Therm. Fluid Sci.*, vol. 82, pp. 450–458, 2017.

[44] H. Ma, B. Borgmeyer, P. Cheng, and Y. Zhang, "Heat Transport Capability in an Oscillating Heat Pipe," *J. Heat Transfer*, vol. 130, no. 14, pp. 1–7, 2008.

[45] J. Chen, "Correlation for Boiling Heat Transfer to Saturated Fluids in Convective Flow," *Ind. Eng. Chem. Process Des. Dev.*, vol. 5, no. 3, pp. 322–329, 1966.

[46] M. M. Shah, "A general correlation for heat transfer during film condensation inside pipes," *Int. J. Heat Mass Transf.*, vol. 22, no. 4, pp. 547–556, 1979.

[47] J. G. Monroe, Z. S. Aspin, J. D. Fairley, and S. M. Thompson, "Analysis and comparison of internal and external temperature measurements of a tubular oscillating heat pipe," *Exp. Therm. Fluid Sci.*, vol. 84, pp. 165–178, 2017.

[48] M. Gonzalez *et al.*, "Heat transfer mechanisms in pulsating heat-pipes with nanofluid Heat transfer mechanisms in pulsating heat-pipes with nanofluid," vol. 013906, no. 2015, 2016.

[49] R. Senjaya and T. Inoue, "Oscillating heat pipe simulation considering bubble generation Part I: Presentation of the model and effects of a bubble generation," *Int. J. Heat Mass Transf.*, vol. 60, pp. 816–824, 1970.

[50] Y. Zhang and A. Faghri, "Heat transfer in a pulsating heat pipe with open end," *Int. J. Heat Mass Transf.*, vol. 45, no. 4, pp. 755–764, 2001.

[51] M. B. Shafii, A. Faghri, and Y. Zhang, "Thermal modeling of unlooped and looped pulsating heat pipes," *J. Heat Transfer*, vol. 123, no. 6, pp. 1159–1172, 2001.

[52] M. B. Shafii, A. Faghri, and Y. Zhang, "Analysis of heat transfer in unlooped and looped pulsating heat pipes," *Int. J. Numer. Methods Heat Fluid Flow*, vol. 12, no. 5, pp. 585–609, 2002.

[53] P. Cheng and H. Ma, "A mathematical model of an oscillating heat pipe," *Heat Transf. Eng.*, vol. 32, no. 11–12, pp. 1037–1046, 2011.

[54] J. Jo, J. Kim, and S. Jin, "Experimental investigations of heat transfer mechanisms

of a pulsating heat pipe," *Energy Convers. Manag.*, vol. 181, no. October 2018, pp. 331–341, 2019.

[55] S. S. Bhakre and R. S. Choudhari, "Experimental Analysis on Effect of Design Parameters on the Performance of Single Loop Pulsating Heat Pipe," *Int. J. Sci. Res.*, vol. 4, no. 4, pp. 2188–2192, 2015.

[56] G. V. Pradeep and K. Rama Narasimha, "Thermal performance of a vertical closed loop pulsating heat pipe and analysis using dimensionless numbers," *J. Mech. Eng. Sci.*, vol. 11, no. 4, pp. 3240–3255, 2017.

[57] G Pundarika, Rudra Naik,K Rama Narasimha, Linford Pinto, R. Naik, V. Varadarajan, G. Pundarika, and K. Rama Narasimha, "Effects of Working fluid on the Performance of a multi turn Pulsating Heat Pipe," *J. Appl. Fluid Mech.*, vol. 6, no. 2, pp. 267–275, 2013.

[58] R. Senjaya and T. Inoue, "Effects of non-condensable gas on the performance of oscillating heat pipe, part II: Experimental study," *Appl. Therm. Eng.*, vol. 73, no. 1, pp. 1393–1400, 2014.

[59] R. Senjaya and T. Inoue, "Effects of non-condensable gas on the performance of oscillating heat pipe, part I: Theoretical study," *Appl. Therm. Eng.*, vol. 73, no. 1, pp. 1387–1392, 2014.

[60] D. Yin, H. Wang, H. B. Ma, and Y. L. Ji, "Operation limitation of an oscillating heat pipe," *Int. J. Heat Mass Transf.*, vol. 94, pp. 366–372, 2016.

[61] S. Khandekar, P. Charoensawan, M. Groll, and P. Terdtoon, "Closed loop pulsating heat pipes - Part B: Visualization and semi-empirical modeling," *Appl. Therm. Eng.*, vol. 23, no. 16, pp. 2021–2033, 2003.

[62] J. Qu and Q. Wang, "Experimental study on the thermal performance of vertical closed-loop oscillating heat pipes and correlation modeling," *Appl. Energy*, vol. 112, pp. 1154–1160, 2013.

[63] T. Katpradit, T. Wongratanaphisan, P. Terdtoon, P. Kamonpet, A. Polchai, and A. Akbarzadeh, "Correlation to predict heat transfer characteristics of a closed end oscillating heat pipe at critical state," vol. 25, pp. 2138–2151, 2005.

[64] V. K. Karthikeyan, S. Khandekar, B. C. Pillai, and P. K. Sharma, "Infrared thermography of a pulsating heat pipe: Flow regimes and multiple steady states," *Appl. Therm. Eng.*, 2014.

[65] N. Mansouri, C. Weasner, and A. Zaghlol, "Characterization of a Heat Sink with Embedded Heat Pipe with Variable Heat Dissipating Source Placement for Power Electronics Applications," *Proc. 17th Intersoc. Conf. Therm. Thermomechanical Phenom. Electron. Syst. ITherm 2018*, pp. 311–317, 2018.

[66] H. Lu, S. M. Thompson, F. F. Laun, and H. B. Ma, "Effect of cooling rate on thermal

performance of an oscillating heat spreader," *J. Thermophys. Heat Transf.*, vol. 30, no. 2, pp. 461–465, 2016.

[67] V. A. Hemadri, A. Gupta, and S. Khandekar, "Thermal radiators with embedded pulsating heat pipes: Infra-red thermography and simulations," *Appl. Therm. Eng.*, vol. 31, no. 6–7, pp. 1332–1346, 2011.

[68] S. M. Thompson, H. Lu, and H. Ma, "Thermal Spreading with Flat-Plate Oscillating Heat Pipes," *J. Thermophys. Heat Transf.*, vol. 29, no. 2, pp. 338–345, 2015.

[69] S. Khandekar and A. Gupta, "Embedded Pulsating Heat Pipe Radiators," in *14th International Heat Pipe Conference*, 2007, vol. 1, no. 1, pp. 258–263.

[70] S. M. Thompson, Z. S. Aspin, N. Shamsaei, A. Elwany, and L. Bian, "Additive manufacturing of heat exchangers: A case study on a multi-layered Ti-6Al-4V oscillating heat pipe," *Addit. Manuf.*, vol. 8, pp. 163–174, 2015.

[71] C. D. Smoot and H. B. Ma, "Experimental Investigation of a Three-Layer Oscillating Heat Pipe," *J. Heat Transfer*, vol. 136, no. 5, p. 051501, 2014.

[72] S. M. Thompson, R. A. Winholtz, and C. Wilson, "Experimental Investigation of Miniature Three-Dimensional Flat-Plate Oscillating Heat Pipe," vol. 131, no. April 2009, pp. 1–9, 2016.

[73] "Hourly forecast for Hamilton, Ontario, Canada." [Online]. Available: https://www.timeanddate.com/weather/canada/hamilton/hourly. [Accessed: 11-Jan-2021].

[74] S. Mohamed, D. Ewing, C. Y. Ching, and A. Zaghlol, "Effect of Fluid Loading on the Performance of Low-Temperature T Thermosyphons," 2018.

[75] R. J. Moffat, "Describing the uncertainties in experimental results," *Exp. Therm. Fluid Sci.*, vol. 1, no. 1, pp. 3–17, 1988.

6 Appendix

The rest plots of transients for the heat spreader cases for the heater block, condenser and saturation temperatures that are not presented in the results chapter are presented here in this chapter as following:

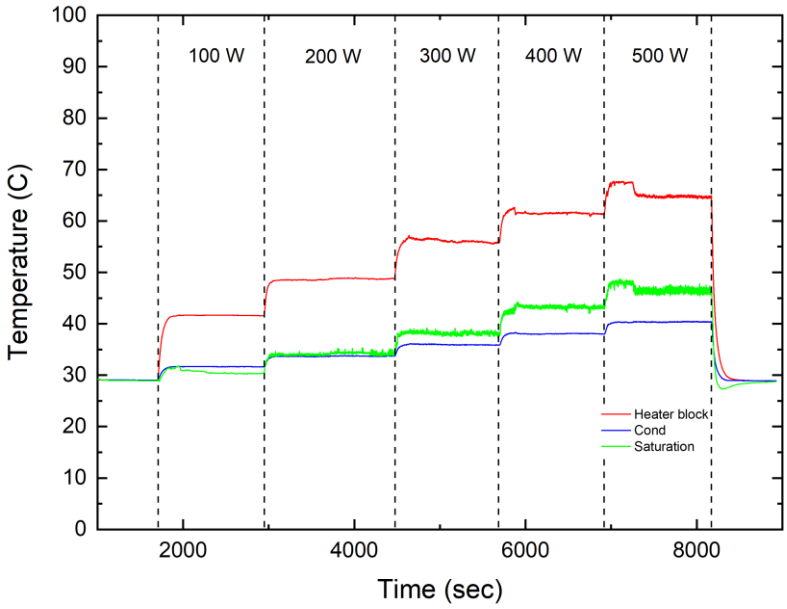

Figure 6-1 Temperature transients for end heating at vertical orientation for cooling water temperature of 30°C with counter-flow cooling water direction.

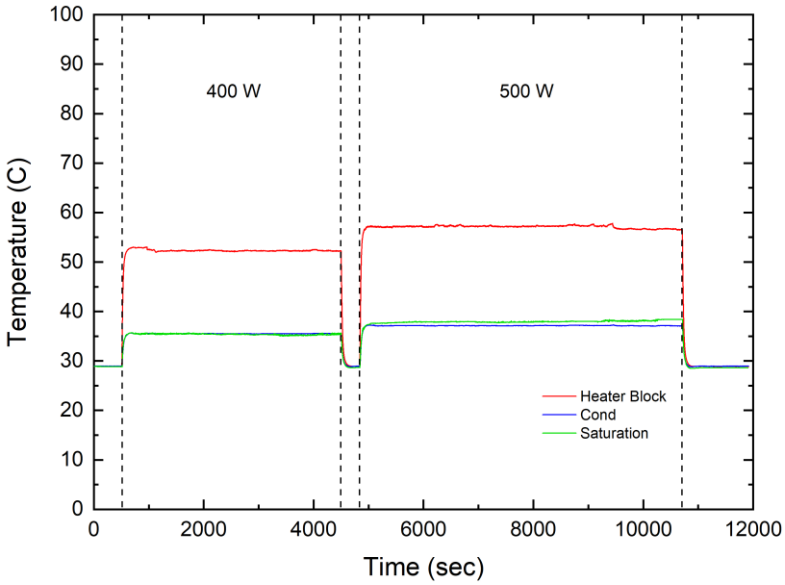

Figure 6-2 Temperature profiles for 400 W and 500 W tests with 30°C cooling water temperature for end heating at vertical orientation with a counter-flow cooling water direction.

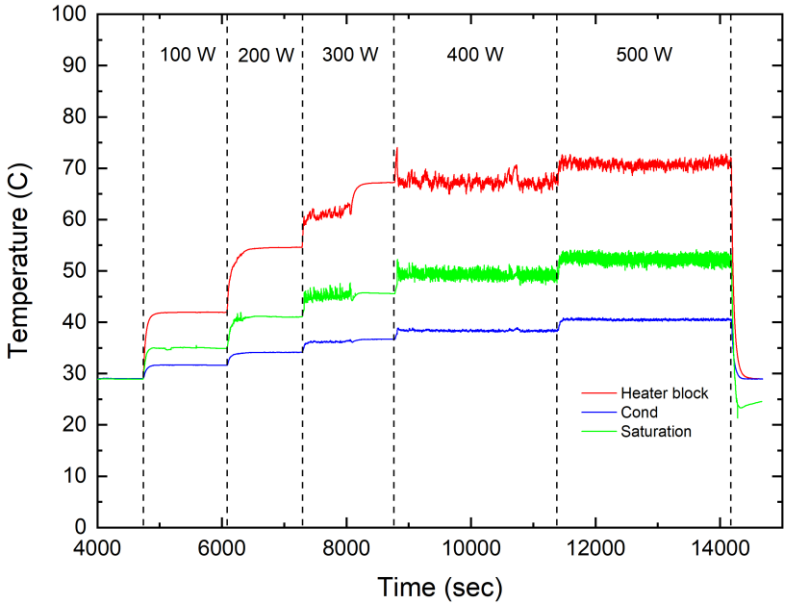

Figure 6-3 Temperature transients for end heating at horizontal orientation for cooling water temperature of 30°C with counter-flow water direction.

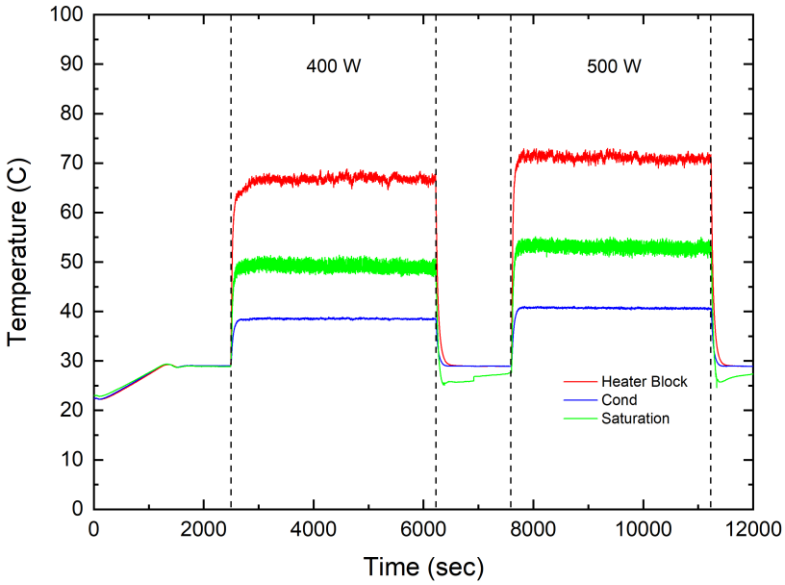

Figure 6-4 Temperature profiles for 400 W and 500 W tests with 30°C cooling water temperature for end heating at horizontal orientation with a counter-flow cooling water direction.

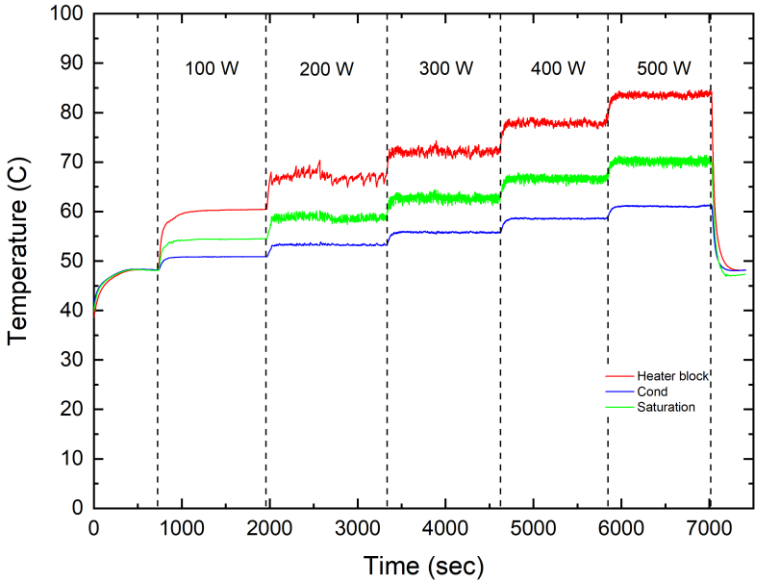

Figure 6-5 Temperature transients for end heating at horizontal orientation for cooling water temperature of 50°C with counter-flow water direction.

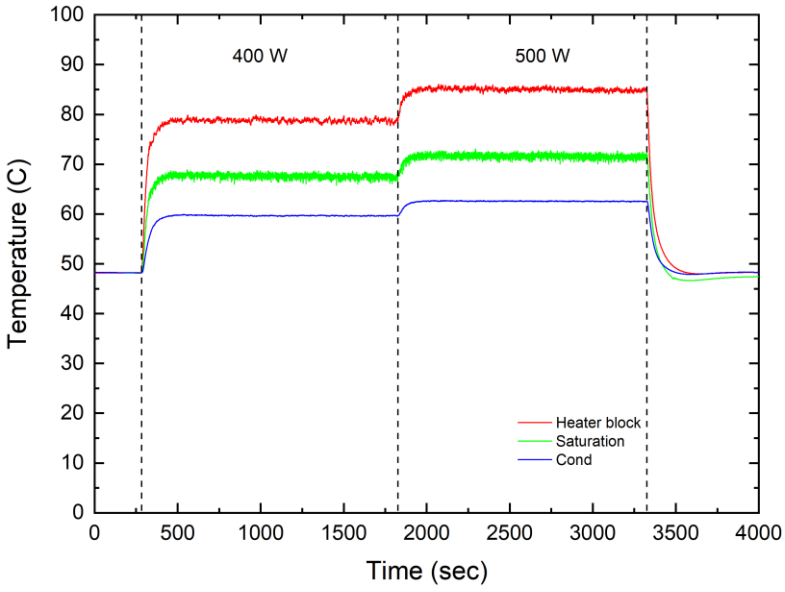
400 W
500 W
Temperature (C)
Time (sec)
Heater block
Saturation
Cond

(a)

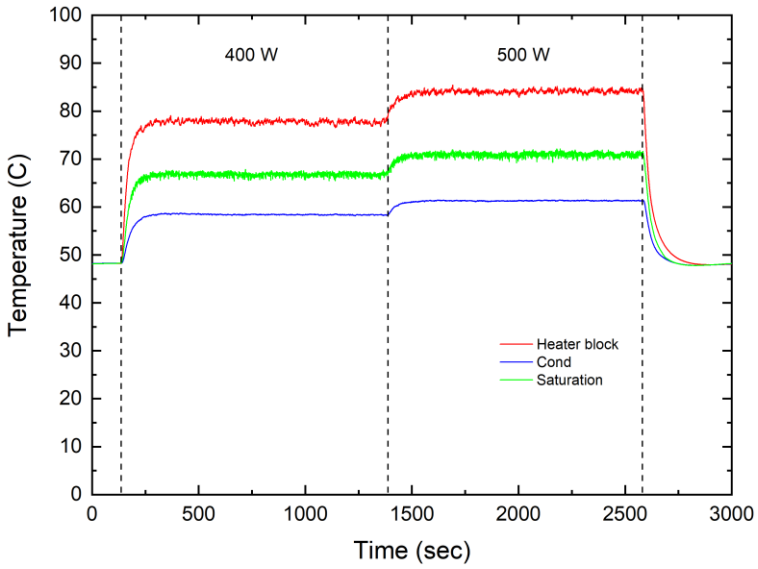
400 W
500 W
Temperature (C)
Time (sec)
Heater block
Cond
Saturation

(b)

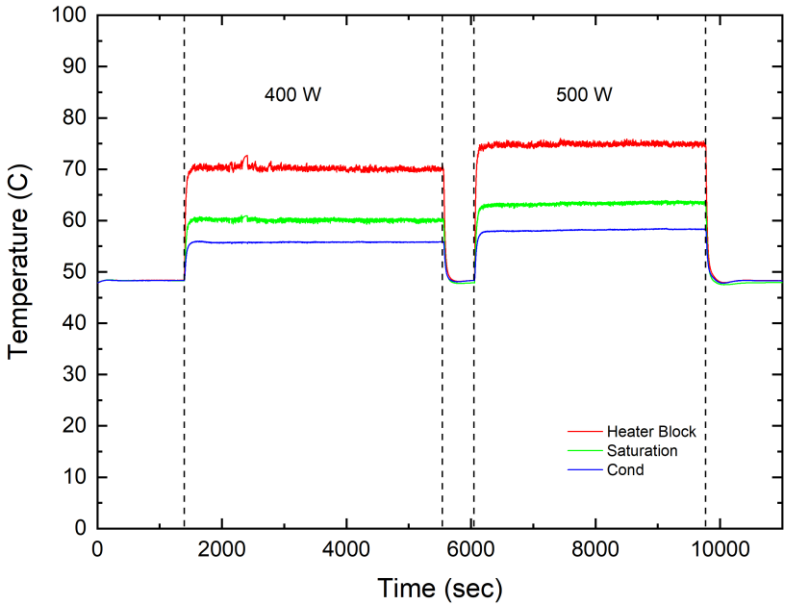

(c)

Figure 6-6 Temperature profiles for 400 W and 500 W tests with 50°C cooling water temperature at horizontal orientation for end heating with a) co-flow and b) counter-flow cooling water direction and c) middle heating.

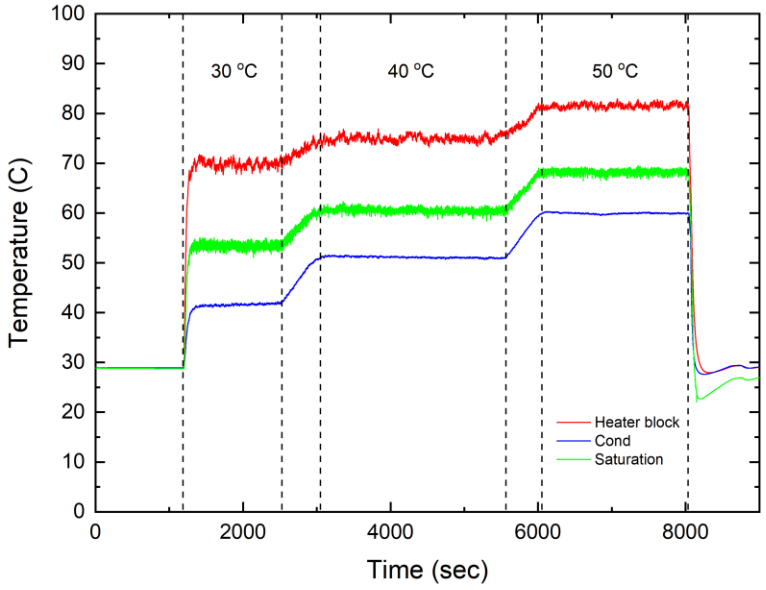

(a)

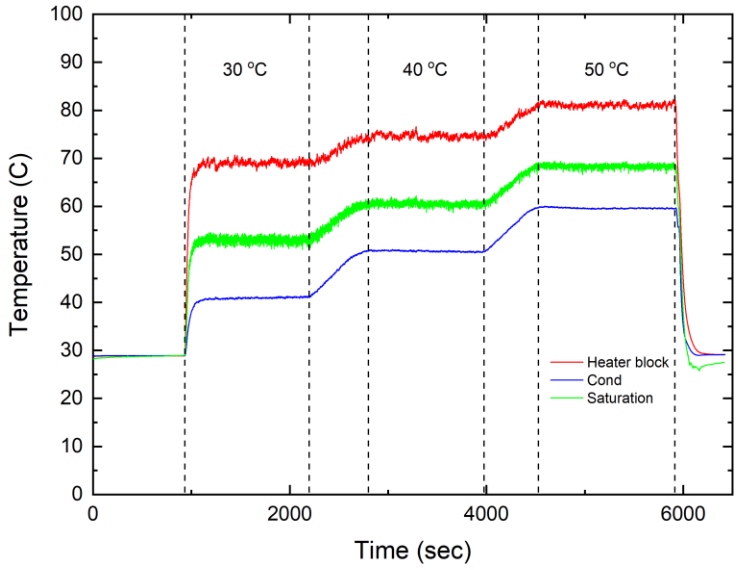

(b)

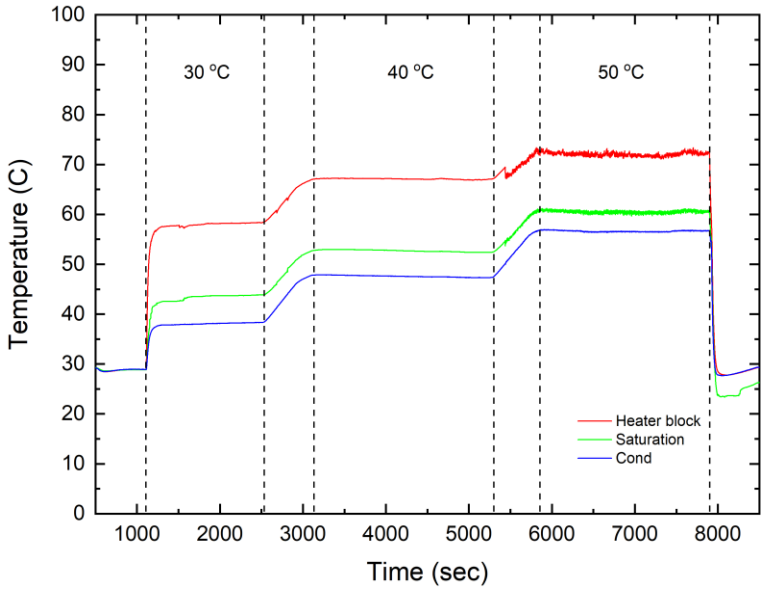

(c)

Figure 6-7 Temperature profiles for 450 W with an increase in the cooling water temperature at horizontal orientation for end heating with a) co-flow and b) counter-flow cooling water direction and c) middle heating.